UNIVERSITY OF CALIFORNIA,
IRVINE

Functional specialization of eye-specific visual pathways into higher visual cortex

DISSERTATION

submitted in partial satisfaction of the requirements
for the degree of

DOCTOR OF PHILOSOPHY

in Biological Sciences

by

Kirstie Jay Salinas

Dissertation Committee:
Associate Professor Sunil P. Gandhi, Chair
Professor Ron Frostig
Associate Professor Alyssa Brewer

2019

DEDICATION

To *my father Adrian*, for his love, support and motivation to stay focused at every level of my education

To *my mother Janie*, for her love, inspiration and insistence that I could overcome any obstacle presented to me

To *my sister Valerie*, for her love, guidance and listening ear

To *my grandparents and ancestors*, whose shoulders I stand on

TABLE OF CONTENTS

LIST OF FIGURES

ACKNOWLEDGMENTS

I would like to acknowledge members of the Gandhi lab who were instrumental to the development of my skills as an experimentalist and as a scientist. My mentor, Sunil Gandhi, provided major support towards this project and made my publications and access to conferences and postdoctoral opportunities possible. All members of the Gandhi lab were influential to my development as a scientist. In particular, Dario Figueroa-Velez assisted me with surgical techniques and as a co-author on my first manuscript in the lab. Xiaoting Zheng, a wonderful lab mate and friend, assisted me with furthering my skills as a scientist by discussing figures and data. Dr. Carey Huh extended career advice, mentorship and assistance with presentations. She also helped with ideas and offered her interpretations when writing my second manuscript in the lab. Hyungtae Kim and Jack Zeitoun provided software development and resources for data analysis that made the experiments possible.

I would like to extend thanks to my committee members, Dr. Sunil Gandhi, Dr. Ron Frostig and Dr. Alyssa Brewer, for their time and support. They have all contributed immensely to my development as a scientist and have provided fundamental feedback for my dissertation. They have also all been integral to my ability to find a postdoc position and I cannot thank them enough for supporting me, believing in me and inspiring me.

I would like to recognize my undergraduate advisor, Dr. Fidel Santamaria, for introducing me to the world of academic research by bringing me into his lab as an undergraduate. He continues to be a huge inspiration and advisor to me. Dr. Gail Taylor, who recruited me into the MARC program as an undergraduate, opened my eyes to life as a researcher, and she continues to support me throughout my endeavors.

I would also like to acknowledge the financial support that I received as a graduate student. I have been awarded the following funding through the University of California Irvine: NIH IMSD Fellowship, Eugene Cota Robles Fellowship and Graduate Dean's Recruitment Fellowship. I also received the NSF-GRFP during my first year of graduate school. I would like to thank Dr. Andrea Tenner, Sunil Gandhi, Fidel Santamaria and Gail Taylor for their assistance with my NSF application.

Finally, I need to thank all of my friends and family who helped me succeed in graduate school. For the countless phone calls, visits to California, trips to the yoga studios, jogging, company, shoulders to cry on, inspiration and motivation to keep me going.

CURRICULUM VITAE

Kirstie Jay Salinas

EDUCATION:

M.S., PhD Candidate, University of California, Irvine, Department of Neurobiology and Behavior, 2014-present

Thesis Advisor: Sunil Gandhi, Ph.D. Expected date of completion: May 2019

B.S., Biology, Neurobiology Concentration, University of Texas at San Antonio, 2009-2013

Honors thesis: Quantifying the effects of gold star-shaped nanoparticles on CA3 Hippocampal neurons; Thesis Advisor: Fidel Santamaria, Ph.D.

RESEARCH EXPERIENCE

University of California, Irvine, Department of Neurobiology and Behavior, 2014-present

Contralateral bias of high spatial frequency tuning and cardinal direction selectivity in mouse visual cortex

-Research Advisor: Sunil Gandhi, Ph.D.

-Characterized eye-specific visual response properties of hundreds of cells within the binocular zone of primary visual cortex using two-photon calcium imaging of GCaMP6s in awake mice, uncovering two seemingly distinct populations within V1: (1) contralateral dominated cells tuned to higher spatial frequencies with high cardinal direction selectivity and (2) binocularly driven cells with lower spatial frequency preferences.

-This work was funded by a NSF GRFP fellowship

Functional segregation of eye-specific visual pathways into higher visual cortex

-Research Advisor: Sunil Gandhi, Ph.D.

-The goal is to understand if two seemingly distinct populations of cells within primary visual cortex are engaged in functional stream/areal specialization. Areas LM and PM have been grouped into the putative mouse dorsal and ventral stream. Using two-photon calcium (GCaMP6s) imaging of hundreds of cells within areas V1, LM and PM, I have characterized eye-specific functional segregation, much like in V1. I have also examined spatiotemporal frequency tuning and characterized preferred speeds to relate eye-dominant populations from V1 to those in higher visual areas. Targeted AAV-Syn-GCaMP6s injections into binocular V1 were used to image V1 projections to areas LM and PM and examine if the cortico-cortical projections reveal distinct routing of information related to separate eye-dominant populations.

-This work is funded by a NSF GRFP fellowship. Manuscript is in preparation

Effects of juvenile monocular deprivation on higher visual areas

-Research Advisor: Sunil Gandhi, Ph.D.

-The goal is to examine the effects of juvenile two-week monocular deprivation on eye-specific population response properties in higher visual areas LM and PM.

-This work is funded by a NSF GRFP fellowship. Manuscript is in preparation.

Pro-inflammatory expression enhanced in the arctic mouse model for Alzheimer's Disease

-Research Advisor: Andrea Tenner, Ph.D.

-Deletion of C5aR expression in the arctic mouse model for Alzheimer's Disease had previously been shown to exhibit a trend for prevention of behavioral deficits, with no apparent differences in number of plaques or microglia. As an entering rotation student, my goal was to assess the pro-inflammatory expression of the Arctic mouse model was different than those that lack C5aR. I developed experience isolating and sorting cortical primary microglia and macrophages and used quantitative PCR to assess the expression of pro-inflammatory cytokines TNFa, IL1b and IL6.

-An NIH IMSD Grant funded this work

Stanford University, 2013

Role of prostaglandin E2 receptors in microglial inflammatory response to oligomeric alpha synuclein

-Research Advisor: Katrin Andreasson, Ph.D.

-Assessed the proinflammatory response to oligomeric alpha synuclein and examined the EP2 and EP4 agonists as potential therapeutics in alleviating this pro-inflammatory response using BV-2 and primary microglial cell cultures

-Amgen funded this work

University of Texas at San Antonio

Transient extracellular application of nanostars increase hippocampal neuronal activity

-Research Advisor: Fidel Santamaria, Ph.D.

-Gold nanostars created in the lab were shown to be particularly useful for photothermal ablation, serving as a potential therapeutic for selective ablation of tissue. The question of how gold nanostars may alter neuronal function was called into question, given that nanoparticles have been shown to bind to proteins. We recorded hippocampal neuronal activity of dissected mouse brain slices and discovered that gold nanostars enhanced firing of hippocampal CA3 cells.

-This work was funded by NIH/NIGMS MARC U*STAR and MBRS-RISE fellowships

FELLOWSHIPS

-National Science Foundation Graduate Research Fellowship, 2015-2019

-Graduate Dean's Recruitment Fellowship, UC Irvine, 2014

-Eugene Cota Robles Fellowship, UC Irvine, 2014

-NIH IMSD Fellowship, UC Irvine, 2014

-Amgen Scholar, Stanford, 2013

-NIH/NIGMS MARC U*STAR Scholar, UT San Antonio, 2011-2013

-NIH MBRS-RISE Scholar, UT San Antonio, 2011

PUBLICATIONS

Salinas, K.J., Velez, D.X.F, Zeitoun, J.H., Kim H., Gandhi, S.P. (2017). Contralateral bias of high spatial frequency tuning and cardinal direction selectivity in mouse visual cortex. *Journal of Neuroscience,* 37(42), 10125-10138.

Pradhan, S.S., **Salinas, K.**, Garduno, A.C., Johansson, J.U., Wang, Q., Manning-Bog, A., Andreasson, K.I. (2017). Anti-inflammatory and neuroprotective effects of PGE2-EP4

Signaling in Models of Parkinson's Disease. *Journal of Neuroimmune Pharmacology,* 12(2), 292-304.

Salinas, K., Kereselidze, Z., De Luna, F., Peralta, X.G., Santamaria, F. (2014). Transient extracellular application of nanostars increase hippocampal neuronal activity. *Journal of Nanobiotechnology*, 12(1), 31.

PREPRINTS

Huh, C.Y.L., Abdelaal K., **Salinas, K.J.**, Gu, D., Zeitoun, J., Velez, D.X.F., Peach, J.P., Fowlkes, C.C., Gandhi, S.P. (2017). Critical-Period Visual Deprivation Disrupts Binocular Integration but Spares Spatial Acuity in the Geniculocortical Pathway. bioRxiv 48774; doi:https://doi.org/10.1101/48774 (In Submission)

TEACHING EXPERIENCE

University of California, Irvine

-Neurobiology (N110) Course Teaching Assistant, Department of Biosciences, 2018

-Neurobiology and Behavior Lab (N113) Teaching Assistant, Department of Neurobiology and Behavior, 2016, 2017

-Biology (BIO93) Course Teaching Assistant, Department of Biosciences, 2016

PRESENTATIONS

-Society for Neuroscience Poster, San Diego, CA, 2017
-UC Irvine annual Neuroblitz, 2014-2017
-Minority Science Program Symposium, 2014, UC Irvine
-MARC/RISE Graduation Symposium, 2013
-Society for Neuroscience Poster, San Diego, CA, 2013
-Society for the Advancement of Chicanos and Native Americans in Science (SACNAS) Poster, San Antonio, Texas, 2013
-Research Centers in Minority Institutions (RCMI) Symposium Poster, San Juan, Puerto Rico, 2012
-Stanford Summer Research Program Symposium, 2013
-College of Sciences Research Conference, 2012, San Antonio, Texas

ABSTRACT OF THE DISSERTATION

Functional segregation of eye-specific visual pathways into higher visual cortex

By

Kirstie Jay Salinas

Doctor of Philosophy in Biological Sciences

University of California, Irvine, 2019

Professor Sunil P Gandhi Irvine, Chair

The brain is able to construct a visual representation of the world by parallel processing of cortical neurons that prefer increasingly complex stimuli. One way the visual cortex has accomplished parallel processing is by creating functionally organized modules that are tuned to unique features and linking them in multiple processing stages of cortex. For example, primary visual cortex (V1) sends functionally distinct information to higher visual areas (HVAs), which are more specialized in their processing of spatiotemporal information. Inherently coupled to this process is the convergence of eye-specific inputs in visual cortex. Shifting the eye-specific tuning of neurons in primary visual cortex by monocular deprivation in early life is known to disrupt tuning for spatial frequency in adulthood. Combining space and time better characterizes the segregation of HVAs. To begin to understand if eye-specific responses could be linked to tuning properties important for the segregation of HVAs, we characterized eye-specific spatiotemporal tuning of layer 2/3 excitatory cells within the binocular zone of V1 and two HVAs grouped into the putative ventral and dorsal streams, LM and PM, using two-photon GCaMP6s imaging of awake mice. An asymmetry was found at the level of V1, such that responses driven

primarily by the contralateral eye were biased towards high spatial frequencies, low speeds, cardinal directions, and were more direction selective than binocular or ipsilateral eye-driven responses. Eye-specific inputs in V1 are tuned to different speeds and also have different degrees of speed tuning, where contralateral eye inputs are more speed tuned than ipsilateral eye inputs. The proportions of eye-specific neurons of LM and PM matched the expected preferences based on eye-specific spatial frequency tuning found at the level of V1. A similar contralateral bias for distinct features, most notably, spatiotemporal tuning, was found within LM and PM, linking neurons with similar eye-specific preferences to their tuning for early feature detectors important for stream specialization. To determine if V1 sends eye-specific functionally distinct information to HVAs, we injected AAV-Syn-GCaMP6s into the binocular zone of V1 and imaged the afferents that targeted either LM or PM. We found that V1 afferents to LM and PM were distinct in their distributions for ocular dominance, suggesting that eye-specific projections from V1 to HVAs contribute to their functional specificity. To determine if the functional specialization of HVAs depend upon eye-specific developmental mechanisms, we deprived mice of visual experience through the contralateral eye (CMD) during the ocular dominance critical period and assessed eye-specific spatiotemporal tuning of V1, LM and PM in adulthood. We found that CMD diminished the functional specificity of V1, LM and PM, resulting in areas without differentiated spatiotemporal preferences. Moreover, the eye-specific functional segregation was also disrupted with CMD. Altogether, our data demonstrates that the maturation of higher visual areas is dependent on proper binocular visual experience and suggests that the functional specialization of eye-specific responses could be an efficient routing mechanism to differentiate higher visual areas.

CHAPTER 1: INTRODUCTION

Overview:

A fundamental goal of neuroscience is to understand how the brain is able to construct an internal representation of an external world. A model of hierarchical parallel organization has played a fundamental role in understanding how the visual system is able to accomplish such a feat. The model suggests that neurons in each stage filter and distribute information related to form, color, orientation/direction and spatial/temporal frequency to higher visual areas suited for more complex visual representations (Zeki, 1978; Mishkin et al., 1983; Van Essen et al., 1992). A common facet to all mammalian species is the simultaneous process of combining inputs from the two eyes. In primates, primary visual cortex has long been attributed as the first site where inputs from the two eyes converge (Hubel and Wiesel 1959; Hubel and Wiesel 1962; Hubel and Wiesel 1969; but see Howarth et al., 2014; Jaepel et al., 2017; Zeater et al., 2015). Hubel and Wiesel, who first demonstrated the columnar organization of eye-specific responses in primary visual cortex (V1) in primates, established a relationship between eye-specificity, which they termed "ocular dominance," and orientation when they discovered that maps (neighboring neurons with similar feature preferences) for orientation and ocular dominance are orthogonal with similar periodicities (Hubel and Wiesel 1974a, 1978). More recently, it has been demonstrated that the maps for spatial frequency, ocular dominance and orientation tuning are aligned in primate V1 (Nauhaus et al., 2016). Particularly, maps for spatial frequency run parallel to eye-specific maps: binocular neurons are high spatial frequency tuned and monocular neurons are low spatial frequency tuned. Consequently, the columnar organization of eye-specificity is intrinsically linked to early encoding for stimulus features

in visual cortex. However, the extent by which eye-specific developmental mechanisms play a role in shaping hierarchical processing remains unknown. Examining the association between eye-specificity and early feature detection will enable a better understanding of how the visual system is wired during development, how visual information may be transformed downstream, and the potential impact of this organization on developmental disorders of visual impairment, particularly amblyopia. We propose that ocularity is intrinsically linked to spatiotemporal selectivity in the mouse, as it is in primates, and that the asymmetry of the spatiotemporal tuning of eye-specific responses may sculpt higher visual area selectivity.

In Chapter 1, I will briefly discuss the background literature for the study, emphasizing the premise behind the hypothesis of the thesis, which is to relate eye-specific organization with parallel stream processing. The relevant background will be divided in three main sections. First, I will discuss the classical model for hierarchical organization of visual cortex, relating to parallel stream processing and, when applicable, eye-specificity. Our current understanding of this framework is largely based on experiments from primates and carnivores. The second section will focus on species relevance, where I introduce the mouse visual system, the current knowledge of mouse higher visual areas and the putative dorsal-ventral stream subnetworks for mice. I would like to point out similarities/differences between primates, our working model for understanding the development of human vision, and mice, as well as the advantages and limitations of using mice to study visual system processing. The third section will focus on visual cortical plasticity and development, as it relates to ocular dominance and other important early features linked to parallel stream specialization.

In Chapter 2, I will describe a study where we demonstrate that primary visual cortex contains eye-specific visual responses with distinct spatial frequency and direction preferences. The findings suggest that ocularity and spatial frequency tuning may be coupled in mouse, and that the functional specificity of eye-specific responses at the level of V1 may encompass distinct channels of information for downstream parallel processing.

In Chapter 3, I extend the findings from V1 to two higher visual areas: LM and PM, grouped into the putative ventral and dorsal stream. I will demonstrate that the functional specificity of eye-specific responses is not restricted to V1, but is found at higher levels of cortex. Moreover, I will further demonstrate that eye-specific tuning may be coupled to orientation and direction selectivity. The findings of these experiments suggest that eye-specific responses may be instrumental in determining the functional specificity of higher visual areas. I will also describe experiments where we characterized the functional specificity of V1 afferents to areas LM and PM. I will demonstrate that these afferents carry information related to both ocularity and spatial frequency, which match the preferences of the target areas. These findings suggest that V1 output specificity may play an active role in the tuning of the cells within higher visual areas.

In Chapter 4, I will describe a set of experiments where we visually deprived mice through either the contralateral or ipsilateral eye for two weeks during the ocular dominance critical period and assessed the spatiotemporal tuning of V1, LM and PM. I will demonstrate that contralateral eye deprivation leads to a de-differentiation of higher visual areas. The deprivation also impacts the functional specificity of eye-specific responses. I will conclude that the specialization of higher visual areas depends upon proper binocular

visual experience, and that eye-specific response properties are required for the establishment of higher visual area selectivity.

In Chapter 5, I will summarize the findings of the dissertation and provide concluding remarks on the studies. I will also provide ideas for future studies that will deepen our understanding and the impact of the findings.

1.1: Hierarchical Organization

There are two routes of visual information flow from retina to cortex: the retinogeniculate and extrageniculate pathway. In the retinogeniculate path, widely described as the central visual pathway, information from the retina is relayed to cells of the lateral geniculate nucleus (LGN), which in turn project to primary visual cortex (V1), or the first cortical processing stage in this circuit. In the extrageniculate path, retinal information is relayed to the superior colliculus and pulvinar before projecting to visual cortex. For primates, the central visual pathway is the predominant route by which information from the two eyes reach visual cortex (Perry et al., 1984). Consequently, the central visual pathway has been extensively studied to understand visual processing in non-human primates, carnivores, and mice alike. Much of our understanding about the transformation of simple spatiotemporal attributes within distinct stream processing pathways (Figure 1) stems from studies on the retinogeniculate pathway. The extrageniculate pathway has received less attention since the superior colliculus receives a minority of RGC innervation in primates, but it does seem to play a role in processing movements (Dec et al., 1978; Liu et al., 2011). V1 cells send their afferents to many higher

visual areas of cortex, who further project to even higher levels and eventually association areas (Mishkin and Ungerleider, 1982).

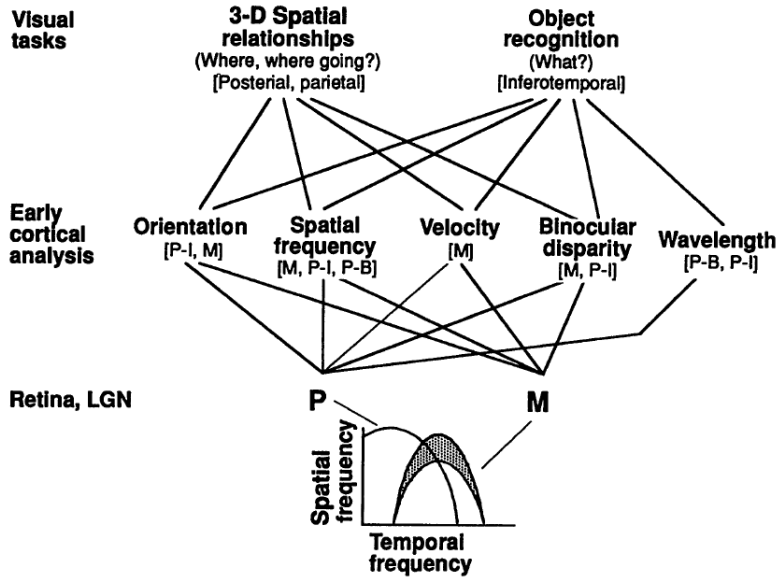

Figure 1.1: Hierarchical model of the visual system. M and P pathways of the primate originating in the retina convey distinct spatiotemporal properties. These diverging and converging pathways can be traced into distinct lamina of LGN and V1, known as the magnocellular layers and parvocellular layers. Further transformations of early features are used to construct more complex receptive fields in higher visual areas. Higher visual areas are important for two broad classes of visual processing: the dorsal stream in visuospatial analysis and the ventral stream in the object recognition. From Van Essen, David C., Charles H. Anderson, and Daniel J. Felleman. "Information processing in the primate visual system: an integrated systems perspective." *Science* 255.5043 (1992): 419-423. Reprinted with permission from AAAS.

Hubel and Wiesel were the first to describe the hierarchical nature of the visual system when they postulated that a feed forward circuit arising from the convergence of LGN inputs could construct the receptive fields of simple cells in primary visual cortex, and the convergence of simple cell inputs could in turn form the receptive fields of complex cells (Hubel and Wiesel 1962, 1965b). Hierarchical organization has since been described for multiple modalities and can be generalized as any network in which well defined levels, or transformations of information, exist. The mammalian cerebral cortex is hierarchically organized and processes information in parallel streams (Felleman and Van Essen, 1991).

Numerous anatomical and physiological studies have demonstrated that these streams begin in the retina (Leventhal et al., 1981; Perry et al., 1984; Schiller et al., 1977; reviewed in Wässle 2004), flow through subcortical regions (Rezak and Benevento, 1979; Ungerleider et al., 1984; Adams et al., 2000), striate and extrastriate cortex (Blasdel and Lund, 1983; Hubel and Livingstone, 1987) and finally to distinct areas of parietal and temporal cortex (Mishkin et al., 1983). The higher visual areas of parietal and temporal cortex are thought to process distinct types of visual information, one suitable for spatial navigation (dorsal stream) and one for object identification (ventral stream), respectively (Mishkin et al., 1983). Similar to the construction of simple cells from the convergence of LGN inputs, the selectivity of higher visual areas are presumed to be based upon convergence from lower levels of cortex specialized for distinct visual stimuli.

Already at the first level of light detection, functional segregation exists in the form of rods and cones in the retina. The rods endow scotopic vision, or the ability to see under dim lights while the cones endow photopic vision and enable the perception of color. Anatomical and physiological evidence suggests that there is functional segregation in the output of the retina (the ganglion cells) and that segregation is largely maintained in the LGN, termed the magnocellular (M) and parvocellular (P) pathways (Conley and Fitzpatrick 1989; Purpura et al., 1990; Schiller and Malpeli 1978; Gouras 1969; Kaplan and Shapley 1982). In primates, these retinal ganglion cells are physiologically distinct and differentially distributed in the retina, such that the alpha cells (M pathway, related to Y cells) are concentrated in the periphery and the beta cells (P pathway, related to X cells) are concentrated in the central retina (Gouras 1969). The alpha cells are more transient in their response and are broadband, encoding information about luminance contrast, while

the beta cells have sustained responses, are optimized for higher temporal frequencies, and are color-opponent (Leventhal et al., 1981; Perry et al., 1984). There is partial overlap in the spatiotemporal information that these cells filter, but in general, the P cells are broadly tuned to spatial frequencies and respond to low and moderate temporal frequencies while the M cells have poor resolution (Figure 1, Van Essen et al., 1992).

The cells in the M and P pathway have physiological distinctions in conduction velocity, contrast sensitivity and color sensitivity (Gouras 1969; Kaplan and Shapley 1982; Schiller and Malpeli 1978; Purpura et al., 1988; Sclar et al., 1990; Shapley et al., 1981; Derrington and Lennie 1984). Most relevant to the current study are differences in sensitivities to temporal and spatial frequencies. The cells of the M pathway (parasol ganglion cells) have higher mean preferred temporal frequency and lower preferred spatial frequency than cells of the P pathway (midget ganglion cells), although overlap of cell preferences exists (Derrington and Lennie, 1984; Hicks et al., 1983). However, there appears to be no difference in spatial resolution or receptive field size between the cell types (Blakemore and Vital-Durand 1986; Crook et al., 1988; Derrington and Lennie 1984). The specialization of the M and P pathways for distinct spatiotemporal tuning has been substantiated by lesion studies (Merigan et al., 1991; Merigan and Eskin, 1986). Anatomical evidence suggests that a potential reason the P pathway is important for detecting high spatial frequency stimuli is due to the high sampling density of retinal P ganglion cells compared to those of the retinal M ganglion cells (Merigan and Katz 1990; Perry et al., 1984; Silveira and Perry 1991).

A third parallel pathway, the koniocellular (K) pathway, has been described for primates (Hendry and Reid, 2000). K cells are also organized in layers of macaque LGN,

which are dominated by input from either retina (Yoshioka and Hendry 1999). These cells have been linked to the cat's W cells, due to their response to S-cone stimulation (Norton and Casagrande, 1982). K cells of the LGN vary broadly in spatiotemporal tuning and the population may consist of multiple subclasses (Norton et al., 1988; Xu et al., 2001). K cells have been thought to contribute to color vision due to the input they receive from S-cones and their innervation of cytochrome oxidase stained blobs in V1 (Hendry and Reid, 2000).

Up the hierarchy, the M, P and K pathways innervate distinct regions of V1 and V2. The segregation is mostly maintained in V1, with projections from the parvocellular and magnocellular layers terminating in distinct subregions of layer 4 (parvocellular connects with Layer 4Ca and magnocellular with Layer 4CB) (Fitzpatrick et al., 1985). The distinct regions of V1 further innervate distinct regions of V2 and beyond (reviewed in Livingstone and Hubel 1987). In the magno pathway, the thick stripes of V2 innervate MT and in the parvo pathway, the interblobs project to the pale stripes of V2. The K pathway makes the third subdivision, projecting to the blobs and then thin stripes of V2. The different pathways are proposed to connect to higher visual areas specialized for more complex visual processing.

1.1.1: Columnar Organization

A cortical column is a group of cells in the cortex that share a preference for one type of visual stimulus. Cortical columns share feature preferences regardless of which layer the cell is in. The retinotopic map of the visual field is a fundamental columnar organization that is repeated throughout the visual cortex in different layers (Talbot and Marshall, 1941; Daniel and Whitteridge, 1961). A congruent alignment of feature maps

overlaid on the retinotopic map permit feature detection in all regions of the visual field and, in the case of higher areas where retinotopic remapping occurs, in a hierarchical fashion. Hubel and Wiesel demonstrated that neurons with eye-specific responses form a columnar organization, termed ocular dominance columns (ODCs), in V1 of both cat and monkey (Hubel and Wiesel 1965a, 1969). Later, they related ODCs to the columnar organization of orientation preference (Hubel and Wiesel, 1974a). In their discussion on the orthogonal relationship between the two maps, they comment on the advantages of repeating functional modules for all parts of the visual field, stating:

"*The tasks that a given region of cortex must fulfill are many and varied and include the machinery for establishing orientation specificity, direction selectivity, degree of complexity, selectivity to color, and binocular convergence, all for a particular region of visual field. It may be that there is a great developmental advantage in designing such a machinery once only, and repeating it over and over monotonously, like a crystal, for all parts of the visual field. The problem is to achieve the uniformity despite the great difference in detail of representation between central and peripheral visual fields." – Hubel and Wiesel 1974a*

Hence, in V1 of primates, in a given region of visual space, each orientation is represented for both eyes, and this pattern is repeated, like a crystal, for other regions of visual space. One way by which the visual system could solve the issue of encoding stimulus features despite differences in the central and peripheral visual fields is by having neurons representing the central visual field with similar receptive field properties as those in the "monocular" region of V1. The functional organization of orientation and ocular dominance established by Hubel and Wiesel has been extended to maps of other features. Using intrinsic signal imaging, Bartfeld and Grinvald revealed the alignment of

maps for orientation preference pinwheels and ODCs as well as maps for cytochrome oxidase stained blobs/interblobs and pinwheels (Bartfeld and Grinvald, 1992). The cytochrome oxidase stained blob/interblobs (Horton and Hubel 1981), convey information of spatial frequency (Tootell et al., 1988) and color (Livingstone and Hubel, 1984). Interestingly, blobs, which are specialized for color detection, fall within monocular zones and the interblobs tend to be binocular (Livingstone and Hubel, 1984).

The alignment between the three phase maps for ocular dominance, spatial frequency and orientation have been described using two-photon calcium imaging of macaque V1 (Nauhaus et al., 2016). Interestingly, the maps of ocular dominance and spatial frequency align such that areas of cortex with preferences for high spatial frequency coinciding with binocular regions. A direct link between eye-specificity and spatial frequency has thus been demonstrated in non-human primates. This raises the question of how these phase maps are aligned during development. Does visual experience and binocular competition play a role in the organization of these phase maps?

Is the same columnar organization found in higher visual areas? It appears that area V2 in macaque also contains orthogonal maps for ocularity and orientation. The columnar organization of V2 also follows a similar periodicity as that of V1, ~1mm (Ts'o et al., 2009). Reports of similar patterns for feature preferences such as orientation, direction and disparity, have been described for higher visual area MT (DeAngelis and Newsome, 1999; Malonek et al., 1999). What are the implications of repeating functional modules in higher levels of cortex? It may be that the alignments of cortical columns are a strategy to improve coding efficiency (Nauhaus et al., 2016). What drives the precise architecture of cortex

during development? How might altering one of the feature maps perturb others? Would the effects of this change be restrictive or expand downstream?

1.1.2: Areal Organization

The visual cortex of humans and primates is highly evolved, comprising multiple representations of the visual field. These "extra" representations of the visual field are thought to offer a new perspective of the visual field, one that is more relevant for understanding the outside world than a series of oriented lines. Subcortically, the levels of the visual processing hierarchy are intuitive to parse out, with a clear starting point (retina) and obvious white matter tracts innervating thalamus and eventually cortex. However, the delineation of higher visual areas and where they sit in the visual hierarchy is not so intuitive. Historically, the identification of visual cortical areas has been based on the combination of three techniques: connectivity analysis, architectonics and topography (Felleman and Van Essen 1991). Connectivity analysis refers to the tracing of the inputs and outputs of an area. When a visual area sends dense projections to a second area we infer that it is closely tied to that area. Felleman and Van Essen used the connectivity patterns, specifically the laminar projections, to determine if areas were sending feed forward information (terminate in layer 4) or feedback information (terminate in superficial and deep layers) and to order areas in a cortical hierarchy. Architectonics describes the morphology of areas using various staining techniques. One useful architectonic method to delineate V1 from higher areas, in particular, is to locate the callosal projections in visual cortex, since primary visual cortex will be largely devoid of such projections (Zeki et al., 1978; Olavarria and Montero, 1989; Wang et al., 2007b).

Finally, visual areas may be delineated based on topographic organization. A visual area should have an orderly map of the visual field, and can the phase reversals of the retinotopic map may be used to designate boundaries if we require a visual area not represent a redundant region of visual space (Garrett et al., 2014). However, and as is the case for visual areas that fall at higher levels of the hierarchy, retinotopic organization can become coarse or irregular, but one would assume this is the case if the area is making higher level computations of the visual field.

The different visual areas have been grouped into parallel pathways that connect to distinct brain regions and process, concurrently, distinct types of visual information (Merigan and Maunsell, 1993; Mishkin et al., 1983). The magnocellular pathway is accredited with motion analysis, depth perception and figure-ground separation while the parvocellular pathway is believed to be important for form, color and pattern discrimination (Livingston and Hubel, 1987). Areas grouped in the dorsal and ventral streams have distinct preferences for early features. For example, direction selectivity is important for the processing of motion, a task attributed to the dorsal pathway, while orientation selectivity is important for form processing, a ventral stream task. As discussed previously, preferences for orientation and direction are mapped on the cortical surface in a columnar organization, a process that seems to be independent of visual experience.

Many lesion studies in primates have demonstrated that higher visual areas are required to perform distinct complex visual processing tasks (Klüver and Bucy, 1937; Mishkin et al., 1983; Mishkin and Ungerleider, 1982; Newsome and Pare, 1988; Maunsell and Newsome 1987). The importance of understanding the function of the multitude of higher visual areas arises from the mismatch between visually evoked activity in V1 and

behavioral readouts (Kiorpes, 2016). With over 30 visual areas described in the macaque, unraveling the function of all of these areas could take quite some time. Perhaps a step towards understanding the function of an area is to understand the general principles of how visual information is organized, combined, distributed and used to generate more complex receptive fields. Using simple features as stimuli while recording from different areas and/or inactivating distinct levels of the cortex helps with this process. Much progress has been made in understanding how cortical transformations occur in the visual hierarchy and in relating early feature detection to more complex visual processing (Maunsell and Newsome, 1987; Movshon and Newsome, 1996).

The validity of the simplistic dorsal-ventral stream segregation has been called into question due to the large crosstalk between areas designated in separate streams (Felleman and Van Essen 1991) as well as neurophysiological (Malpeli et al., 1981; Ferrera et al., 1992) and behavioral evidence (Schiller et al., 1990) that contradicts strict functional segregation. An approach that emphasizes cell-type specific connectivity over laminar, and perhaps even areal, connectivity seems to resolve the concerns of crosstalk while preserving fundamental ideas taken from the hierarchical model (Nassi and Callaway, 2009). Thus, an understanding of cell-type specific connectivity between layers/areas/columns could be informative for resolving the significance of dorsal vs. ventral stream processing and the machinery used to compute different visual perceptions.

1.2 Species relevance: Organization of Mouse Visual Cortex

Much of our understanding of vision stems from studies conducted on humans, non-human primates and cats. However, the mouse is emerging as a prominent model organism

for understanding the underlying circuitry involved in visual processing and plasticity, due to the amount of available tools we can use to dissect neural circuitry in vivo. Novel techniques in neuroimaging and neuroanatomy make it possible to reveal detailed organization of the mouse visual system (Callaway and Luo 2015; Osakada et al., 2011). The current technological advances of genetic tools available in the mouse allow one to reveal cell-type specific circuitry and its relation to anatomy and physiology. Revealing what the mouse visual system can tell us about human visual processing is becoming increasingly valuable. The relatively easy access to the entire visual cortex and surrounding areas makes studying mouse vision highly attractive. Mice, like primates, have multiple visual areas which can be grouped into a hierarchical framework and putative parallel streams (Wang and Burkhalter 2007a; Marshel et al., 2011; Berezovskii et al., 2011; Wang et al., 2011; Wang et al., 2012; D'Souza et al., 2016). Undoubtedly, the mouse visual system has evolved to benefit the mouse in its own ecological niche. Consequently, expecting the mouse visual system to behave as a miniature primate visual system is impractical. Despite the multitude of dissimilarities between mice and primates, there are some fundamental resemblances, and the feasibility of studying mouse visual cortex allow researchers to discover detailed levels of understanding the underlying circuitry and potentially formulate hypotheses about human visual processing.

1.2.1 General Architecture of the Mouse Visual System

Mouse retinal organization is somewhat similar to that of the primate retina, at least in the peripheral retina. Rods outnumber cones in mice, as they do in humans and non-human primates. Mice have a functional cone system endowing them with color vision,

with photoreceptors sensitive to short (centered at 360nm, or ultraviolet) and medium (centered at 510nm, or green) wavelengths of light (Calderone and Jacobs 1995). The mouse retina contains a gradient of sensitivity to different opsins, which endow them with specialization for coding color in the lower vs. upper visual field (Applebury et al., 2000; Baden et al., 2013; Haverkamp et al., 2005; Szel and Rohlick 1992). This is recapitulated in V1 and higher visual areas of cortex (Rhim et al., 2017). Despite being afoveate, mice are not blind, and are able to perform complex visual tasks. Interestingly, the densest retinal ganglion cell (RGC) type, the output neurons of the retina, (called "W3") in mouse retina is sensitive to dark, small moving objects and has been hypothesized to be sensitive to predators in the sky (Zhang et al., 2012). Interestingly, this RGC type exists predominantly in the ventral retina where the cones prefer dark contrasts (Baden et al., 2013). The presence of many different retinal ganglion cell types and densities is a shared property of mice and primates alike.

Retinal ganglion cell types innervate different regions of the thalamus, often projecting to distinct laminar zones (Ecker et al., 2010; Huberman et al., 2008, 2009; Kay et al., 2011; Kim et al., 2008; Rivlin-Etzion et al., 2011; reviewed in Seabrook et al., 2017, Figure 2). Notably, on-off direction selective ganglion cells innervate the shell of the LGN while non-direction selective alpha RGCs innervates the core (Bickford et al., 2015; Cruz-Martin et al., 2014; Krahe et al., 2011; Seabrook et al., 2017). The outputs of the two eyes also innervate different regions of the thalamus, with the ipsilateral RGCs projecting to the core region of LGN. While there is a clear demarcation within the retina of RGCs that project to the contralateral or ipsilateral eye in primates, there is no such distinction in mice (Seabrook et al., 2017). Instead, uncrossed RGCs are overlaid on crossed RGCs, which

outnumber them greatly (only about 5% of ipsilateral projecting RGCs (Dräger and Olsen 1980)). However, the core and the shell of the LGN have distinct cell types that can be related to those of cat and primate: the X and Y-like cells are densest in the core while the W-like cells are distributed in the shell (Krahe et al., 2011).

The cells of the shell and the core region of LGN terminate in segregated layers of V1 (Figure 2, reviewed in Seabrook et al., 2017). Cells of the shell region are tuned to both orientation and direction and innervate the superficial layers of V1, while cells of the core region innervate the deeper layers (Bickford et al., 2015; Cruz-Martin et al., 2014; Kondo and Ohki 2016; Piscopo et al., 2013; Lien and Scanziani 2013; Seabrook et al., 2017). These parallel pathways may route information into distinct processing streams, akin to primates. Thus, the mouse visual system has a functional architecture that includes morphologically distinct retinal ganglion cells, regionally distributed thalamic cells and some functional segregation into the cortex, akin to the general structural properties of cats and primates.

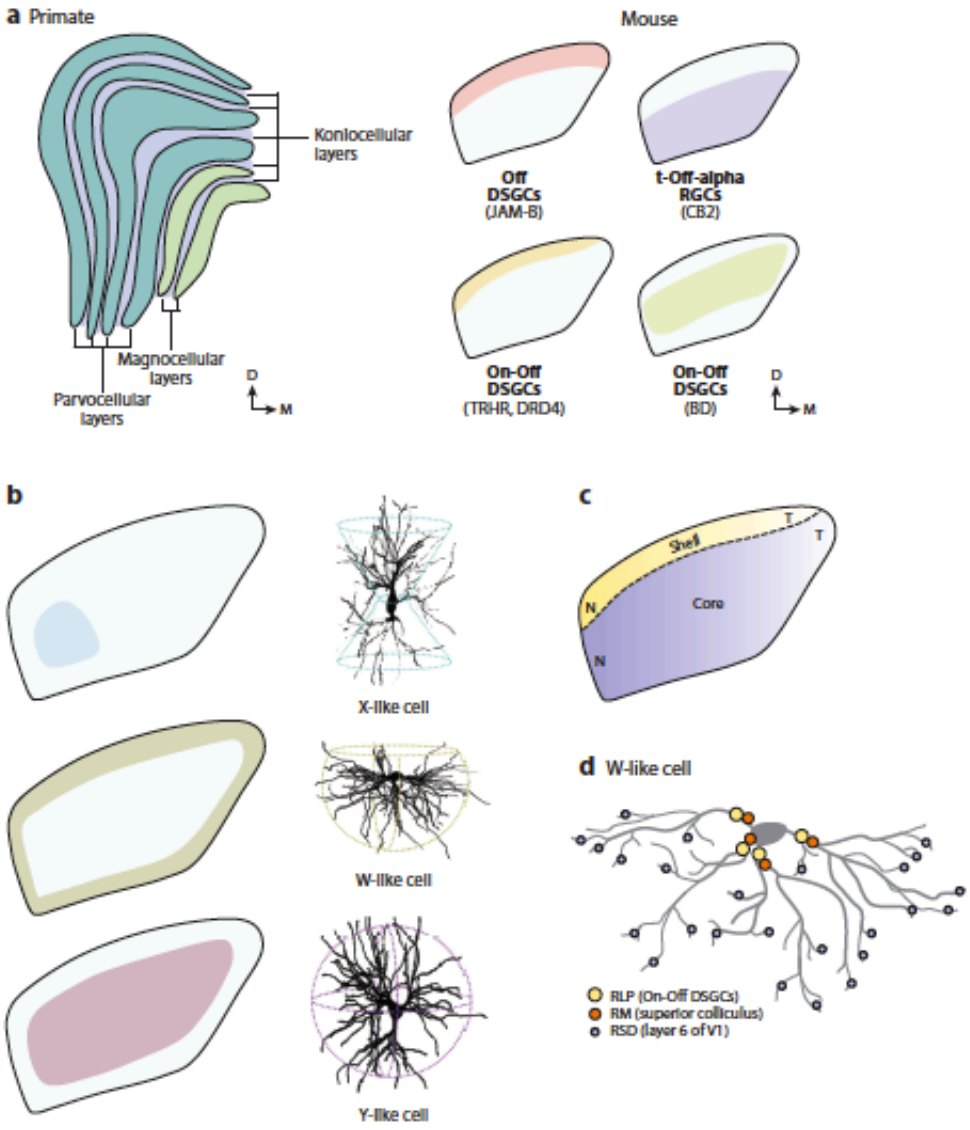

Figure 1.2: Schematic of mouse retinal ganglion cells and their connectivity patterns with thalamus. A. Left: Primate LGN with segregation of M and P pathways, each layer also received input form one eye. Right: Distinct retinal ganglion cells innervate different regions of mouse LGN. B. Mouse LGN contains cells that are X-like, Y-like and W-like, as in other higher mammals. These cells innervate different parts of the thalamus preferentially. C. Separation of core and shell, which contain distinct cell types. Y and X-like cells are found in the core while W-like cells are found in the shell. From Seabrook, Tania A., et al. "Architecture, function, and assembly of the mouse visual system." *Annual review of neuroscience* 40 (2017): 499-538.

As mentioned previously, the superior colliculus (SC) is an alternate route for RGCs in the mammalian visual system. The SC is especially important for head and eye movements (Wurtz and Goldberg 1972; Harris 1980). While in primates only 10% of the RGCs project to the SC (Perry and Cowey 1984), almost all (90%) of mouse RGCs have

terminations in the SC (Ellis et al., 2016). Like the LGN, the SC is retinotopically organized and contains eye-specific segregation (Mrsic-Flogel et al., 2005; Dräger and Hubel 1975, 1976). Interestingly, the SC projects to the outer shell of the dLGN (Bickford et al., 2015; Harting et al., 1991), a region which is known to contain cells that are highly direction selective and dominated by input from the contralateral eye, as well as to the lateral posterior nucleus (LP), the pulvinar equivalent for mice. The LP is connected bidirectionally to higher visual areas (Hughes 1977; Herkenham, 1980). The density of RGC projections to SC vs. LGN in mice (90% vs. 30-40% (Martin, 1986)), suggests that the extrageniculate pathway may be a prominently important system for the mouse that the non-human primate system has replaced with a more elaborate retinogeniculate system. The LP system thus remains a caveat in our use of mouse visual cortex as a working model for classical hierarchical organization, especially considering that inactivating V1 does not alter the spatiotemporal tuning of HVAs while inactivating SC does (Tohmi et al., 2014). Moreover, the weaker projection from the SC to the dLGN has also been demonstrated to modulate responses in V1, in a manner that is independent of LP (Ahmadlou et al., 2018). However, similar loss of function of some HVAs has been reported with SC inactivation in cats (Lomber et al., 2002; Ogino and Ohtsuka 2000; Dean and Redgrave, 1984a,b) as well as in primates, albeit less robustly (Bruce et al., 1986; Rodman et al., 1990). Thus, the extrageniculate system in any species tests the validity of the canonical classical hierarchical framework of the central visual pathway; especially considering that V1 inactivation does not alter higher visual area MT activity in macaque (Girard et al., 1992; Rodman et al., 1989). In addition to its suggested role in “blindsight” (Brindley et al., 1969;

Pasik and Pasik 1971), the extrageniculate path has been proposed to provide context and modulate visual processing (Dean and Redgrave, 1984b; Roth et al., 2016).

The complexity of the mouse visual system has recently been revealed, first with triple anterograde tracing (Wang and Burkhalter, 2007), and later established with functional imaging of retinotopic maps (Garrett et al., 2014; Wekselblatt et al., 2016; Zhuang et al., 2017). Complex visually guided behaviors have also been demonstrated, calling to question how rudimentary the mouse visual system really is (Andermann et al., 2010; Hoy et al., 2016; Poort et al., 2015; Prusky et al., 2000). Recent evidence suggests parallel stream organization in the mouse, akin to humans and primates, with some visual areas projecting more densely to ventral regions, and some visual areas projecting more densely to dorsal regions of the brains (Wang et al., 2011; Wang et al., 2012).

1.2.2 Identifying Extrastriate Areas

Recent efforts to gain an understanding of mouse visual cortex have led to an evolution in the description of areas surrounding V1. As noted previously, retinotopic maps can be used to segregate regions of mouse visual cortex, given the definition that a visual area does not contain a redundant region of visual space. Olavarria and Montero were the first to study the organization of mouse visual cortex using tracer injections into V1 in combination with tracer injections into the contralateral hemisphere as a way to label callosal connections (Olavarria and Montero 1989). They identified 8-9 patches of projections surrounding V1 with the callosal projections serving as landmarks between V1 and surrounding extrastriate cortex. Wang and Burkhalter first presented the widely accepted area map of visual cortex using triple anterograde tracing with different

fluorescent dextrans into V1 (Wang and Burkhalter, 2007). Using this method, in combination with retrograde tracing of bisbenzimide to label callosal connections, ten extrastriate areas were identified and their receptive fields mapped.

Today, the area map of visual cortex can be determined using intrinsic signal optical imaging (Garrett et al., 2014) and widefield calcium imaging (Wekselblatt et al., 2016; Zhuang et al., 2017). Garrett et al., 2014 were the first to present a modification to the mapping technique of Kalatsky and Stryker (Kalatsky and Stryker, 2003), which used a temporally periodic stimulus (drifting bar in azimuth or elevation in each direction) and Fourier analysis of the hemodynamic signal to map retinotopy. The modification of stimulating the mouse's entire contralateral visual field and holding the size of the drifting bar constant at the edges of the monitor generates azimuth and elevation phase maps that may be used to generate borders. A visual field sign map is taken as the sine of the difference in the gradients of the two orthogonal phase maps. Using this technique, similar areas were identified as those by Wang and Burkhalter 2007, with a total of 10 extrastriate areas identified. Zhuang et al., 2017 present an extended retinotopic map, which includes 14 proposed areas. Zhuang et al also confirmed borders obtained by widefield calcium imaging at the cellular level using two-photon calcium imaging. Further, they illustrate nicely how the higher visual areas are biased to certain parts of the visual field, specializing in different subfields. The use of widefield calcium and intrinsic signal optical imaging to obtain maps of higher visual areas, which can then be probed psychometrically, has already greatly facilitated our understanding of the function of higher visual areas (Juavinett et al., 2015; Juavinett et al., 2017; Rhim et al., 2017).

1.2.3 Evidence for Hierarchical Organization

As in primates, information from the retina may reach higher visual areas of mice by two routes. Although the proportion of RGCs that project to the dLGN in mice is far fewer than in primates, primary visual cortex is necessary for visual tasks (Glickfeld et al., 2013b; Marques et al., 2018). In the classical hierarchical model, LGN projects only to the primary visual cortex. However, the LGN of both mice and primates projects to higher visual areas (Benevento and Yoshida, 1981; Bullier and Kennedy, 1983; Fries 1981; Lysakowski et al., 1988). Tracing studies based on laminar projections indicate that rodent visual cortex is hierarchically organized (Coogan and Burkhalter, 1993; Wang and Burkhalter, 2007; Wang et al., 2011). V1 projects to higher visual areas, with the densest projections sent to areas LM, AL, RL, A, AM, PM, LI, P and POR (Wang et al., 2007). The information flow from the retina may also be as follows: superior colliculus to the lateral posterior nucleus to V1 and directly to all higher visual areas.

As visual information is relayed to higher visual areas, receptive fields become larger, magnification factor increases (Espinoza and Thomas, 1983) and fewer neurons are responsive to simple stimuli, such as drifting gratings, preferring more complex visual stimulation (Marshel et al., 2011). In the primate visual cortex, interareal projections either terminate in layer 4 if they are feed forward or superficial and deep layers if they are feedback (Felleman and Van Essen 1991). For the mouse and rodent, feedforward terminations extend all areas but are strongly biased towards layer 2/3 and 4, while feedback terminations are densest in layer 1 and least dense in layer 4 (Coogan and Burkhalter 1993, D'Souza et al., 2016). Recently, D'Souza et al. 2016 examined the laminar projection biases of areas V1, LM and PM using anterograde-tracing techniques. They

injected biotinylated dextranamine (BDA) into each area and measured the density of projections in different layers of seven higher visual areas. By calculating the ratio of the density of terminations in layer 2/3 and 4 to layer 1, with the terminations in layer 2/3 and 4 indicating feedforward projections (or lower to higher level processing) and layer 1 indicating feedback (or higher levels to lower level processing), they were able to assess the relative contribution of each area to other areas in terms of feedforward and feedback processing. Higher layer 2/3 and 4 to layer 1 ratio indicates more feedforward processing, and V1 was the most feedforward processing area of the three, indicating it was at the bottom of the hierarchy between the three. PM was at the top, with the smallest layer 2/3 to layer 4 density ratios. They also found evidence of a scaling down of the inhibition/excitation ratio from the most feedforward to the most feedback.

In an earlier study, Berezovskii et al., 2011 found distinct circuits for feedforward and feedback information by using retrograde and anterograde tracing techniques. They counted the number of double-labeled neurons within LM after injecting a retrograde tracer into AL and an anterograde tracer into V1. Using this approach, approximately 2% of cells were double labeled in LM. This suggests feedforward and feedback pathways in the mouse involve distinct cell-type specific circuits. It has been shown that the functional projections of V1 cells to higher visual areas are target-specific (Glickfeld et al., 2013a). However, feedforward projections of single neurons in mouse visual cortex often target multiple areas at a time, but the likeliness of their connectivity seems to link areas with similar visual tuning properties (Han et al., 2018). Thus, it seems that the there is functionally specific circuits linking different levels of cortex, as expected from the classical hierarchical model.

Unfortunately, despite the extensive knowledge we now have on the regional connectivity of extrastriate cortex, we still do not know the function of many of these higher visual areas. Moreover, there is still uncertainty regarding the types of complex visual processing mice are capable of. Using visual stimuli that are more complex than drifting gratings, others have identified cells that participate in the encoding of global motion of a plaid pattern (Juavinett and Callaway 2015; Muir et al., 2015; Palagina et al., 2017), demonstrating that higher visual areas, and V1, are capable of processing pattern motion. A study on rats also concluded that the lateral extrastriate areas LM, LI and LL might represent an object identification pathway (Tafazoli et al., 2017). Thus, although we don't know the functions of each individual area in mouse extrastriate cortex, evidence suggests that rodents are capable of more complex visual processing tasks than previously appreciated, and thus, warrant probing into the underlying circuitry (Bussey et al., 2001; Vermaerke et al., 2012; Tafazoli et al., 2017; Matteucci et al, 2019; Hoy et al., 2016; Baroncelli et al., 2013).

1.2.4 Evidence for parallel stream processing

Functional and anatomical evidence suggests that mouse visual cortex may be parsed into putative dorsal and ventral streams. Numerous studies have established that the higher visual areas have distinct spatiotemporal frequency selectivity and, in general, are more selective in their responses to drifting gratings than V1 (Marshel et al., 2011; Andermann et al., 2011; Roth et al., 2012). By identifying mean area preferences in spatial frequency, temporal frequency, direction and orientation selectivity, the segregation of areas into dorsal vs. ventral-related areas began to be inferred. Moreover, visual

stimulation propagates through distinct regions of visual cortex in parallel after V1 is activated (Polack and Contreras, 2012). A more recent study examined correlated activity of higher visual areas through development and found two distinct subnetworks whose areas match their anatomical assignments of dorsal and ventral streams (Smith et al., 2017). Analysis of a series of tracing experiments allowed Wang and colleagues to group the higher visual areas into putative dorsal and ventral streams (Wang et al., 2012). In each study, LM is grouped in the ventral stream and PM is grouped in the dorsal stream.

A prominent area grouped into the primate dorsal stream is area MT, the motion responsive area. Early filtering for motion processing is selective for neurons that are sensitive to the direction of a visual stimulus. For example, area MT in macaque contains a high proportion of directionally tuned neurons—much more than primary visual cortex (Movshon and Newsome 1996). Further, in this area exists neurons that respond to global motion, or motion of a complex pattern. Using antidromic stimulation of area MT, Movshon and Newsome found a small number of V1→MT projections that were highly direction selective and responded only to the motion of the components of patterns. This indicates that in the primate cortex, cells from V1 may send functionally specific information to higher area MT, which is important for dorsal stream processing. The same appears to be true also for mice (Glickfeld et al., 2013). Whether cells involved in one stream processing are unique to those involved in another remains elusive. The output of V1 is functionally specific to the target regions in terms of spatiotemporal selectivity and cells linked to different target areas with distinct spatiotemporal selectivity appear to be distinct from another (Kim et al., 2017).

1.2.5 Area LM: Mouse V2?

Area LM has been described as mouse V2 because it shares the vertical meridian with V1 and V1 sends its densest projections to LM (Wang et al., 2012). LM is the largest of the extrastriate areas, sitting adjacent to V1 on the lateral side, adjacent to two areas grouped into the putative ventral stream, LI and LL. Due to its bias for the upper nasal visual field (Zhuang et al, 2017), LM is a good candidate to understand the transformations of binocular cells along the cortical hierarchy. Perhaps depending on the state of the animal and stimuli shown, LM may have a similar mean spatial frequency tuning as V1 or slightly lower (Glickfeld and Olsen 2017). Area LM has been associated with ventral stream processing (Wang et al., 2012; Smith et al., 2017) although others have provided evidence associating it with dorsal stream processing as well (Juavinett and Callaway, 2015). Equally valid, it may be that area LM is more like V2, in that it contains cells that are functionally specialized for each processing stream. In line with possessing ventral stream capabilities, rodents are able to discriminate objects (Bussey et al., 2001; Vermaerke et al., 2012; Tafazoli et al., 2017). Evidence for an object-processing pathway in rodent suggests that V1, LI and LL comprise a hierarchical cortical object identification pathway (Tafazoli et al., 2017; Matteucci et al, 2019). No evidence was found that suggests LM is grouped into this hierarchical object identification pathway (Tafazoli et al., 2017). Thus, more experiments are needed to determine the role of LM in the putative dorsal/ventral streams of mice. Anatomically, it appears to connect preferentially to ventral areas, but functionally, there is a lack of evidence for this area in object processing.

1.2.6 Area PM: A high spatial frequency dorsal area?

Area PM sits adjacent to V1 on the medial side and is more biased to the lower temporal visual field (Zhuang et al., 2017). PM has consistently been shown to prefer relatively high spatial frequencies and lower temporal frequencies than other higher visual areas (Andermann et al., 2011; Marshel et al., 2011; Roth et al., 2012; Glickfeld et al., 2013) as well as a bias for cardinal directions (Roth et al., 2012). Due to its projections to retrosplenial cortex and cardinal tuning preferences, it has been proposed that PM might be important for visuospatial navigation (Roth et al., 2012). Excitingly, mice use landmarks to navigate through their virtual environment and exhibit many correlates of spatial navigation in the hippocampus and retrosplenial cortex (Harvey et al., 2009; Czajkowski et al., 2014; Mao et al., 2017). PM has been shown to be responsive to slow speeds, indicative of dorsal stream processing (Andermann et al., 2011; Roth et al., 2012) and possibly playing a role in coding natural scenes of the periphery due to its cardinal bias (Girschick et al., 2011; Hansen et al., 2003).

1.2.7 How Mouse Visual Circuitry Informs Our Understanding of Visual Processing

Historically, the mouse visual system was largely overlooked due to their low-resolution acuity. Acuity thresholds for mice are far lower than humans and primates and their binocular visual field is quite small. Despite these differences, mice can perform visually guided tasks (Prusky et al., 2000, Bussey et al., 2001; Andermann et al., 2010; Hoy et al., 2016). They also have a constellation of higher visual areas surrounding V1, much like primate visual cortex with properties that fall within dorsal and ventral like stream processing. The organization of cortex is also similar, although by no means reiterated, in

the mouse: they have a six-layer cortex whose organization seems to generally follow the feedforward and feedback organization of primates, inhibitory and excitatory cell types and retinotopic organization. Moreover, a comparison of the neurophysiology of cells within V1 in mice and primates is quite similar. For instance, both contain simple and complex cells (Dräger 1975; Niell and Stryker 2008; Hubel and Wiesel 1974b) orientation/direction tuned cells, spatial frequency tuning and cells that respond preferentially to one of either or both eyes. Thus, understanding the underlying circuitry involved in the components of visual processing that are shared by primates and mice alike could reveal much about how these cortical computations are solved in primates.

Owing to Hubel and Wiesel's discovery of ocular dominance columns in primates and carnivores, an intensely studied process is binocularity in the visual cortex. While primates and carnivores have prominent ocular dominance columns, mice do not (Gordon and Stryker, 1996; Antonini et al., 1999). This may be in part due to vastly different amount of retinal territory dedicated to the ipsilateral eye (Merlin et al., 2013). The eyes of the mouse are placed largely on the sides of their heads so their binocular visual field is limited to that of humans and non-human primates (30° for mice, 120° for humans). Until recently, it was widely believed that V1 in mice, like humans and primates, was the first site of binocular convergence, but studies have demonstrated that there is binocularity in LGN of mice (Howarth et al., 2014; Rompani et al., 2017; Jaepel et al., 2017; Huh et al., 2018). These studies have prompted detailed examination of primate LGN and binocularity has also been found in the koniocellular layers of primate LGN (Zeater et al., 2015). Moreover, the genetic tools available for studying mouse circuitry continue to improve, allowing researchers to correlate brain activity with behavior. Thus, studies of the mouse visual system, in light of

the known species differences, can inform hypotheses about human vision which can be directly tested in primates.

A shift in favor of using the mouse as a model organism to study visual processing coincides with an expansion in the use of genetically encoded calcium indicators (GECIs) to understanding neural processing. The improvements in GCaMPs and coupling CRE recombinases allow researchers to image activity deep within the brain, at multiple layers and for multiple cell types. However, the switch of GECIs for electrophysiological techniques results in trade offs for each. GECIs, like GCaMP, are correlates of neural activity, detecting calcium transients in a graded but non-linear fashion (Chen et al., 2013). Although improvements to GCaMPs enable the detection of single action potentials, insight into electrophysiological markers of physiologically distinct cell types (simple vs. complex, for example) are lost without using some type of deconvolution algorithm to transform the fluorescence signals into action potentials, or a very fast indicator. Moreover, the ability to detect weak signals for both recording techniques is likely not the same due to the difference in noise characteristics for each system. Resolving the mounts of historical data fathered by single unit recordings with the explosion of new data generated by calcium imaging is a challenge that is still ongoing. However, genetically encoded voltage indicators may bypass the need for this resolution (Panzera and Hoppa 2019). Moreover, a benefit to imaging methods in comparison with electrophysiological methods is the ability to actually see many cells during a single experiment, trace their activity chronically and to quantify cells that are not excited by probed stimuli. This contributes immensely to our understanding of the types of processing single cells and whole areas are capable of.

There are numerous practical reasons for conducting vision studies on mice. Mice are inexpensive, small, can be trained to complete behavioral tasks and their entire visual cortex can be studied with a 5 mm cranial window. Many more caveats exist than have been explained in the previous sections for choosing to use mice in vision studies. One important caveat is the emphasis on the central visual pathway, in both primates and mice, in a system where the dominant output of the retina is to the superior colliculus. On the other hand, extensive probing of the extrageniculate pathway in mice may lead us to a better understanding of its role in mediating visually guided behaviors in primates. Any potential inconsistencies between mouse and primate visual systems will prompt researchers to consider the ethological relevance/ implications of their findings and to think of the organism as a whole, thus providing a context by which to move forward in our understanding of brain function.

1.3: Visual Cortical Plasticity- Critical Periods

Although mice may lack some of the cortical functional architecture described in cats and primates, such as the columnar organization (Gordon and Stryker, 1996; Antonini et al., 1999; Ohki et al., 2005; Ohki and Reid, 2007, but see Fahey et al., 2019), they share many of the neurophysiological characteristics described in primates, such as tuning for eye-specificity, orientation, direction, spatial frequency and temporal frequency. Endowed with the machinery to perform cortical computations important for more complex visual processing downstream, the mouse visual system has become the most prominent model in understanding mechanisms of visual cortical plasticity. Of the most central forms of cortical plasticity are those that arise during a critical period in life. A critical period is assigned

when experience is vital for the maturation of some form of processing. The critical period usually falls within a discrete window, although the boundaries can be fuzzy, during which absence of experience leads to deleterious effects later in life. There are many critical periods for different types of information and particular visual processing already established in mice: for example, ocular dominance, acuity and interocular orientation matching (reviewed in Espinosa and Stryker 2012; Gordon and Stryker 1996; Prusky and Douglas 2003; Wang et al., 2010). Historically, much of the research on these forms of plasticity has been restricted to V1. With the recent rise in our understanding and ability to examine mouse extrastriate areas, fundamental questions about the development and plasticity of higher visual areas can now be probed in mice.

It has since been discovered that many aspects of the functional architecture of the visual system do not require external visual stimuli, while others do. For example, the retinotopic map formation happens before eye opening but is dependent on spontaneous retinal waves (Cang et al., 2008). In the next few sections of the chapter, I will briefly review what is known about the development and experience-dependence of features discussed in the dissertation: ocular dominance, orientation and direction selectivity, spatial frequency and temporal frequency. I will conclude the section with what is currently known about the development of mouse higher visual areas.

1.3.1 Ocular Dominance Plasticity

In their early studies, Hubel and Wiesel discovered an early window for enhanced cortical plasticity by depriving animals of visual input through one eye and recording the responsivity to visual stimuli later in life. Generally, neurons respond preferentially to one

eye over the other, termed ocular dominance (OD) by Hubel and Wiesel (Hubel and Wiesel, 1962). Depriving an animal of visual experience from one eye (monocular deprivation, MD) during the critical period results in a shift in responsiveness away from the deprived eye and towards the non-deprived eye when probed with visual stimuli, typically drifting oriented lines (Wiesel and Hubel, 1963; Hubel and Wiesel 1970; Hubel et al., 1977). This change in plasticity is accompanied by shrinkage of ocular dominance columns (ODCs) of the closed eye in favor of the open eye (Hubel et al., 1977; Le Vay et al., 1980; Swindale et al., 1981; Horton and Hocking, 1997). This disruption of binocular organization and shift in ocular dominance tuning is called ocular dominance plasticity (ODP). The discovery of MD-induced ODP and its long lasting effects on cortex by Hubel and Wiesel led to an explosion of research on the mechanisms of ODP and the hunt for more critical periods.

The effect on the shapes of ODCs induced by early monocular deprivation suggests that the initial formation of ODCs does not require visual experience. In fact, the functional organization of the cortical column, in terms of ocular dominance and orientation, does not require visual experience for its formation (Wiesel and Hubel, 1963; Sherk and Stryker, 1976, Crair et al., 1998; Rakic 1976; Horton and Hocking, 1996; Des Rosiers et al., 1978). Thus the initial formation of the functional organization of cortex appears to be largely innate—although visual experience can modify the existing columnar organization by modifying column widths, switching eye territory for ODCs. This also seems to be the case when considering V1 outputs to V2 (which also maintains its columnar organization), where visual deprivation does not alter the functional segregation of V1 outputs to V2 in amblyopic macaques (Sincich et al., 2012).

Is there any information on how monocular deprivation may impact one stream of visual processing over the other? Horton and Hocking found that the ocular dominance columns in the parvocellular layer (Layer 4Cb) were more impacted than those in the magnocellular layer of V1 (Layer 4Ca) and no discernable effect on the koniocellular layer of V1 (Layer 3) (Horton and Hocking, 1997). However, to date there is little information on the effects of monocular deprivation during the critical period on ocular dominance plasticity of higher visual areas. One study compared the effects of monocular deprivation in V1 and an extrastriate area lateral suprasylvian (LS) in cats. Despite LS having an earlier termination of its critical period for ODP, the effects of MD were comparable in magnitude in regards to the OD shift of V1 (Jones et al., 1984).

The genetic tools available to the mouse led researchers to shift their attention toward the mouse to understand cellular and molecular mechanisms of ODP. Cells in V1 of normal adult mice have a high contralateral eye bias (Dräger, 1975; Gordon and Stryker, 1996), which shifts towards the ipsilateral eye when visually deprived through the contralateral eye between P19 and 32 (Gordon and Stryker, 1996). Accompanied by this shift in ODP is a decrease in acuity (Prusky and Douglas 2003). Initial studies demonstrating that neurons of the dLGN did not display functional changes after MD led many to believe that the site of ODP began in V1 (Wiesel and Hubel, 1963; Blakemore and Vital-Durand, 1986), even though dLGN afferents do differ with MD (Shatz and Stryker, 1978; Antonini and Stryker, 1993; Antonini et al., 1999; Coleman et al., 2010). Thus, extensive work has evolved from the initial findings that MD induces ODP in mice, especially on the effects of MD in V1 (reviewed in Levelt and Hübener, 2012). However, recent studies have demonstrated ODP at the level of the dLGN in mice (Huh et al., 2018;

Jaepel et al., 2017; Sommeijer et al., 2017), pointing towards the thalamus as an earlier site of MD-induced ODP.

For mice, cats and primates alike, there is a gap in our understanding of the critical period for ocular dominance plasticity in higher visual areas of cortex. Filling this gap is important for understanding how plasticity is relayed downstream. V1 has been described as the first step in the cortex for visual processing, yet there is extensive work solely focusing on V1 plasticity. If the critical period for ODP is as important as presumed, it should cause perceptual alterations in vision, especially if ODP is used as a model for the developmental disorder amblyopia. Amblyopia, which is associated with impaired visual acuity, is insufficiently described by functional deficits at the level of V1 alone (Kiorpes and McKee 1999; Kiorpes et al., 1998) and it is likely that higher visual areas are more severely impacted by abnormal visual experience (Kiorpes, 2016).

1.3.2 Spatial and Temporal Frequency Tuning

Acuity, a measurement of the ability to see fine details, matures with age and also appears to be experience-dependent (Boothe et al., 1985; Maurer et al., 1999; Kang et al., 2013). Monocular deprivation (MD) in early development disrupts the proper development of acuity, particularly in the eye that is deprived (Dews and Wiesel, 1970; Hess and Howell, 1977; Levi and Harwerth, 1977; Fagiolini et al., 1994; Kiorpes et al., 1998; Prusky et al., 2000). Although the shift in ocular dominance induced by MD has been associated with a disruption in acuity, recent evidence suggests that the circuits establishing ODP and acuity are distinct (Stephany et al., 2018). The effect of MD on maps for spatial frequency remains elusive. However, it appears that disrupting the ocular dominance map in ferrets via

monocular enucleation disrupts the layout, but not the presence, of maps of spatial frequency and orientation in the hemisphere contralateral to the remaining eye (Farley et al., 2007).

There are far fewer studies on the development and experience-dependence of temporal frequency tuning. As with spatial frequency tuning, temporal frequency matures after eye opening (Zheng et al., 2007). Interestingly, the developmental time course for this maturation is faster in V1 than it is in V2. It appears that the development of temporal modulation sensitivity is experience-dependent, with monocular deprivation disrupting the tuning of the deprived eye in particular (Harwerth et al., 1983). While functional maps have been found for spatial frequency, a modular organization for temporal frequency tuning has not been established in visual cortex. Notably, Khaytin et al., 2008 searched for and could not find maps of preferred temporal frequency in primates (Khaytin et al., 2008). However, neurons may change their response properties depending on stimulus conditions for spatial frequency, temporal frequency, orientation and direction (Priebe et al., 2006; Ayzenshtat et al., 2016; Basole et al., 2003). In fact, Basole and colleagues found that many stimulus conditions could activate the same neural populations, and argue that the functional organization of V1 be described as a map of spatiotemporal energy (Basole et al., 2003). Given that higher level processing involves the integration of both spatial and temporal frequency, this idea of V1 serving as a spatiotemporal energy map has implications for how higher visual areas could acquire their distinct responsiveness for spatiotemporal tuning, providing that they are dependent on V1 output. What could be the downstream consequences, if any, of altering V1 spatiotemporal tuning early in development?

1.3.3 Orientation and Direction Selectivity

Orientation and direction are early features that can be linked to form and motion processing. In ferrets, maps for direction form later than maps of orientation (White and Fitzpatrick, 2007). Consequently, developments of orientation and direction tuning in cortex are believed to be independent processes in ferrets (Li et al., 2006). When mice are dark reared, orientation and direction selectivity appear to develop normally (Rochefort et al., 2011). Orientation selectivity is present around the time of eye opening and, unlike direction selectivity, appears to sharpen during the course of development (Chapman and Stryker 1993; Wiesel and Hubel, 1963; White et al., 2001; Wiesel and Hubel 1974; Rochefort et al., 2011). Although dark rearing does not appear to disrupt the orientation selectivity of cells in V1, other sensory experience manipulations do have an effect on orientation tuning in the juvenile (Kreile et al., 2011; Kim and Bonhoeffer, 1994; Crair et al., 1997b; Kang et al., 2013). Importantly, monocular deprivation during the critical period drastically reduces binocular matching for orientation tuning (Wang et al., 2010), demonstrating that the two are linked developmentally. The distinction between orientation and direction tuned cells and their association with stream segregation has yet to be explored in depth in mouse V1 and HVAs. If and how orientation and direction tuning are selectively perturbed in circuits, or even if they are separable in development of mouse visual cortex, has still yet to be discerned.

1.3.4 Development of Higher Visual Areas

Much of the work centered on critical period plasticity, particularly in mice, or the experience-dependence of some visual attribute is based on the activity of V1. This is

largely due to the widely accepted fact that the first level of functional differences induced by monocular deprivation appears to be in V1, where the eye-specific afferents were altered. The development of more complex image analysis is less intensely studied, but perhaps more important for understanding how hierarchical information is computed (Kiorpes, 2016). The limitations of restricting studies to V1 are demonstrated by the inability to describe with single unit recordings from V1 visual perceptual deficits in models of amblyopia (Kiorpes et al., 1998). A cascade of developmental trajectories, following their hierarchical order has been proposed for describing the development of the visual system (Kiorpes, 2016). This postulation is largely based on the fact that the detection of simple visual features develops faster than more complex ones (Figure 1.3).

What do we currently know about the experience-dependence of higher order features or higher visual areas? In one study, a deficit was found at the level of V2 in amblyopic primates in terms of orientation tuning and acuity, where none could be found in V1 (Bi et al., 2011). It appears that amblyopia induces deficits in processing motion (Tychsen et al., 2004; El-Shamayleh et al., 2010) and difficulties with global perception (Hess et al., 1999; Kovács et al., 1999; Kozma and Kiorpes, 2003; Norcia et al., 2005).

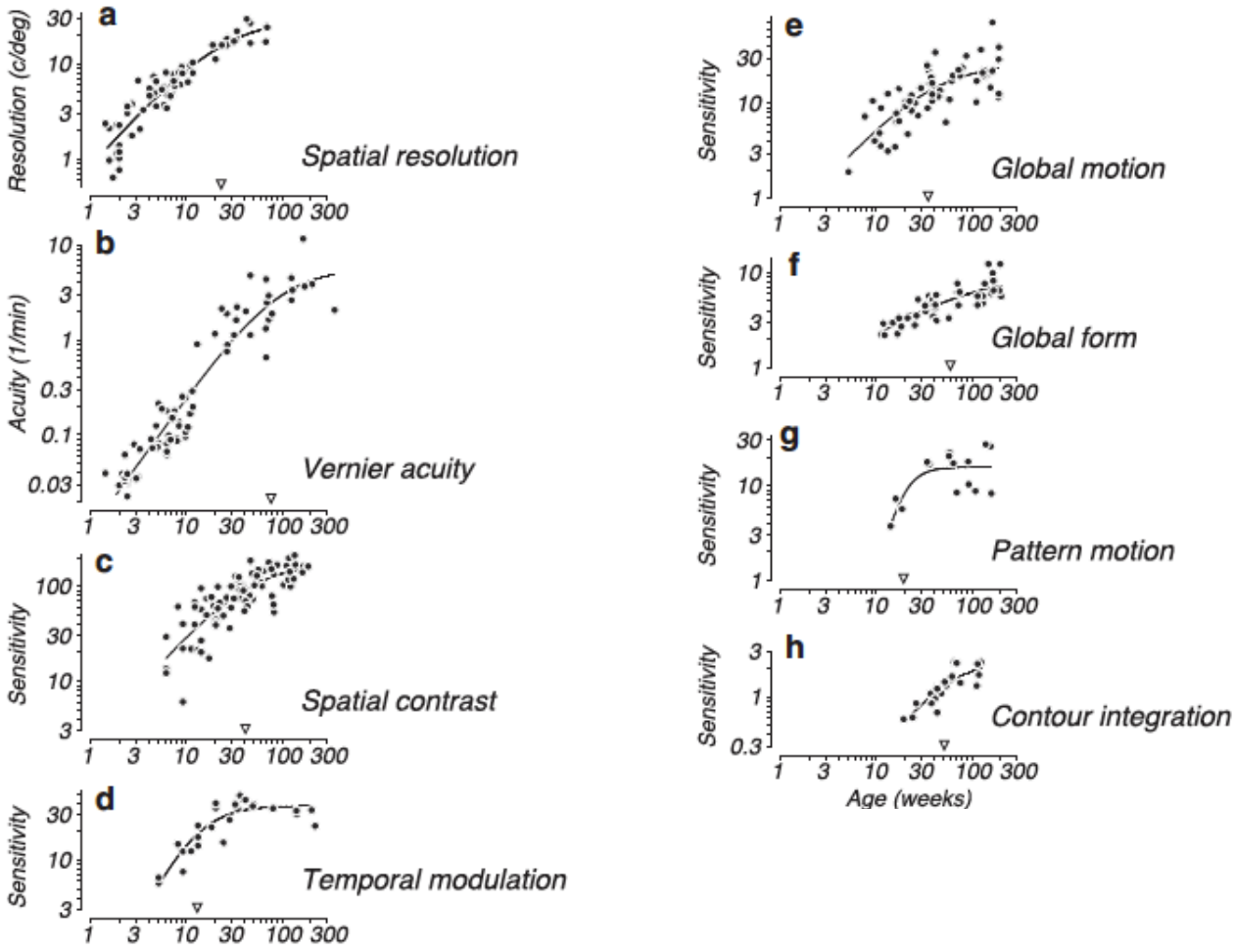

Figure 1.3: Developmental timeline for various visual functions. Left column (a-d) are developmental trajectories for simple features (x-axis indicates Age (weeks)). Right column (e-h) are developmental trajectories for more complex visual features. Modified (re-ordered) from Kiorpes, Lynne. "The puzzle of visual development: behavior and neural limits." *Journal of Neuroscience* 36.45 (2016): 11384-11393.

In terms of the mouse literature, only recently has the development of higher visual areas been probed. Two studies in particular have pioneered this work, but neither used monocular deprivation. Using widefield calcium imaging, Murakami et al., 2017 demonstrated that the higher visual areas gain their unique spatiotemporal tuning profiles over time, and become more functionally segregated with increasing days of eye opening, until they plateau around ~P25. This report agrees with other studies using cats and monkeys (DeAngelis et al., 1993; Chino et al., 1997; Zheng et al., 2007). With intrinsic signal

imaging, Smith et al., 2017 demonstrated that higher visual areas grouped into the putative ventral stream are close to maturity, in terms of response amplitude elicited by visual stimulation, at the time of eye opening; whereas areas grouped into the putative dorsal stream take longer to develop. They all show that dark rearing preferentially disrupts the maturation of the response magnitude of dorsal stream areas. However, this study did not examine the spatiotemporal tuning properties of areas in their respective streams or determine which populations in particular are vulnerable to disrupted visual experience.

How might the developmental maintenance of eye-specificity in the cortex shape or instruct the spatiotemporal selectivity of higher visual areas? Orientation has been coupled to spatial frequency and now ocular dominance in macaque. Can a shift in ocular dominance plasticity coincide with a consequential disruption in other tuning properties, for instance, in the spatiotemporal domain, to the point where higher visual area selectivity is degraded downstream? If the higher visual areas develop in a hierarchical fashion, as has been hypothesized in higher order primates, we might expect that the deficits seen at the level of V1 (shift in ODP, disrupted acuity) may just be the first step in a developmental cascade that leads to a immature higher cortical organization. Even if higher visual area selectivity is not strictly dependent on V1 during the development and HVAs develop rather independently than V1 (which has yet to be determined), the extrageniculate path houses eye-specific maps in the SC and LP and may also yield downstream consequences for HVA selectivity.

1.4 Significance Statement

Understanding the circuits underlying mouse vision is important for understanding principles that may relate to human visual processing. The functional architecture of the mouse visual system is closer to the primate than previously appreciated. This work adds to this by demonstrating functional motifs at V1 and higher visual areas: LM and PM. It furthers the field by linking ocularity with functional specificity at multiple levels of cortex and then determining if functional specialization is dependent on eye-specific visual experience. By using monocular deprivation and its known effect on ocular dominance plasticity as a way to determine the experience-dependence of higher visual area specialization, we may also provide insight into models of amblyopia (Hoyt, 2005).

CHAPTER 2: Eye-specific Functional Properties in binocular V1

2.1 Introduction

The mammalian visual cortex processes spatial information using neurons that are narrowly tuned to specific spatial frequencies (Maffei and Fiorentini, 1973; Schiller et al., 1976a,b, Movshon et al., 1978a,b, De Valois et al., 1982a). Given the narrow bandwidth of cortical responses, neurons tuned to the highest spatial frequencies should set the limit of visual acuity. Psychophysical studies have long suggested that binocular vision enhances spatial acuity over monocular viewing by enhancing the sensitivity of signal detection (Pirenne, 1943; Campbell and Green, 1965; Blake et al., 1981). Together, these observations suggest that individual neurons in visual cortex tuned to the highest spatial frequencies are likely to receive eye-specific inputs whose response properties are well matched. Hubel and Wiesel's initial description of binocular receptive fields reported that eye-specific inputs to cortical neurons are similar (Hubel and Wiesel, 1962). Subsequent studies that explicitly explored spatial frequency tuning in binocular neurons found significant but quantitatively modest asymmetries in the preferred spatial frequencies and bandwidth of eye-specific responses (Skottun and Freeman, 1984; Bergeron et al., 1998; Saint-Amour et al., 2004). Other studies, however, found many spatial frequency mismatched binocular responses in cat visual cortex (Hammond and Pomfrett, 1991; Hammond and Fothergill, 1994).

The mouse system has emerged as a prominent model for studying precise wiring and developmental plasticity in the central visual pathway (Huberman and Niell, 2011; Espinosa and Stryker, 2012). In particular, the spatial acuity of mouse cortical responses has been used extensively to assess cellular and molecular mechanisms for binocular

system development (e.g. Porciatti et al., 1999; Huang et al., 1999; Beurdeley et al., 2012; Davis et al., 2015). Since these studies used indirect measures of neuronal activity, such as visually evoked potentials and intrinsic signal imaging, they cannot address whether binocular responses at the level of individual cells are matched at the highest spatial frequencies. Although many aspects of neuronal response properties have been studied extensively in mouse binocular visual cortex (Dräger, 1975; Wagor et al., 1980; Gordon and Stryker, 1996; Mrsic-Flogel et al., 2007; Wang et al., 2010; Scholl et al., 2013), the investigation of spatial frequency tuning in mice has been largely restricted to the monocular zone (Niell and Stryker, 2008; Durand et al., 2016; Hoy and Niell, 2015). Little is known about binocular matching of spatial frequency responses in mouse visual cortex at the level of single neurons.

In this study, we set out to characterize the eye-specific spatial frequency tuning of neurons in the binocular zone of mouse area V1. Using calcium imaging of excitatory neurons, we found that contralateral-eye dominated neurons in binocular area V1 are tuned to higher spatial frequencies than their binocular counterparts. In binocular neurons, responses that are matched in spatial frequency preference are matched in orientation preference, whereas cells mismatched in spatial frequency preference are more mismatched in orientation preference. Furthermore, we found that contralateral eye dominated, high spatial frequency tuned neurons are biased to the cardinal axes. These results suggest that distinct circuit mechanisms process binocular and high acuity vision in the mouse visual system.

2.2 Materials and Methods

2.2.1 Animals

All protocols and procedures followed the guidelines of the Animal Care and Use Committee at the University of California, Irvine. To image evoked activity in excitatory neurons, a Camk2a-tTA driver line (RRID: IMSR_JAX:007004) was crossed to a line expressing the calcium indicator GCaMP6s under the control of the tetracycline-responsive regulatory element (tetO) (RRID: IMSR_JAX:024742; Wekselblatt et al., 2016). The founder line was heterozygous for both transgenes and maintained by breeding with wildtype C57BL/6 mice (RRID: IMSR_CRL:642). Wildtype mice were used in experiments for AAV-mediated expression of GCaMP6s. Mice were weaned at P18-21 and co-housed with one or more littermate until the day of window implantation (P63-91). In awake recordings, 4 female and 8 male mice were used, while in anesthetized recordings 3 males were used.

2.2.2 Cranial Window Implantation

Mice were anesthetized with isoflurane in O_2 (2% for induction, 1-1.5% for maintenance). Headplate attachment and craniotomy were performed in one surgery. Carprofen (5 mg/kg, s.c.) and topical xylocaine (2%, 20mg/mL) was administered to provide analgesia. Dexamethasone was administered 4-8 hours before surgery (4.8 mg/kg, i.m.). Atropine (0.15 mg/kg, s.c.) was administered to reduce secretions and aid in respiration. To attach custom-printed ABS headplates, the skull was cleared of connective tissue and dried with ethanol. A thin layer of Vetbond was applied to the skull and the headplate was attached using dental acrylic at an angle parallel to the site of imaging (~20 degrees from horizontal). A craniotomy (5 mm diameter) was performed over the left or right hemisphere using previously described methods (Figueroa Velez et al., 2017). A 5 mm

glass coverslip (World Precision Instruments) was placed over the exposed brain and sealed with Vetbond and black dental acrylic. Sterile eye ointment (Rugby) was used to protect the eyes. Body temperature was maintained at 37.0^{o}C using a heating pad under feedback control from a rectal thermoprobe. Mice were allowed to recover on a warm heating pad following surgery (<15 minutes). Mice were given daily injections of Carprofen (5mg/kg, s.c.) for at least two days post-surgery.

2.2.3 GCaMP6s Virus Delivery

To assess visual responses in binocular visual cortex, AAV-Syn-GCaMP6s (Chen et al., 2013) (Upenn Vector Core AV-1-PV2824) was injected into wildtype mice two weeks prior to imaging. Virions were diluted 10-fold with ACSF to ~2x10^{12} GC/mL and 400nL was injected at a rate of 10nL/min. Lactated Ringer's (0.2mL/20g/hr, s.c.) was given to prevent dehydration. Mice were allowed to recover on a warm heating pad following surgery (<15 minutes).

2.2.4 Widefield Visual Area Mapping

Mapping of the visual areas was performed at least one week after window installation using widefield imaging of GCaMP6s (Wekselblatt et al., 2016; Zhuang et al., 2017). Widefield fluorescence images were acquired using a SciMedia THT macroscope (Leica PlanApo 1.0X; 6.5x 6.5 mm imaging area) equipped with an Andor Zyla sCMOS camera. The surface vasculature and GCaMP6s signal was visualized using a blue 465 nm LED (LEX2). The camera was focused ~600 μm beneath the surface. Image acquisition and visual stimulus presentation was controlled by custom written software in python using the PsychoPy 1.8 library.

2.2.4.1 Visual Stimuli for Area Mapping

To perform visual area segmentation, awake mice were shown a 20° wide visual noise stimulus that swept periodically every ten seconds in each of the four cardinal directions. The sweeping visual stimulus was created by multiplying a band limited (<0.5 c/d; >2 Hz), binarized spatiotemporal noise movie with a one dimensional spatial mask (20°) that was phase modulated at 0.1 Hz. A gamma corrected monitor (54" LED LG TV model 55LB5900) with maximum luminance of 30 cd/m^2 was placed 20 cm from the contralateral eye and angled at approximately 30^o from the long axis of the animal. The stimulus was spherically corrected to cover 140^o visual angle in elevation and 120^o in azimuth. The stimulus was presented to the contralateral eye for 5 minutes for each direction. To confirm the location of the binocular zone, we also presented the sweeping, binarized noise stimulus confined to the central 30^o of visual azimuth.

2.2.4.2 Analysis for Area Mapping

Retinotopic maps of azimuth and elevation were used to generate a visual field sign map (Sereno et al., 1994; Garrett et al., 2014) to designate borders between visual areas. Recordings from binocular V1 were confined to regions adjacent to the intersection of the horizontal and vertical meridians at the border of V1 and LM. Recordings from monocular V1 were confined to regions medial to the binocular zone of V1 along the horizontal meridian.

2.2.5 Two-Photon Calcium Imaging

Fluorescence was gathered with a resonant two-photon microscope (Neurolabware, Los Angeles, CA) with 920 nm excitation light (Mai Tai HP, Spectra-Physics, Santa Clara, CA). Emissions were filtered using a 510/84nm BrightLine bandpass filter (Semrock,

Rochester, NY). A 16x (Nikon NA=0.8) or a 20x water immersion lens (Olympus NA=1.0) was used. Image sequences typically covered a field of approximately 700 μm by 500 um and were acquired at 7.7 or 15.4 Hz (1024 lines) using Scanbox acquisition software (Scanbox, Los Angeles, CA) at a depth of 200-250 μm below the pia.

2.2.5.1 Two-Photon Visual Stimuli

Visual stimuli were generated by custom-written python code using the PsychoPy 1.8 library. Full field drifting sinusoidal gratings were presented eight orientations (0-315, 45^{o} steps) and six spatial frequencies (0.03-0.96 c/d, logarithmically spaced) at a fixed temporal frequency (2Hz) using an Acer V193 gamma corrected monitor (53 x 33 cm, 60 Hz refresh rate, 20 cd/m^2). The visual stimulus was spherically corrected. In addition to the 48 grating stimuli, we also showed a blank condition and a condition in which the whole monitor flickered at 2 Hz (FF). The 50 total stimulus conditions were presented in a random order for each of the 10 repetitions. In one subset of experiments, 20 repeats were used. For each trial, the stimulus was presented for 2 seconds, followed by 3 seconds of grey screen. For anesthetized recordings, mice were sedated during recordings using isoflurane in O_2 (0.6-0.9%) supplemented with chlorprothixene (2 mg/kg, i.p.). For awake and anesthetized recordings, the visual stimulus was presented either first to the ipsilateral or the contralateral eye. In awake recordings, four of eight animals were presented with the stimulus through the contralateral eye first. In anesthetized recordings, two of three mice were presented with the stimulus through the contralateral eye first.

2.2.6 Data Analysis

2.2.6.1 Cellular Responses

Custom-written Python routines were used to remove motion artifact, identify cell ROIs, extract calcium fluorescence traces, and perform analyses. First, we implemented motion correction by using an efficient algorithm that corrects for translational artifacts by minimizing the Euclidean distance between frames and a template image using a Fourier transform approach (Dubbs et al., 2016). To identify the region of pixels associated with distinct neuronal cell bodies, we used the maximum intensity projection of the images. Only cell bodies that could be visually identified throughout the 80-minute recordings were included in analysis. The fluorescence signal of a cell body at time *t* was determined as $F_{cell}(t) = F_{soma}(t) - (R \times F_{neuropil}(t))$ (Chen et al., 2013; Kerlin et al., 2010). R was empirically determined to be 0.7 by comparing the intensity of GCaMP6s signal in the blood vessels to the intensity in the neuropil across recordings. The neuropil signal $F_{neuropil}(t)$ of each cell was measured by averaging the signal of all pixels outside of the cell and within a 20 μm region from the cell center.

To determine a cell's response to each stimulus trial, the cell's trace during the stimulation period was normalized to the baseline value averaged over the 0.75 seconds preceding stimulus presentation. The cell's response to a given orientation θ_i was defined as the average response across the 10 repeats of each condition: $F(\theta_i)$. An estimate of the cell's spontaneous calcium fluctuation was determined using the cell's trace during the blank condition. At each spatial frequency, a cell's responsiveness was determined using a one-way ANOVA ($p<0.01$) across orientations against the blank condition (Figure 2A). To assess spatial frequency tuning and directional selectivity, we restricted our analysis to

neurons whose responses at the peak spatial frequency reached significance and whose responses to drifting gratings across all spatial frequencies reached significance when compared against the blank condition (ANOVA $p<0.01$; Figure 2B; analyzed cells).

2.2.6.2 Preferred Orientation

For each cell, preferred orientation (θ_{pref}) was determined at the spatial frequency that gave the strongest response by calculating half the mean of the directional vectors weighted by the response $F(\theta)$ at each orientation:

$$\theta_{pref} = \frac{\sum F(\theta) e^{2i\theta}}{\sum F(\theta)}$$

For each spatial frequency, a tuning curve, $R(\theta)$, was determined by fitting $F(\theta)$ to a sum of two Gaussians centered on θ_{pref} and $\theta_{pref} + \pi$, with different amplitudes and equal width, and a constant baseline. The amplitude of the response at the preferred orientation (R_{pref}) was $R(\theta_{pref})$.

2.2.6.3 Preferred Spatial Frequency

To determine the preferred spatial frequency, responses at the preferred orientation (R_{pref}) across all spatial frequencies were fitted with a difference of Gaussians function (DoG) (Hawken and Parker, 1987). For each fitted neuron, the preferred spatial frequency was determined by the maximum of the DoG functional fit. In addition, the bandwidth was calculated by taking the square root of the width at half the maximum of the fit.

2.2.6.4 Orientation and Direction Selectivity

Orientation selectivity for a cell was determined using a method derived from the circular variance of the cell's response $F(\theta)$ (Niell and Stryker, 2008; Kerlin et al., 2010, Hoy and Niell, 2015). The circular variance method for calculating orientation selectivity is

closely correlated to an alternative measure that uses a sum of two Gaussians (Velez et al., 2017). Since the circular variance based method is sensitive to the sign of F and because F fluctuates above and below 0 at baseline (sd = ±0.032% dF/F), we added an offset to F for each cell which set the minimum average response to 0: F(θ_i))=F(θ_i) - min(Fθ_i). Following this correction, the orientation selectivity index was calculated as

$$\text{OSI} = \left(\sqrt{(\sum_i (F(\theta_i) * \sin(2\theta_i)))^2 + (\sum_i (F(\theta_i) * \cos(2\theta_i)))^2} / \sum_i F(\theta_i)\right)$$

The direction selectivity index was calculated as:

$$\text{DSI} = \left(\sqrt{(\sum_i (F(\theta_i) * \sin(\theta_i)))^2 + (\sum_i (F(\theta_i) * \cos(\theta_i)))^2} / \sum_i F(\theta_i)\right)$$

2.2.6.5 Ocular Dominance Index

The ocular dominance index (ODI) for each cell was calculated as (C-I)/(C+I), where C is R_{pref} for the contralateral eye and I is R_{pref} for the ipsilateral eye. Contralaterally dominated neurons have an ODI value near 1 and ipsilaterally dominated neurons have an ODI value near -1. In cases where no significant response was detected for one eye, R_{pref} for that eye was set to 0. Therefore, responses that were purely a result of contralateral or ipsilateral eye stimulation were assigned ODI values of 1 and -1, respectively.

2.2.7 Pupil Tracking

Contralateral and ipsilateral eyes were recorded simultaneously using GigE cameras (Teledyne Dalsa, Mako G, Waterloo, Ontario, Canada). The cameras were positioned 30° above the mouse's eyepoint and 45° from the mouse's midline on each side. The eyes were illuminated by the infrared laser (MaiTai HP, Spectra-Physics, Santa Clara, CA) used for two-photon imaging.

To identify the pupils, each frame was thresholded and contours were extracted (Suzuki and Abe, 1985) using routines from the OpenCV library (3.2.0). Artifacts that

distorted the pupil contours were removed by 1) converting all contours to convex hulls (Sklansky 1982), 2) filtering the hulls using a predefined range, and 3) assigning the pupil to be the hull whose centroid was located closest to the center of the eye. Frames in which the contrast dropped significantly or those in which the mouse blinked produced erroneous pupil identification. To address this issue, we established a scoring system that would exclude frames in which the pupil exceeded a maximum circularity score. The circularity score was determined by calculating the ratio between the longest distance from the centroid to the hull and the shortest distance from the centroid to the hull. A score of 1.25 was selected as the cutoff based on the distribution of circular scores for a recording.

2.2.8 Experimental Design and Statistical Analyses

The statistical determination of cellular responsiveness is described in detail above. The Kolmogorov-Smirnov test was used to assess differences in the distributions of cellular spatial frequency preferences. The Mann-Whitney U test and Kruskal-Wallis test were used to assess differences between groups of cells (e.g. monocular vs. binocular cells). For animal-by-animal analyses of median eye-specific differences in binocular responses, we used a pair-wise Wilcoxon signed-rank test for comparing two groups and, for more than two groups, a Friedman test with a Dunn's multiple comparison post hoc test. Correlations were determined using Spearman rank correlation. For the analysis of direction selectivity, a Mann-Whitney U test was used to determine the significance of cardinality for a group and a Chi-squared test was used to test differences in cardinality between groups. Statistical analyses were performed using Prism v7.01 (GraphPad). To find the standard error of the median for preferred spatial frequency of a group of cells, we estimated the

sampling distribution using a bootstrap methodology that resampled 500 times with replacement (MATLAB, Mathworks).

2.3 Results

To systematically probe the spatial frequency tuning of binocular area V1, we used a transgenic mouse line that expresses GCaMP6s under the control of the CaMK2 promoter (CaMK2-tTA; tetO-GCaMP6s; Wekselblatt et al., 2016). The line restricts GCaMP6s expression to excitatory neurons only and excludes inhibitory interneurons, which are known to have distinct spatial frequency tuning properties (Kerlin et al., 2010). Binocular area V1 was identified using a widefield imaging procedure to retinotopically map visual areas in posterior mouse cortex (visual field sign map; Garrett et al., 2014; Figure 2.1a). Next, GCaMP6s imaging of cellular responses was performed using 2-photon microscopy. Recordings were directed to the central visual field by situating the field of view adjacent to the map coordinates for the V1/LM border and centered on the horizontal meridian. Cellular imaging was performed in awake, head-fixed mice that were acclimated to the setup over several days. Mice were shown a visual stimulus through either the contralateral or ipsilateral eye that consisted of two second presentations of drifting visual gratings at one of eight directions and one of six spatial frequencies (0.03-0.96 c/d spaced logarithmically; see Figure 2.1b). We interleaved the presentation of a full field flickering stimulus with the gratings to detect neurons tuned to very low spatial frequencies. Each stimulus condition was repeated 10-20 times per eye. Eye movement and pupil dilation were also recorded for the eye shown the visual stimulus. Half of the fields were imaged with the ipsilateral eye shown the stimulus first and half with the contralateral eye first.

Typical excitatory neurons responded to low spatial frequencies (<0.12 c/d) and had binocularly matched preferences for spatial frequency and direction (Figure 2.1c). The contralateral response (black; Figure 2.1c) was typically stronger than the ipsilateral response (red). Beyond these binocularly matched, low spatial frequency preferring responses, three other types of responses are also found in binocular area V1: cells that had mismatched spatial frequency tuning between the two eyes, cells that were dominated by the contralateral eye and cells dominated by the ipsilateral eye (Figure 2.1d). A typical field of view reveals overt differences in the spatial frequency tuning of the contralateral and ipsilateral eye inputs to binocular visual cortex (Figure 2.1e, f).

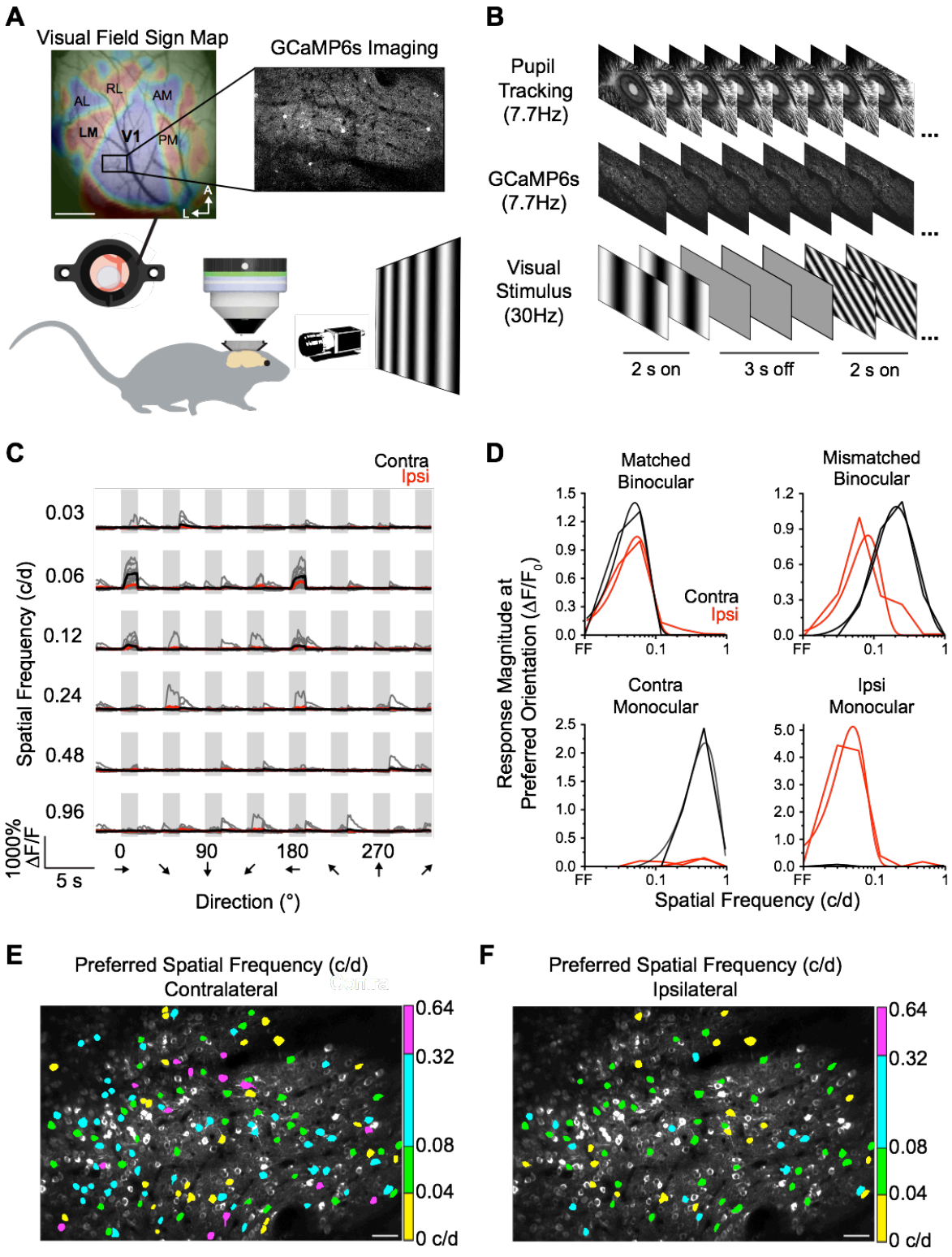

Figure 2.1: Assessment of Binocular Spatial Frequency Tuning in Primary Visual Cortex Using GCaMP6s Mice. A. Experimental Setup. (Top Left) Widefield imaging produces a visual field sign map that identifies the boundaries of primary visual cortex (V1). Scale bar is 1mm. (Top Right) Two-photon imaging was done in central binocular cortex adjacent to the border of areas V1 and LM. Visual responses were

measured in head-fixed, awake mice while they viewed drifting sinusoidal gratings. Mice walked freely while pupil dilation and eye movements are tracked by IR camera. **B.** Each trial consists of a two second presentation of a drifting grating at one of eight directions and one of six spatial frequencies, followed by a three second off period. The stimulus was shown to either the contralateral or ipsilateral eye. **C.** Example binocular responses from a cell. Grey boxes indicate when the visual gratings were shown. Individual trials shown in gray traces, averaged traces in black for contralateral eye stimulation and red for ipsilateral stimulation. This cell prefers vertical gratings at 0.06 c/d moving along the horizontal axis. **D.** Four types of spatial frequency responses in binocular V1 revealed by contralateral (black) and ipsilateral (red) eye stimulation: spatial frequency matched binocular, spatial frequency mismatched binocular, contralateral monocular and ipsilateral monocular cells. The average responses at each spatial frequency are overlaid with a Difference of Gaussians fit. Preferred spatial frequency is determined by the maximum of the fit. **E, F.** Maps of spatial frequency preference for contralateral (E) and ipsilateral (F) eye stimulation shown for a field of view. Scale is 50 μm. Most neurons are tuned to low spatial frequencies (yellow and green). Higher spatial frequency tuning (cyan and magenta) is found predominantly in contralateral responses.

2.3.1 Higher Spatial Frequency Tuning of Contralateral Eye Responses

Altogether, 1850 cells were imaged in ten animals. Across all cells, more neurons responded at high spatial frequencies for contralateral than for ipsilateral eye stimulation (Figure 2.2a, all cells). To characterize spatial frequency selectivity, we restricted our analysis to those cells (Figure 2.2b; analyzed cells) whose responses at the peak spatial frequency reached significance and whose responses to drifting gratings across all spatial frequencies reached significance when compared against the blank condition ($p<0.01$, ANOVA, total: 61.6%; contra: 48.97%; ipsi: 34.59%). These cells also responded to high spatial frequency stimuli through the contralateral and not the ipsilateral eye (Figure 2.2b). Composite spatial frequency response curves for all (Figure 2.2c) and analyzed (Figure 2.2d) cells confirm that these cells responded to high spatial frequencies through the contralateral and not the ipsilateral eye.

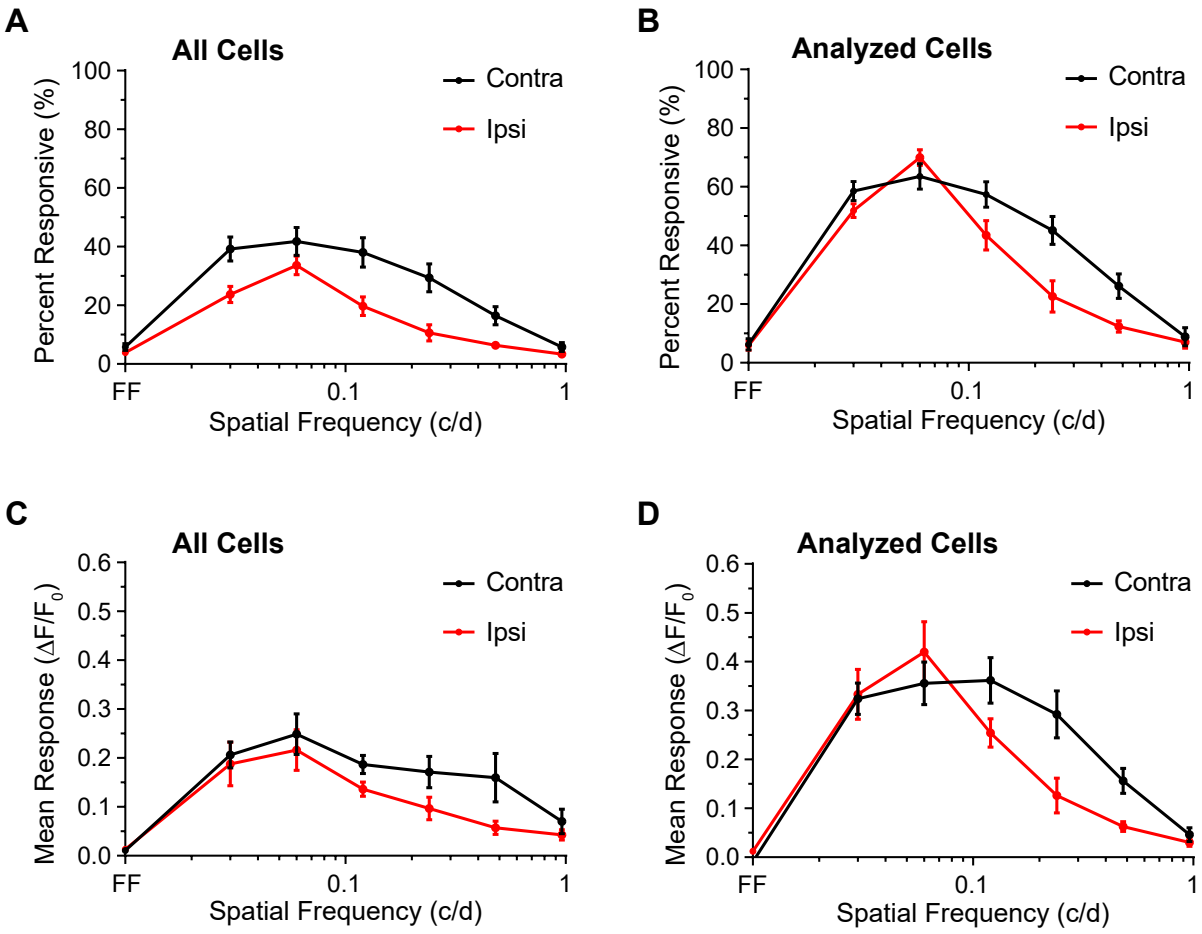

Figure 2.2: Higher Spatial Frequency Tuning of Contralateral Eye Responses in Binocular Visual Cortex A. Percent of all recorded cells are plotted with significant responses at each spatial frequency for contralateral eye (black) and ipsilateral eye (red) stimulation. Error bars reflect standard error of percent responsive across ten animals. **B.** Spatial frequency tuning and directional selectivity were only analyzed in cells whose responses at the peak spatial frequency reached significance and whose responses to drifting gratings across all spatial frequencies reached significance when compared against the blank condition. Among these analyzed cells, the percent with significant responses at each spatial frequency are plotted. Error bars reflect standard error of percent responsive across ten animals. **C, D.** Composite tuning curves for responses to contralateral (black) and ipsilateral (red) eye stimulation are plotted for all cells (C) and those cells that met our statistical criteria for spatial frequency tuning analysis (D). In both cases, the composite spatial frequency responses to the contralateral eye extended to higher spatial frequencies than the responses to the ipsilateral eye. Error bars reflect standard error of response strength across ten animals.

We found that the preferred spatial frequency of contralateral eye responses in binocular area V1 was overall ~35% higher than ipsilateral responses (median ipsi: 0.073 c/d, contra: 0.099 c/d Figure 2.3a, b). The animal-by-animal distributions of preferred spatial frequency for contralateral (black) and ipsilateral (red) responses show a consistent

pattern of higher tuning in the contralateral pathway. In contrast, we found that the spatial tuning bandwidths of contralateral and ipsilateral responses were nearly identical (Figure 2.3c, d). The amplitude of the response to the preferred stimulus across cells was somewhat higher for contralateral eye recordings (Figure 2.3e), raising the possibility that ipsilateral responses at high spatial frequencies were too weak to be detected. We found, however, no relationship between spatial frequency preference and response amplitude in our recordings (Figure 2.3f; all responses: $r=-0.02$; $p=0.556$). These results reveal an eye-specific asymmetry in the responses of binocular area V1.

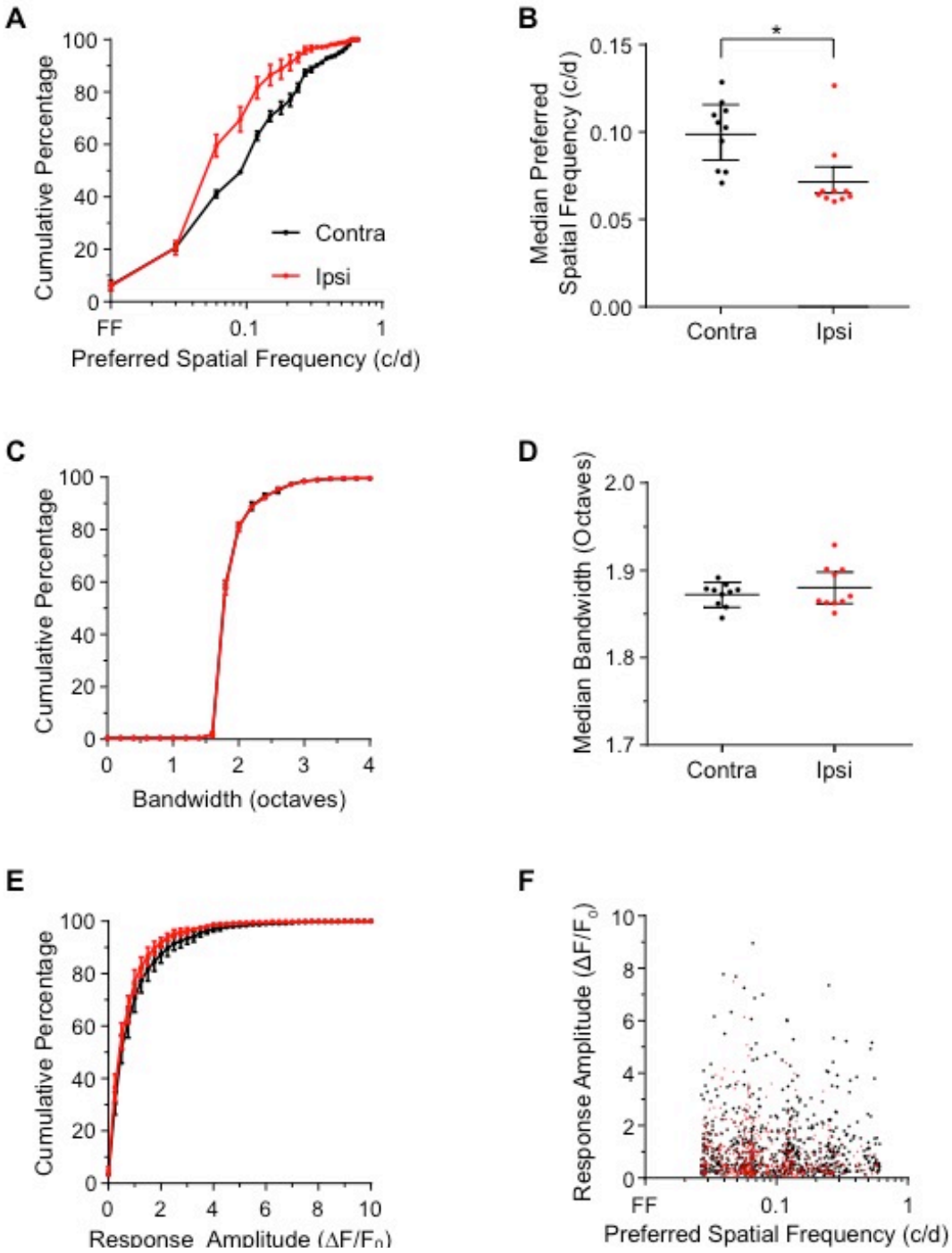

Figure 2.3: Spatial Frequency Preferences of Contralateral Responses is Higher than Ipsilateral Responses in Binocular Visual Cortex. A. Preferred spatial frequency for contralateral (black) and ipsilateral (red) eye responses. The distributions from ten mice were binned and the mean is plotted. Error bars reflect standard error of the mean. The preferred spatial frequency for contralateral responses is significantly higher than for ipsilateral responses (median contra= 0.099 c/d, n=908 neurons; median ipsi=0.0653 c/d, n=641 neurons; KS D=0.178, $p<0.0001$; MW(U)=245465, $p<0.0001$). **B.** Data grouped by animal confirm that the preferred spatial frequency of contralateral responses is significantly greater than ipsilateral responses (contra median=0.108 c/d; ipsi median=0.0653 c/d; Wilcoxon's rank sum test (W)=-40, $p<0.0391$, N=10 mice). Error bars reflect standard error of the median. **C.** The spatial frequency bandwidth

for contralateral (black) and ipsilateral (red) responses are very similar (contra median=1.867; ipsi median=1.867). Error bars reflect standard error of the mean. **D.** Data grouped by animal confirm that the spatial frequency bandwidths do not differ by eye (contra median=1.876 octaves; ipsi median=1.869 octaves, Wilcoxon rank sum test (W)=11, ns, p=0.6094, N=10 mice). Error bars reflect standard error of the median. **E.** Averaged responses at the peak spatial frequencies are shown for contralateral (black) and ipsilateral (red) eye stimulation. Responses to the contralateral eye are higher than responses to the ipsilateral eye (median contra= 0.620 ΔF/F, median ipsi= 0.518 ΔF/F; KS D=0.084, p<0.0099; MW(U)=258651, p<0.0002). **F.** Peak responses for contralateral (black) and ipsilateral (red) stimulation are plotted against preferred spatial frequency. The amplitudes of contralateral responses are similar at low and high preferred spatial frequencies.

2.3.2 Higher Spatial Frequency Tuning of Monocular Responses

Next, we examined the binocularity of cortical responses in binocular area V1 (Figure 2.4a). Surprisingly, we found that 62% of neurons recorded in binocular area V1 responded to one eye only (Figure 2.4b; ipsi: 19%; contra: 43%), while the remainder responded to both eyes (gray). The spatial distribution of monocular responses (ODI=1 or -1; see Figure 2.4a) appeared widely dispersed, discounting the possibility that our recordings had been made on the edge of the binocular zone. The number of trials and the order of eye presentation were also not found to be a factor in the prevalence of monocular responses.

It was possible that the prevalence of monocular neurons we observed in binocular area V1 stemmed from a non-linear sensitivity of calcium signals to neuronal firing. The amplitude of the monocularly responsive neurons (red=ipsilateral, black=contralateral) was less than half of what is predicted by the linear extrapolation of the eye-specific responses from binocular neurons (Figure 2.4c; ipsi monocular=0.743 ± 0.059 ΔF/F; contra monocular=1.084 ± 0.091 ΔF/F; y-intercept ipsi binocular=2.03; y-intercept contra binocular=2.38). The smaller amplitude of the monocular responses may mean that non-dominant eye inputs to these cells fall below a detection threshold for calcium imaging.

Alternatively, the smaller amplitude of these monocular responses may make them challenging to detect with traditional electrophysiological recording techniques.

Next, we compared the spatial frequency tuning of contralaterally dominated responses with their binocular and ipsilateral counterparts. We found that the preferred spatial frequency of contralaterally dominated responses is significantly higher than for binocularly responsive and ipsilateral only responsive neurons (Figure 2.4d; $p=0.0002$; $p=0.0161$). These findings reinforce our overall observation that the contralateral pathway is tuned to higher spatial frequencies than the ipsilateral pathway.

In some animals, we also recorded from a monocular region of area V1 that was centered at the horizontal meridian in the visual field map. The spatial frequency tuning of neurons in monocular area V1 (blue) was similar to contralaterally dominated neurons (black) in binocular area V1 (Figure 2.4d). In these experiments, we showed a brief ipsilateral stimulus to confirm that no ipsilateral responses were present. Across animals, the contralateral-eye dominated neurons were found to consistently prefer higher spatial frequencies than binocular neurons (Figure 2.4e; $p=0.0278$) and ipsilateral-eye dominated neurons (Figure 2.4e, $p=0.0073$). Together, these results reveal that contralateral-eye dominated neurons are tuned to higher spatial frequencies than their binocular and ipsilateral counterparts.

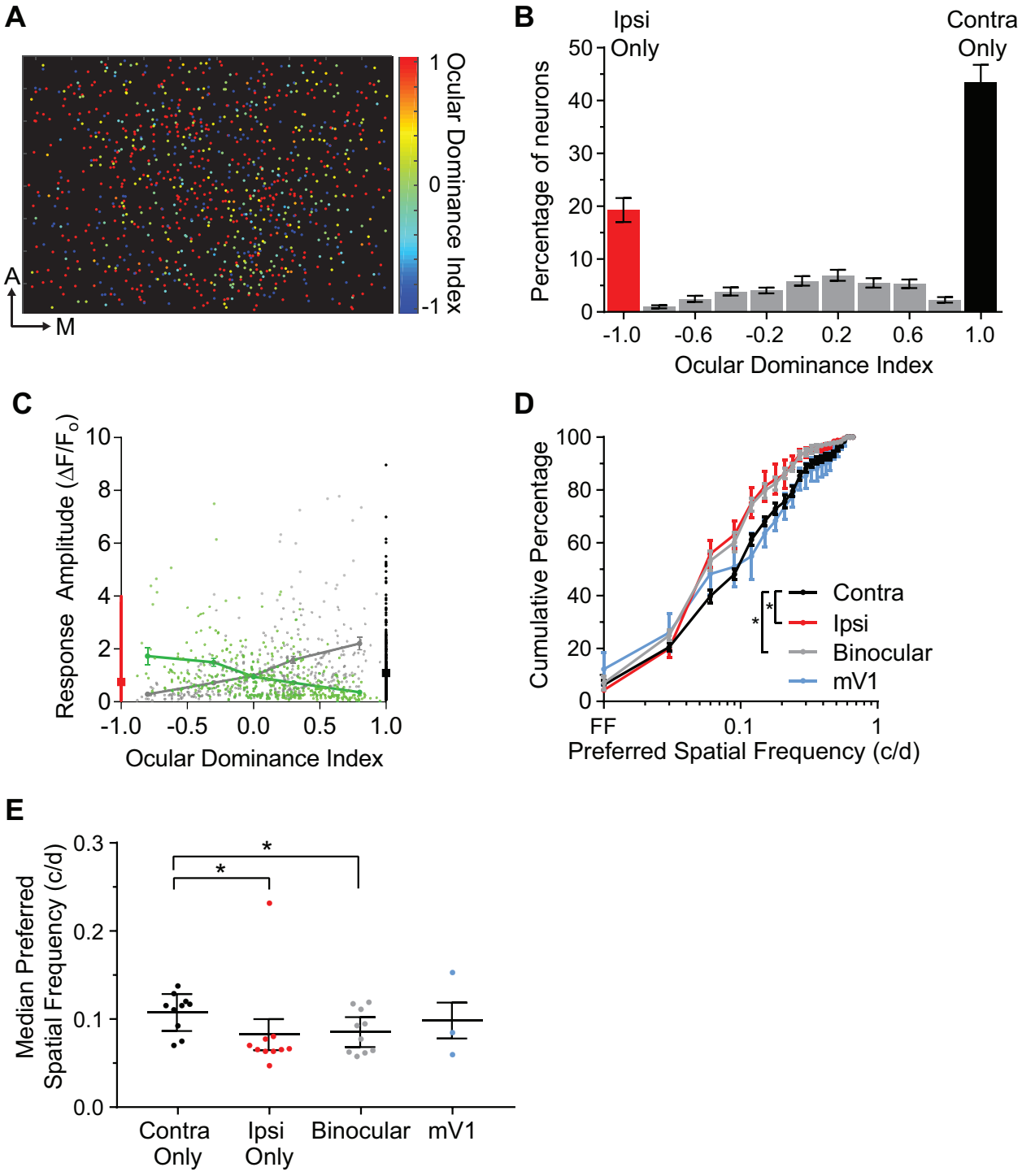

Figure 2.4: Contralaterally Dominated Cells are Tuned to Higher Spatial Frequencies than Binocular and Ipsilaterally Dominated Cells A. Ocular dominance index (ODI) was calculated as C-I/C+I. Single cells are color coded by ODI (N=10 mice, n=994 cells) for cells in binocular V1 (bV1). Scale bar is 50 µm. **B.** Binocular cells are shown in gray, cells that respond to the ipsilateral eye only are shown in red and cells that respond to the contralateral eye only in black. Error bars show standard error across animals (Overall ODI=0.268; Binocular only ODI=0.117, n=994 cells, N=10 mice). **C.** Binocular responses to the contralateral eye (gray dots) and ipsilateral eye (transparent green dots) are plotted as a function of ODI. Binned averages

are shown in solid lines. Monocular responses to the contralateral eye (solid black dots) and ipsilateral eye (solid red dots) are shown with their averages plotted as squares. **D.** Preferred spatial frequency for contralateral monocular (black), ipsilateral monocular (red), binocular (gray) cells and cells recorded in monocular V1 (mV1; blue). The preferred spatial frequency of the dominant eye response was used to plot the distribution for binocular cells. In binocular V1, the spatial frequency preferences for contralateral monocular cells are higher than for binocular cells and ipsilateral monocular cells (contra only median=0.113 c/d, n=481 cells; binocular median=0.0759 c/d, n=426 cells, KW, $p<0.0002$; ipsi only median=0.0687, n=214 cells, KW $p<0.0161$, N=10 mice; mV1 median=0.116 c/d n=226 cells, KW ns, N=3 mice). **E.** Data grouped by animal confirm that the preferred spatial frequency of contralateral monocular responses is significantly greater than ipsilateral monocular and binocular responses (contra only median=0.115 c/d; ipsi only median: 0.0658 c/d, Friedman test $p<0.0073$; binocular median=0.0850, $p<0.0278$, FM=9.8, N=10 mice). The preferred spatial frequency of contralateral monocular responses is not different from monocular V1 responses (mV1 median=0.0846 c/d, Friedman test ns, N=3 mice).

2.3.3 Binocular Matching of Spatial Frequency Tuning and Orientation Preference

During the ocular dominance critical period, the eye-specific orientation preferences of binocular neurons become better aligned in mouse area V1 (Wang et al., 2010; Wang et al., 2013). These binocular matching studies were performed at lower spatial frequencies (0.01-0.32 c/d) than in this study (0.03-1.0 c/d). In this lower range of preferred spatial frequencies, we found that neurons are largely matched in spatial frequency preference and orientation tuning (see example Figure 2.5a-left). In contrast, at high spatial frequencies, we found that binocular responses are more mismatched in spatial frequency and preferred orientation (see example Figure 2.5a-right). Overall, we found that contralateral and ipsilateral preferred spatial frequencies are moderately matched (Figure 2.5b, $r=0.372$, $p=0.0001$).

By using the spatial frequency bandwidth of cells as a threshold, we partitioned the binocularly responsive population into spatial frequency matched and mismatched groups (Figure 2.5b, gray area). 21.4% of binocular responsive neurons are mismatched in spatial frequency. For responses matched in spatial frequency (black), the orientation preferences of contra- and ipsilateral responses are also similar (Figure 2.5c; mean difference=18.5 degrees), in line with previous reports (Wang et al., 2010). In contrast, for cells mismatched

in spatial frequency preference (gray), orientation preferences are more discordant (mean difference=36.8 degrees), similar to the mismatch found after monocular deprivation during the juvenile critical period (Wang et al., 2010). We observed that neurons mismatched in spatial frequency tend to be more mismatched in orientation preference at spatial frequencies in which both the ipsilateral and contralateral eye were responsive (Figure 2.5d, $p<0.0001$). Moreover, high spatial frequency tuned neurons are more mismatched in orientation preference than low spatial frequency tuned neurons (Figure 2.5e, $p<0.0001$). These results reveal a significant population of neurons in binocular area V1 that have largely discordant response properties between the two eyes.

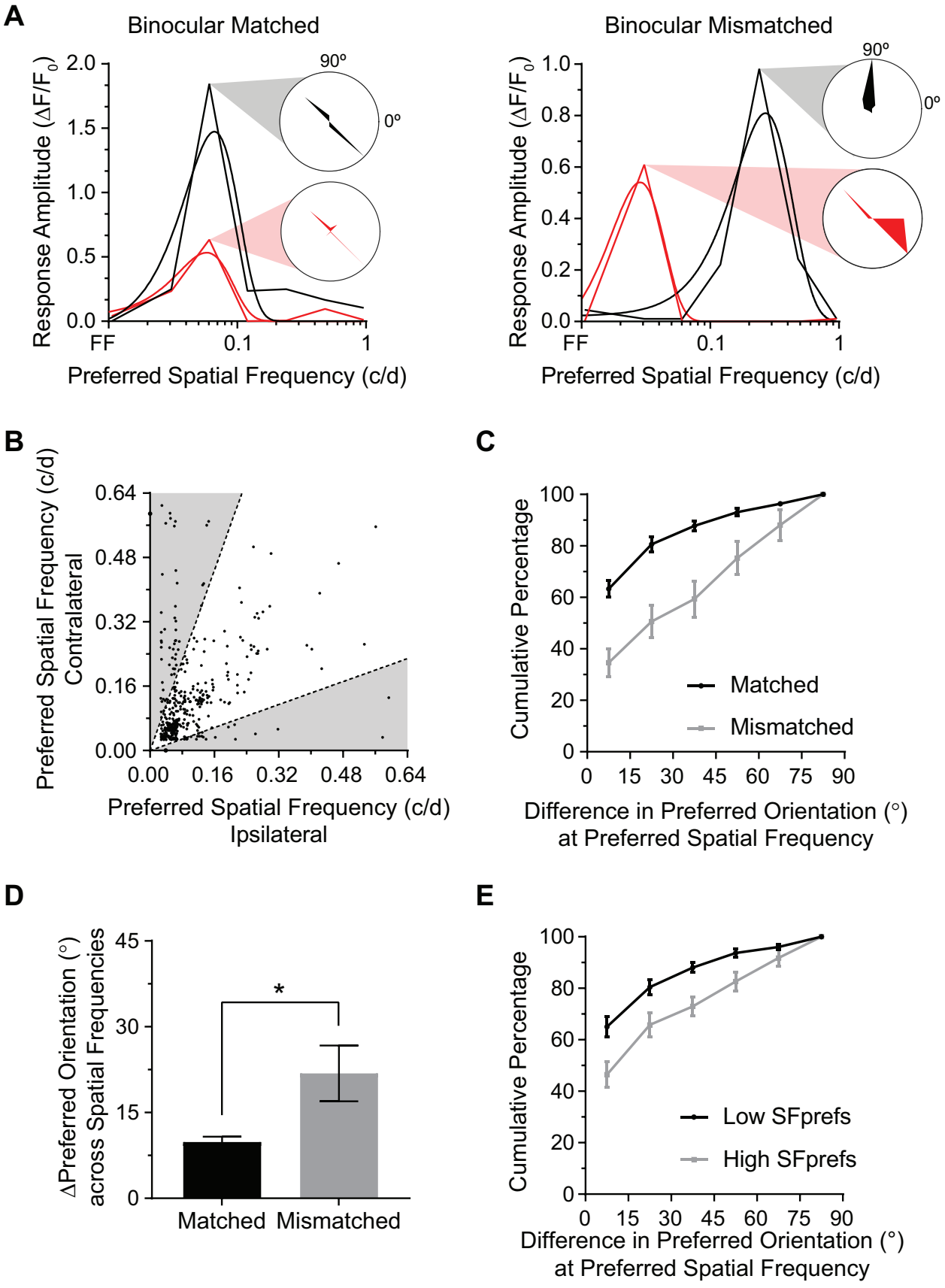
A
Binocular Matched
Response Amplitude (ΔF/F0)
2.0
1.5
1.0
0.5
0.0
90°
0°
FF
0.1
1
Preferred Spatial Frequency (c/d)
Binocular Mismatched
1.0
0.8
0.6
0.4
0.2
0.0
90°
0°
FF
0.1
1
Preferred Spatial Frequency (c/d)
B
Preferred Spatial Frequency (c/d)
Contralateral
0.64
0.48
0.32
0.16
0.00
0.00
0.16
0.32
0.48
0.64
Preferred Spatial Frequency (c/d)
Ipsilateral
C
Cumulative Percentage
100
80
60
40
20
0
Matched
Mismatched
0
15
30
45
60
75
90
Difference in Preferred Orientation (°)
at Preferred Spatial Frequency
D
ΔPreferred Orientation (°)
across Spatial Frequencies
45
30
15
0
*
Matched
Mismatched
E
Cumulative Percentage
100
80
60
40
20
0
Low SFprefs
High SFprefs
0
15
30
45
60
75
90
Difference in Preferred Orientation (°)
at Preferred Spatial Frequency

Figure 2.5: Binocular Neurons Mismatched in Spatial Frequency are Also Mismatched in Orientation Preference. A. (Left) Example cell with matched ipsilateral (red) and contralateral (black) eye spatial frequency tuning. The spatial frequency responses are overlaid with a Difference of Gaussians fit. Polar plots show matched orientation preferences of the ipsilateral and contralateral inputs at ~~the~~ peak spatial frequencies. (Right) Example cell with binocularly mismatched spatial frequency preferences. The orientation preferences of this cell are mismatched. **B.** The preferred spatial frequencies of binocular cells are shown for contralateral and ipsilateral eye stimulation (n=425 cells, N=10 mice). Dashed lines indicate a bandwidth-derived threshold (mean bandwidth+2*s.d.) used to separate spatial frequency matched cells from mismatched cells. **C.** The binocular differences in preferred orientation shown for spatial frequency matched (black) and mismatched cells (gray; mismatched n=75 cells; matched n=351 cells, N=10 mice). Cells that are binocularly mismatched in spatial frequency are also binocularly mismatched in orientation (matched mean orientation: 18.5 degrees, mismatched mean orientation: 36.8 degrees; MW(U)=7891, $p<0.0001$; KS D=0.309, $p<0.0001$). Error bars indicate standard error across animals. **D.** The difference in preferred orientation for binocularly matched (black) and mismatched (gray) cells calculated across all spatial frequencies in which there are significant responses to both the contralateral and ipsilateral eye. Error bars indicate standard error of the median. Mismatched cells are more orientation mismatched across common spatial frequencies than matched cells (matched median =9.85 degrees, n=493 cells; mismatched median= 21.8 degrees, n=87 cells; MW(U)=15181, $p<0.0001$). **E.** The binocular difference in preferred orientation shows that high spatial frequency preferring cells (gray, n=251 cells) are more mismatched in orientation than low spatial frequency preferring cells (black, n=175 cells; high spatial frequency cells mean difference in orientation: 27.5 degrees, low spatial frequency cells mean difference in orientation: 17.6 degrees; MW(U)=16593, $p<0.0001$; KS D= 0.206, $p<0.0003$). Error bars indicate standard error across animals.

2.3.4 Spatial Frequency Preferences are Similar for Contralateral Eye Viewing and Binocular Viewing

The finding that contralateral eye responses are significantly higher in preferred spatial frequency than ipsilateral eye responses and dominant-eye binocular responses calls to question how binocular viewing might influence the tuning of these cells. In a subset of recordings, we imaged responses to visual stimulation through each eye as well as through both eyes and compared the single cell tuning (Figure 2.6). Spatial frequency preferences of binocular viewing are strongly correlated with monocular viewing for responses to the contralateral eye and weakly correlated for ipsilateral responses (Figure 2.6, contra: r=0.992, ipsi: r=0.298). When we determine the composite spatial frequency tuning curve for ipsilateral, contralateral and binocular viewing, we find that the spatial frequency preferences are similar for contralateral eye stimulation and binocular

stimulation. These results suggest that the contralateral eye predominantly determines binocular cortical responses to high spatial frequency stimuli in mice.

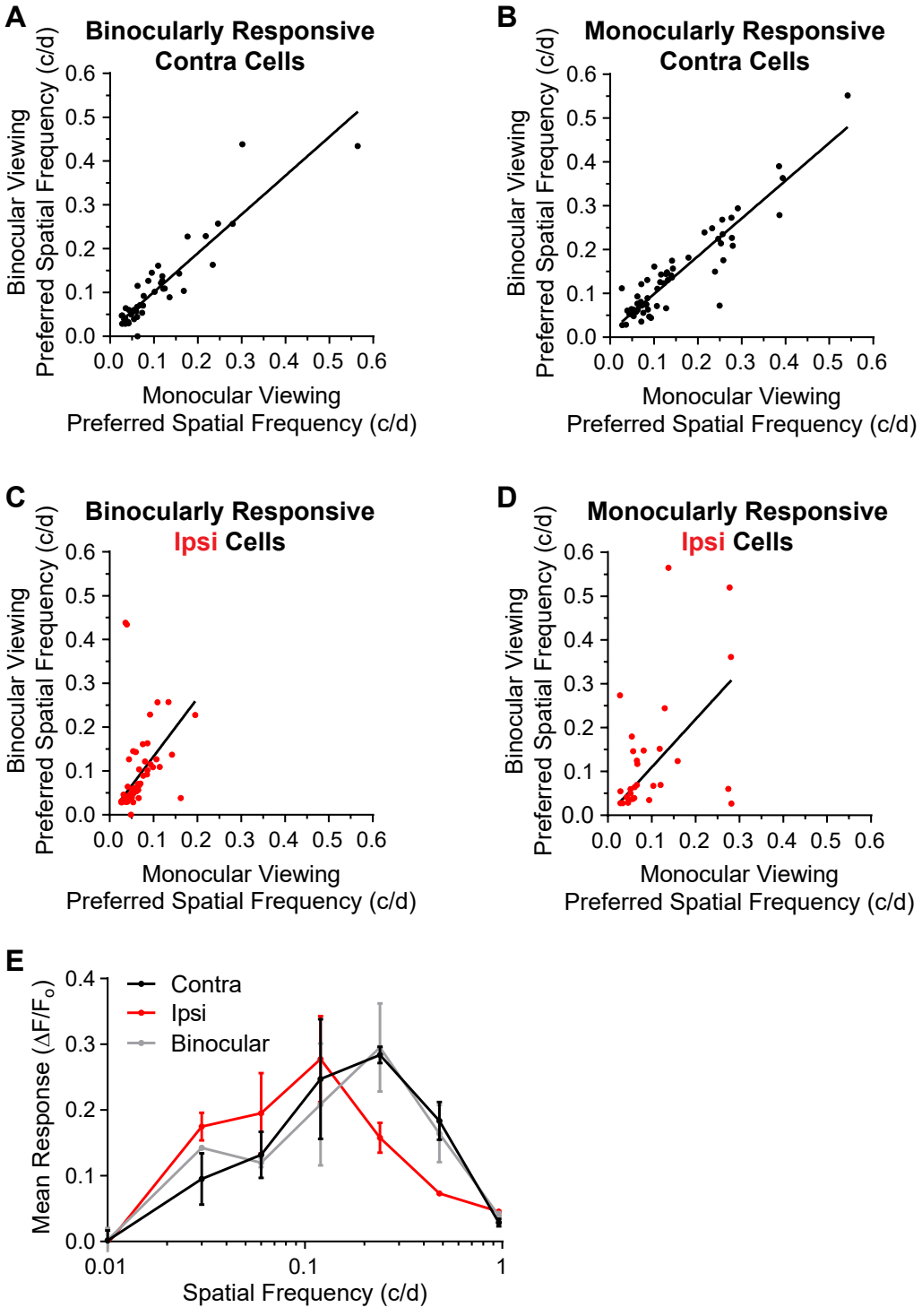

Figure 2.6: Binocular Viewing Does Not Increase Spatial Frequency Tuning of Contralateral Eye Responses. A, B. Spatial frequency preference of binocularly responsive cells (A) and monocularly

responsive cells (B) during binocular viewing is strongly correlated to monocular viewing through the contralateral eye (Binocular: Pearson r=0.922, p<0.0001, n=49 cells; Monocular: Pearson r=0.934, p<0.0001, n=67 cells). **C, D.** Spatial frequency preference of binocularly responsive cells (C) and monocularly responsive cells (D) during binocular viewing is weakly correlated to monocular viewing through the ipsilateral eye. (Binocular: Pearson r=0.451, p<0.0124, n=30 cells; Monocular: Pearson r=0.298, p<0.03, n=67 cells). **E.** Composite spatial frequency responses shown for contralateral (black), ipsilateral (red) and binocular viewing (gray).

2.3.5 Cardinal Direction Selectivity of Contralateral Responses

Next, we examined the direction selectivity of responses in binocular area V1. To highlight the differences in ipsilateral and contralateral responses, we used a spatial frequency threshold of one standard deviation above the mean preference to split the contralateral responses into high and low spatial frequency subpopulations (ipsi responses in red; <0.24 c/d contra in black; ≥0.24 c/d contra in dashed black). We found that the direction selectivity of high spatial frequency tuned contralateral responses is higher than low spatial frequency tuned contra- and ipsilateral responses (Figure 2.7a). We also found lower orientation selectivity in high spatial frequency selective contralateral responses (Figure 2.7b). It may be that the absence of a matching ipsilateral input prevents high spatial frequency selective, contralateral dominated neurons from sharpening orientation tuning during the critical period for binocular orientation matching (Wang et al., 2010). After eye opening, cortical responses are initially biased towards cardinal axes (0-180 and 90-270 degree axes; Rochefort et al., 2011; Hoy and Niell, 2015). By adulthood, the directional preference of cortical responses becomes balanced between cardinal and intercardinal directions (Hoy and Niell, 2015). Whereas the orientation-tuned ipsilateral (red) and low spatial frequency preferring (closed black) responses in our recordings are selective for both cardinal and intercardinal directions (ipsi: 55%; contra low: 54%, Figure 2.7c) the high spatial frequency preferring neurons (open black) prefer cardinal directions

(high contra: 82%, p=0.0001; Figure 2.7c). In monocular area V1, high spatial frequency, orientation-tuned neurons also responded with a strong preference for cardinal directions (Fig 2.5d; mV1 low 55%; mV1 high 91%, p=0.0024). Together, these results reveal the strong cardinal bias of high spatial frequency tuned contralateral responses.

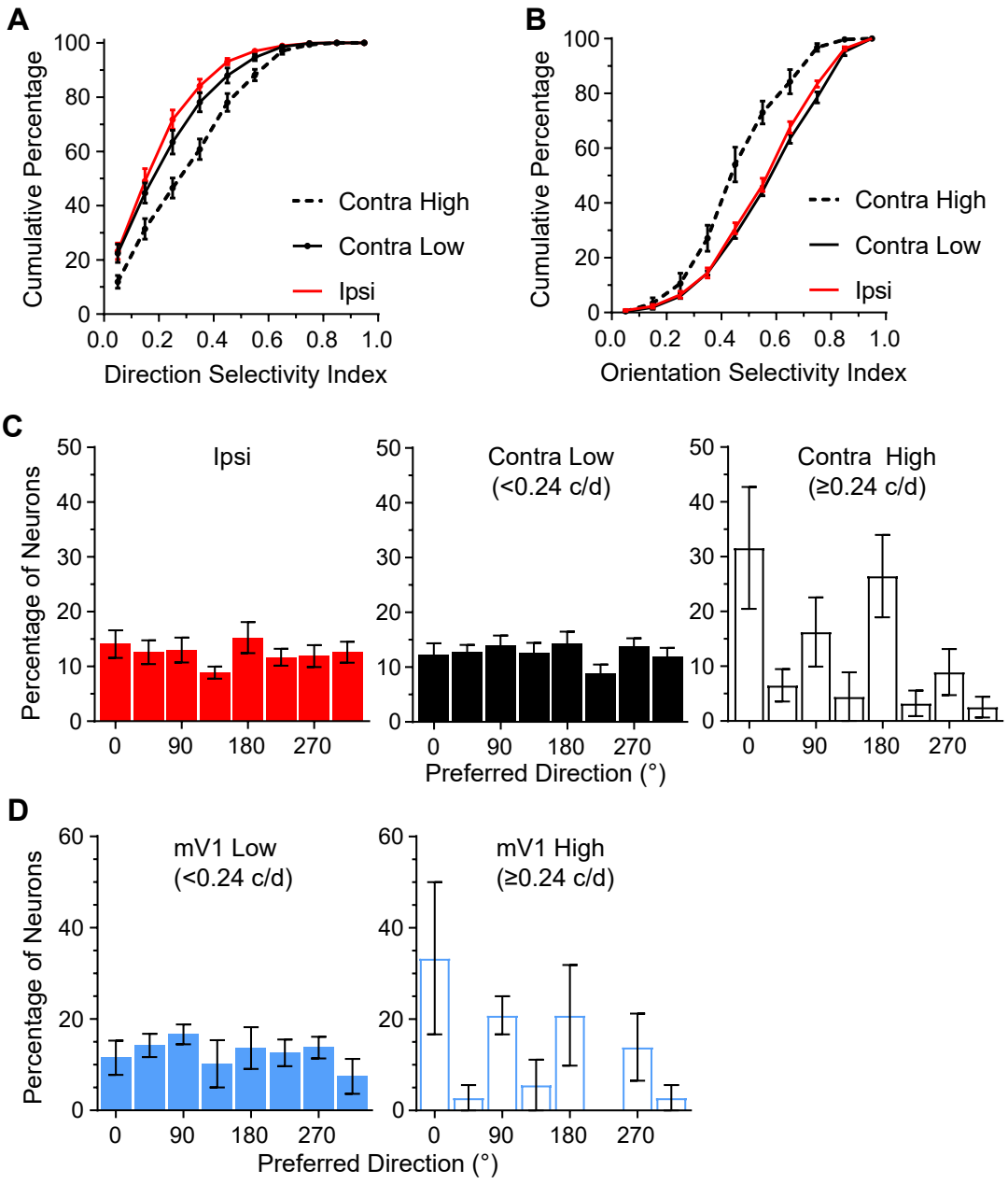

Figure 2.7: Higher Direction Selectivity and Cardinal Preference of Contralateral Responses. A. The direction selectivity for ipsilateral responses is shown in red and for contralateral responses in black. High spatial frequency preferring cells (dashed black) were separated from lower spatial frequency preferring cells (black) using one standard deviation above the population mean (0.24 c/d). Contralateral high spatial

frequency selective responses are more direction selective than contralateral lower spatial frequency selective and ipsilateral responses (median contra high: DSI=0.344, n=161 cells; median contra low: DSI=0.229, n=627 cells, p<0.0001; median ipsi DSI=0.203, n=561 cells, KW, p<0.0001, N=10 mice). Contralateral low spatial frequency selective responses were also slightly more direction selective than ipsilateral responses (KW, p<0.0405). **B.** Contralateral high spatial frequency tuned responses are less orientation selective than contralateral lower spatial frequency tuned and ipsilateral responses (contra high median OSI: 0.490, n=161 cells; contra low median OSI: 0.629, n=627 cells; KW, p<0.0001; ipsi median OSI: 0.611, N=10 mice, p<0.0001). **C.** Histograms of preferred direction are shown for ipsilateral responses (red bars), contralateral responses that prefer lower spatial frequencies (<0.24 c/d; black bars) and contralateral responses that prefer high spatial frequencies (≥0.24 c/d, black open bars), in all cases for responses that are orientation selective (OSI>0.5). Ipsilateral and contralateral low spatial frequency preferring cells are not biased towards cardinal directions (ipsi: 55% cardinal, MW(U)=529, ns; contra low: 54% N=10 mice). In contrast, orientation selective high spatial frequency preferring contralateral responses are more biased to cardinal directions (contra high: 82% cardinal MW(U)=341.5, p<0.0001, N=10 mice) than ipsilateral and contralateral low spatial frequency tuned cells (Chi-squared test, p<0.0001, contra high: n=78 cells; ipsi: n=388 cells, N=10 mice). **D.** In monocular V1 (mV1), high spatial frequency tuned cells (≥0.24 c/d, open blue) are more biased to cardinal directions than low spatial frequency tuned cells (<0.24 c/d, blue; high cells: 91% cardinal n=24 cells, low cells: 55% n=150 cells, MW(U)=24, p<0.0024; Chi-squared test, p<0.0002; N=3 mice). All error bars reflect standard error across animals.

2.3.6 Contralateral Bias for High Spatial Frequencies Present in Wildtype Mice

Since we were using transgenic GCaMP6s mice, it is possible that the eye-specific asymmetries of spatial frequency tuning we found are not representative of typical responses in wildtype mice. To confirm our findings we injected AAV-Syn-GCaMP6s into the binocular visual cortex of wildtype C57Bl6J mice. Despite the fact that this injection method does not label excitatory cells exclusively, we found a similar contralateral bias of high spatial frequency tuning in virally labeled animals as compared to the transgenic GCaMP6s mice (Figure 2.8a, p<0.0001). Although the spatial frequency preference for both contralateral and ipsilateral eye stimulation is overall higher with AAV injection, the ratios of contralateral to ipsilateral preferred spatial frequency are similar (tetO-GCaMP6s median ratio: 1.54, AAV injected median ratio: 1.7). The differences in spatial frequency tuning preferences are not attributable to differences in bandwidth (Figure 8b). We also found a similar ocular dominance distribution in wildtype and the transgenic line (Figure 2.8c; percent ipsi or contra only: tetOGCaMP6s: 62.7%, AAV injected: 50.8%). These results

confirm that the differences in spatial frequency tuning between contralateral and ipsilateral eye stimulation generalizes to the wildtype C57Bl6J strain.

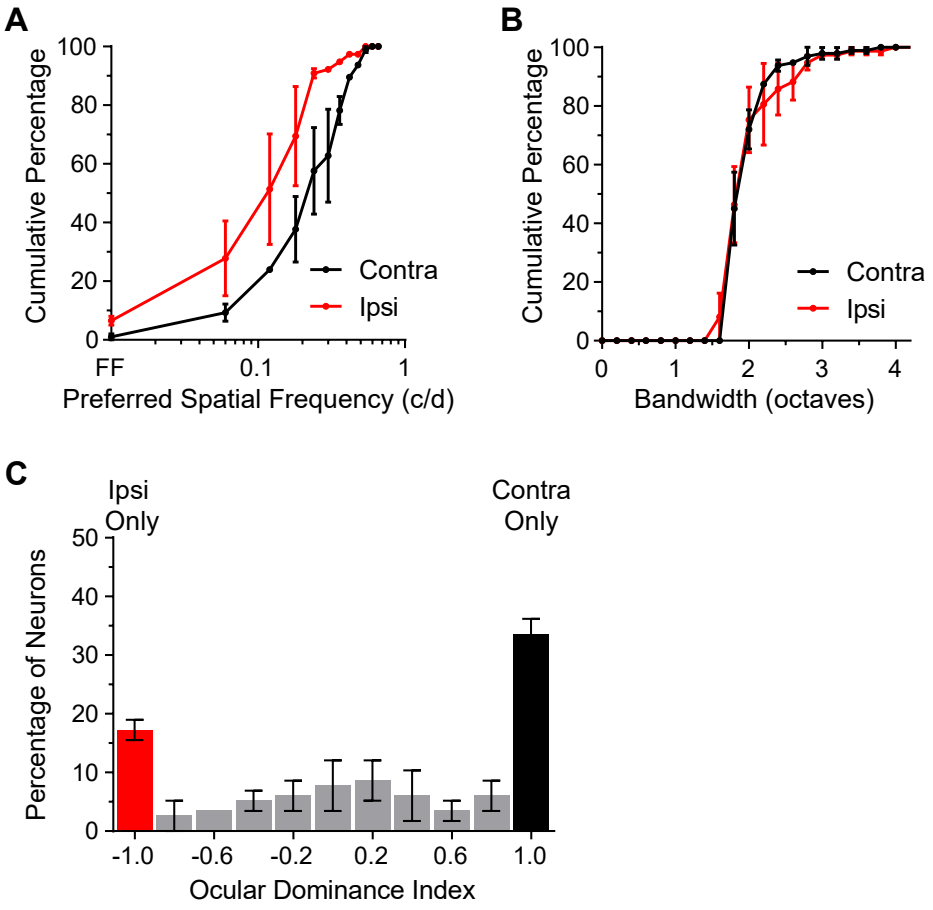

Figure 2.8: Spatial Frequency Preferences of Contralateral Responses is Higher than Ipsilateral Responses in AAV-SynGCaMP6s Injected Mice. A. The preferred spatial frequency is significantly higher for contralateral (black) than ipsilateral (red) responses (median contra=0.251 c/d, n=96 cells; median ipsi=0.148 c/d, n=76 cells; KS D=0.403, p<0.0001; MW(U)=1918, p<0.0001, N=2 mice). **B.** Distributions of bandwidth are plotted for contralateral (black) and ipsilateral (red) responses. The bandwidth for contralateral responses and ipsilateral responses are very similar (contra median=1.919; ipsi median=1.922; MW(U)=3579, p=0.717; KS(D)=0.139, p=0.372). **C.** Histogram of ocular dominance for neurons. Binocularly responsive cells shown in gray, cells that only respond to the ipsilateral eye shown in red and cells that only respond to the contralateral eye in black. Error bars show standard error of the mean across animals (overall mean ODI=0.202; binocular only ODI=0.077, n=116 cells, N=2 mice).

2.3.7 Contralateral Bias of Tuning Properties Not Explained by Behavioral State

The animal's behavioral state can strongly regulate the level of visual responsiveness in area V1 (Niell and Stryker, 2010; Lee et al, 2014; Fu et al., 2014)

particularly for neurons tuned to high spatial frequencies (Mineault et al., 2016). Since our recordings were performed in awake animals, we sought to rule out the possibility that fluctuations in behavioral state produced our results. We repeated our characterization of binocular spatial frequency tuning under anesthesia (Figure 2.9). We analyzed 582 neurons across three animals (total responsive: 70.32 ± 8.08%; contra responsive: 62.57 ± 8.11%; ipsi responsive: 28.91 ± 10.84%). Just as in awake recordings (Figure 3), we found higher spatial frequency tuning in contralateral responses (Figure 2.9a; median contra=0.0928 c/d vs. median ipsi=0.068 c/d). Approximately half of anesthetized cortical responses were monocular, similar to the percentage in our awake recordings (Figure 2.9c; anesthetized: 60%; awake: 62%). Altogether, these results discount the possibility that behavioral state fluctuations could account for our results.

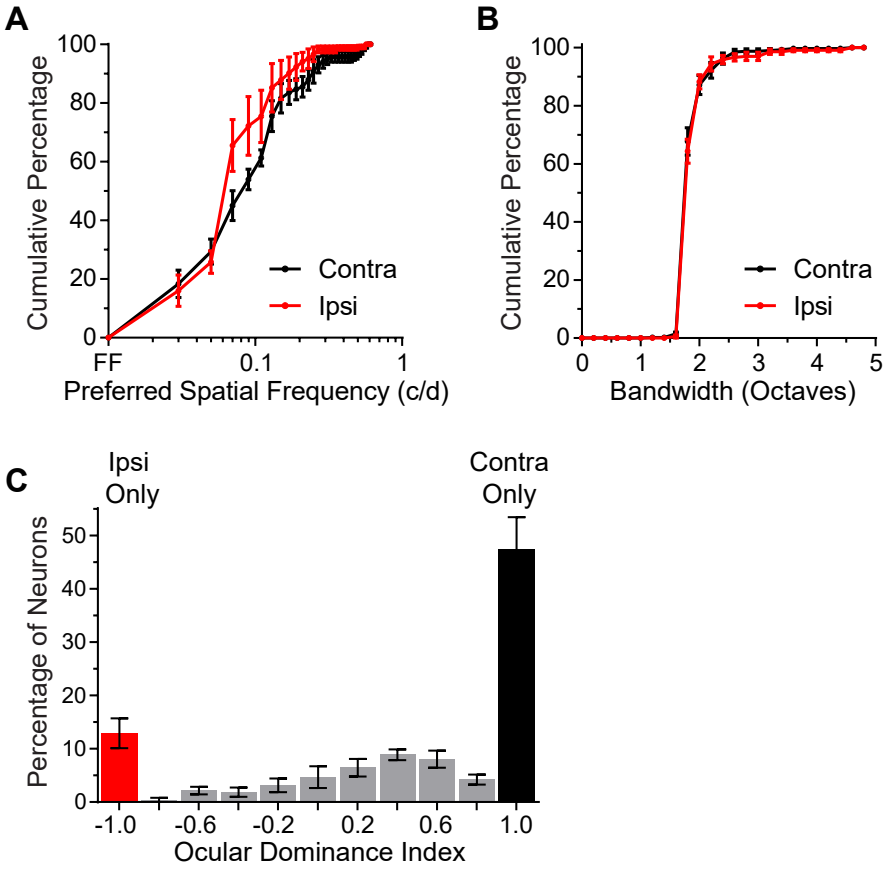

Figure 2.9: Higher Spatial Frequency Tuning of the Contralateral Responses Also Found in Anesthetized Animals. A. Cumulative distributions of preferred spatial frequency to contralateral (black, n=332 cells, N=3 mice) and ipsilateral (red, n=197 cells, N=3 mice) eye stimulation in binocular V1 of anesthetized mice. The preferred spatial frequency of contralateral responses is significantly higher than for ipsilateral responses (median contra=0.0928 c/d vs median ipsi=0.068 c/d; KS D=0.179, p=0.0007; MW(U)=29333, p=0.0474). **B.** Spatial frequency bandwidth distributions are similar for contralateral and ipsilateral responses (median contra=1.853 vs median ipsi=1.859; KS D=0.826, p=0.826; MW(U)=31645, p=0.752). **C.** Histogram of ocular dominance for neurons. Binocularly responsive cells are shown in gray. Cells that only respond to the ipsilateral eye are shown in red and cells that only respond to the contralateral eye in black. All distributions were binned and the mean across animals plotted. Error bars show standard error of the mean across animals.

It is possible that other visual circuits outside of binocular visual cortex respond selectively to high spatial frequency, cardinal oriented visual gratings and trigger a change in the animal's behavioral state. If so, then these stimulus-dependent behavioral state changes might be indirectly responsible for producing our results. Pupil size has been used as a sensitive metric for behavioral state changes in visual cortex (Vinck et al., 2015). We examined the pupillary dilation and eye velocity from a subset of our experiments (Figure 10). We found that eye velocities during ipsilateral and contralateral recordings were minimal, similar to a recent study of awake mice shown gratings of varying spatial frequencies and directions (Figure 10b; Mineault et al., 2016). To determine whether certain stimulus conditions modulated behavioral state directly, we examined the pupillary dilation across trials and stimulus conditions according to the eye shown the stimulus (Figure 10c). We observed no obvious relationship between pupil dilation and stimulus condition. Also, the pupillary dilations during contralateral and ipsilateral eye imaging sessions were comparable, suggesting that the behavioral state was not systematically different (Figure 10d). Altogether, these analyses do not reveal any overt behavioral state confound in our study.

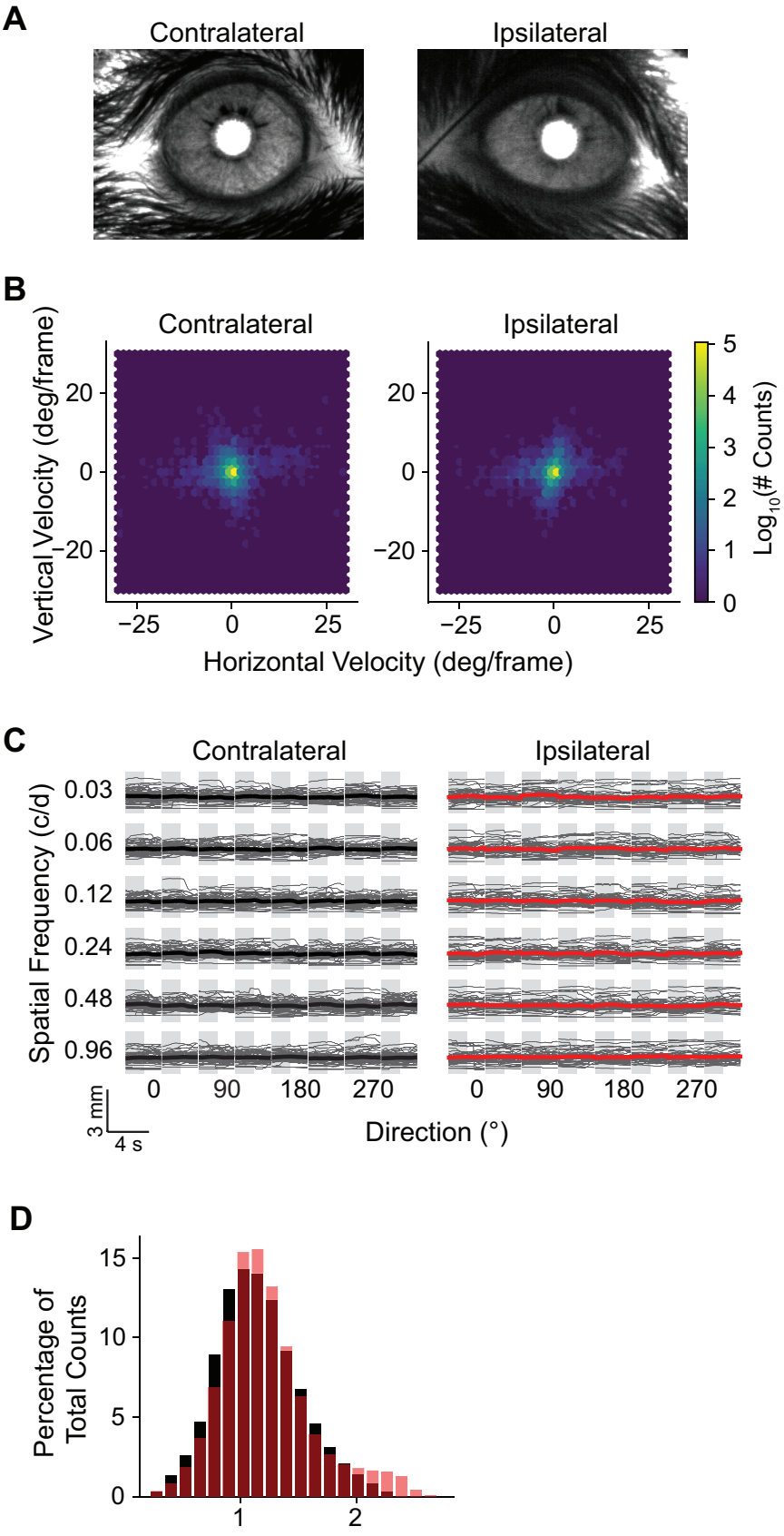
A
Contralateral
Ipsilateral
B
Contralateral
Ipsilateral
Vertical Velocity (deg/frame)
20
0
−20
−25
0
25
Horizontal Velocity (deg/frame)
Log10(# Counts)
5
4
3
2
1
0
C
Contralateral
Ipsilateral
Spatial Frequency (c/d)
0.03
0.06
0.12
0.24
0.48
0.96
0
90
180
270
3 mm
4 s
Direction (°)
D
Percentage of Total Counts
15
10
5
0
1
2
Pupil Diameter (mm)

Figure 10: Comparable Eye Movements and Pupillary Dilation during Contralateral and Ipsilateral Recordings. Sample snapshot of the contralateral (left) and ipsilateral (right) eyes revealed by two-photon IR laser light scattered through the brain. **B.** Spatial histogram of angular pupil velocity observed during calcium imaging for contralateral (left) and ipsilateral (right) eye presentation (contra, n=149,965 counts; ipsi, n=109,225 counts; N=2 mice). Pupil position remains largely static during recordings. **C.** Pupil diameter plotted as a function of spatial frequency and orientation for contralateral (black) and ipsilateral (red) recordings (contra, n=5 recordings; ipsi, n=4 recordings). No relationship between spatial frequency or orientation and pupil dilation is observed. **D.** Histograms comparing pupil diameter during contra (black) and ipsilateral (red) viewing. Counts are normalized as the percentage of total counts (contra, n=133,747 counts, mean=1.19 mm, SD= 0.36; ipsi, n=98,109 counts, mean=1.26 mm, SD=0.40, N=2 mice).

2.4 Discussion

Our study of the spatial frequency tuning of eye-specific cortical responses reveals pronounced asymmetries in spatial and direction processing in binocular area V1 of mice. Previous studies of binocular response properties in mouse area V1 only probe to 0.32 c/d (Wang et al., 2010; Vreysen et al., 2012), not to 1.0 c/d, as in our study. For this reason, previous studies likely missed many mismatched binocular cells and the highest spatial frequency tuned, contralateral-dominated cells. Also, previous binocular cortical recordings were performed under anesthesia. Arousal has been shown to influence the spatial frequency tuning of cortical responses in mice (Mineault et al., 2016). Nevertheless, we found the same asymmetry of the spatial frequency tuning of contralateral and ipsilateral responses in our anesthetized recordings (Figure 2.9) as we did in our awake experiments (Figure 2.3).

We found more contralateral and ipsilateral eye dominated responses in binocular area V1 (62%; Figure 2.3) than has previously been reported. While Dräger's initial study of binocularity in mouse area V1 reported a high prevalence of monocular neurons within binocular area V1 (Dräger 1975: ~32%), other studies reported fewer (Mrsic-Flogel et al., 2007: 5%; Gordon and Stryker, 1996: 11-23%). A recent study using the calcium indicator OGB-1 reports ~50% monocularly-dominated responses in binocular V1 (Scholl et al.,

2017). The high signal-to-noise of GCaMP6 recordings may have allowed us to pick up cells other techniques missed. Indeed, we found that the responses from monocular neurons was approximately half that expected from binocular responses (Figure 2.3). It is possible, however, that calcium imaging may be unable to detect very weak responses, missing the non-dominant eye input to cells that we identify to be monocular. Nevertheless, the ocular dominance of neuronal responses in our recordings was skewed towards the contralateral eye (mean ODI=0.289), in agreement with previous studies of single-cell binocularity (Dräger 1975; Gordon and Stryker 1996; Mrsic-Flogel, 2007; Wang et al., 2010; Gandhi et al., 2008). Monocularly dominated neurons in binocular area V1 may exhibit other distinctive response properties as compared to binocular cells.

One implication of our findings is that monocular mechanisms may be more important than binocular interactions in determining the spatial acuity of mice. At the limits of visual detection, binocular visual processing has been shown extensively to be more sensitive than monocular processing (Campbell and Green, 1965; Blake and Levinson, 1977; Anderson and Movshon, 1989). The perceptual facilitation of visual acuity by binocular viewing was initially corroborated by evoked potential studies of human visual cortex (Campbell and Maffei, 1970; Blake et al., 1981). Some psychophysical studies performed above contrast threshold later revealed that binocular facilitation of monocular processing is weak at high spatial frequencies (Apkarian et al, 1981; Bagolini et al., 1988; Tobimatsu and Kato, 1996). Our observation in mice that binocular neurons have lower spatial frequency tuning than contralaterally-dominated cells may provide a possible explanation for the lack of binocular facilitation at high spatial frequencies in humans.

In cat visual cortex, there is a strong correlation in the spatial frequency tuning of each eye for binocular neurons (Skottun and Freeman, 1984: preferred spatial frequency r=0.92; Saint-Amour, 2004: r=0.82). In contrast, we find a moderate degree of correlation in the preferred spatial frequency tuning of binocular neurons in mouse visual cortex (r=0.372, Figure 2.5b). One study in cat cortex finds more prevalent mismatch in the spatial frequency tuning of binocular neurons (Hammond and Pomfrett, 1991). Another study reports a small but significant tendency for spatial frequency mismatch in monocularly biased neurons (Skottun and Freeman, 1984). These findings may reflect functional asymmetries in eye specific visual pathways in the cat visual system that is more pronounced and amenable for study in mice. It is also possible that our findings reveal that housing conditions and/or genetic limitations may prevent the two distinct genotypes of laboratory mice studied here (wildtype c56/bl6 and tetO-GCaMP6s) from developing full high acuity binocular vision.

Our results in mice agree with classical findings that cortical neurons with the highest spatial frequency tuning are more directionally selective (De Valois et al., 1982b). The asymmetry of contralateral and ipsilateral cardinality, however, has not been examined previously. Humans perform better at making judgments about stimuli oriented along the cardinal axes (Girshick et al., 2011). Behavioral studies of visual acuity in mice typically use cardinally oriented stimuli (Prusky et al., 2000). Since we have found that the highest spatial frequency responses in binocular area V1 are cardinal and monocular, comparing mouse acuity using cardinal versus oblique stimuli may reveal a monocular bias.

The more accurate portrayal of binocular spatial frequency tuning elucidated in this study supports the possibility of distinct developmental mechanisms for acuity and binocularity. Psychophysical data from primates suggest that the critical periods for spatial acuity and binocular processing may be distinct (Harwerth et al., 1986). In addition, studies in mice (Kang et al., 2013; Stephany et al., 2014) and in cats (Murphy and Mitchell, 1986) have dissociated acuity development from binocular plasticity. Cellular and molecular studies of visual acuity development in mice have made the assumption that changes in high spatial frequency responses reflect binocular mechanisms yet we find that high spatial frequency responses are strongly dominated by the contralateral eye. Might monocular visual deprivation have distinct effects on monocular, contralaterally dominated responses in binocular visual cortex as compared to their lower spatial frequency selective binocular counterparts?

The contralateral bias of cardinal direction selectivity and high spatial frequency tuning we find in mouse binocular visual cortex is reminiscent of the functional segregation recently found in early stages of the mouse visual pathway. Direction selectivity along the cardinal axes has been found in the dendrites of retinal ganglion cells (Yonehara et al., 2013) while orientation selectivity has been found in the retina (Nath and Schwartz 2016). Furthermore, certain types of ganglion cells specialize in processing high spatial frequency information (Jacoby and Schwartz, 2017). Downstream, in the lateral geniculate nucleus (LGN), a distinct region has been identified that contains neuronal responses that have direction selectivity and cardinal bias (Marshel et al., 2012; Zhao et al., 2013; Piscopo et al., 2013). Interestingly, Piscopo et al., reported that these direction selective cells in LGN are higher spatial frequency tuned. More recently, thalamic afferents to mouse visual cortex

have also been reported to respond with directional and orientation tuning (Cruz-Martin et al., 2014; Kondo and Ohki, 2016; Sun et al., 2016; Roth et al., 2016). Furthermore, anatomical (Rompani et al., 2017) and functional (Howarth et al., 2014) evidence suggest that there may be eye-specific segregation of response properties in the LGN. Combining these observations, we postulate that in the mouse visual system high spatial frequency tuned and direction selective signals from the eye project contralaterally while lower spatial frequency tuned, non-or weakly- direction selective signals project ipsilaterally. To confirm whether the functional segregation we find in binocular visual cortex is present in the thalamus, tracing and eye-specific functional analysis of thalamocortical axons is needed.

Recent studies suggest that higher visual areas in mouse cortex are divided in a dorsal and a ventral stream (Wang et al., 2011; Wang et al., 2012; Smith et al., 2016). Given that area V1 sends functionally specific projections to different higher visual areas (Glickfeld et al., 2013), it may be that binocular low spatial frequency tuned and monocular high spatial frequency tuned cells bifurcate into dorsal and ventral streams. Since area LM, lateral to area V1, has been shown to be broadly tuned to spatial and temporal frequencies (Marshel et al., 2011), we might predict that it receives input from binocular, lower spatial frequency tuned V1 neurons. This pathway may mediate more complex binocular visual processing. Since Area PM, medial to area V1, prefers higher spatial frequencies and cardinal directions (Andermann et al., 2011; Glickfeld et al., 2013; Roth et al., 2012), we might predict it receives input from contra-dominated, monocular high spatial frequency neurons. Tracing studies with calcium imaging can test these predictions about the functional segregation of visual processing in mouse visual cortex.

CHAPTER 3: Eye-specific functional properties of higher visual areas LM and PM

3.1 Introduction

The functional architecture of the mammalian visual system is modular and hierarchically organized (Felleman and Van Essen, 1991; Van Essen, 1992). Maps of neurons encoding similar stimulus features are repeated multiple times along the cortical hierarchy, presumably to build complex representations from simpler ones. For instance, the visual field is encoded in all visually defined cortical areas, although retinotopy may vary in coarseness and have biases towards certain regions of visual space (Felleman and Van Essen, 1991; Zhuang et al., 2017). The re-mapping may allow the simultaneous processing of distinct aspects of the visual scene by parallel pathways (Ungerleider and Mishkin 1982; Maunsell and Newsome, 1987; Goldman-Rakic, 1988). In a similar manner, maps for spatial frequency, orientation, direction and eye-specificity are parsed and organized among higher visual areas, which are specialized for processing distinct visual features (Zeki, 1978; Marshel et al., 2011; Andermann et al., 2011; Glickfeld et al., 2013). In primates, the functional maps of spatial frequency, orientation and ocular dominance are interrelated in the cortical columns of primary visual cortex (V1) (Nauhaus et al., 2016). Moreover, the output of V1 has been demonstrated to parse functionally specialized information to higher visual areas (Movshon and Newsome, 1996).

Akin to humans and primates, mice also have distinct processing streams, interconnecting regions important for spatial navigation and form processing (Wang et al., 2011; Wang et al., 2012). There is also evidence that mouse V1 is modular and contains a broad distribution of spatiotemporal frequency tuned cells, capable of parsing stream-

related information to higher visual areas of cortex (Gao et al., 2013; Ji et al., 2015). Due to a lack of columnar organization of orientation, ocular dominance and spatial frequency in the mouse visual system, little is known about the relationship between these functionally specific neurons or how they relate to neurons downstream in higher visual areas. Despite a lack of columnar organization, neurons within mouse V1 share fundamental properties with primate V1. V1 neurons are tuned to each eye distinctly, carry spatiotemporal frequency information and vary in the degree of tuning for direction and orientation (Drager, 1975; Niell and Stryker, 2008). The relation between maps for ocularity, spatial frequency and orientation in primate V1 poses the question if the parcellation of distinct spatiotemporal tuning properties of higher visual areas is linked to the eye by which the information is coming from.

We have recently discovered an asymmetry in the tuning of eye-specific visual processing within mouse V1 (Salinas et al., 2017), suggesting that the functional specificity of V1 and higher order cortex could be regulated by eye-specific mechanisms. It is currently unknown whether eye-specific visual processing relates to stream segregation outside of V1. We sought to investigate if the eye-specific functional organization in V1 is also present in higher order areas of cortex, potentially serving a purpose for stream specialization. To characterize the eye-specific spatial and spatiotemporal frequency tuning of neurons in the putative ventral and dorsal stream, we recorded from hundreds of excitatory layer 2/3 neurons from areas V1, LM and PM while mice viewed drifting sinusoidal gratings through the contralateral or ipsilateral eye. We found conserved functional motifs in V1, LM and PM that are linked to eye-specificity and ocularity. Contralateral-dominated cells are tuned to the highest spatial frequencies, binocular cells are selective for orientation and monocular

cells are selective for direction. The distribution of eye-specific responses also match the expectation based on their spatial frequency tuning profile: PM contains more contralateral dominated cells and LM contains more binocular cells. Differences in eye-specific spatial frequency tuning could be a reflection of differences in speed preferences between the two eyes. Indeed, we do find contralateral eye responses are tuned to slower peak speeds than ipsilateral eye responses throughout V1, LM and PM. These results suggest that eye-specificity and ocularity are linked to feature preferences for orientation, direction, spatial frequency and temporal frequency in the mouse.

3.2 Materials and Methods

Most of the materials and methods are the same for the previous experiments probing eye-specific spatial frequency tuning in binocular V1 (Salinas et al., 2017). Refer to the materials and methods section for more information on previously reported methods. Exceptions to this will be indicated.

3.2.1 Animals

All protocols and procedures followed the guidelines of the Animal Care and Use Committee at the University of California, Irvine. To image evoked activity in excitatory neurons in areas, a Camk2a-tTA driver line (RRID: IMSR_JAX:007004) was crossed to a line expressing the calcium indicator GCaMP6s under the control of the tetracycline-responsive regulatory element (tetO) (RRID: IMSR_JAX:024742; Wekselblatt et al., 2016). The founder line was heterozygous for both transgenes and maintained by breeding with wildtype C57BL/6 mice (RRID: IMSR_CRL:642). Mice were weaned at P18-21 and co-housed with one or more littermate until the day of window implantation (P73-200). Mice of either sex were used in the experiments.

3.2.2 Cranial Window Implantation

See Section 2.2.2 Cranial Window Implantation

3.2.3. GCaMP6s Virus Delivery

To assess visual responses of boutons from primary visual cortex to higher visual areas, AAV-Syn-GCaMP6s (Chen et al., 2013) (Upenn Vector Core AV-1-PV2824) was injected into wildtype mice two to three weeks prior to two-photon imaging. Intrinsic signal imaging maps of retinotopy were used to target injections into the binocular zone of primary visual cortex. Virions were diluted with ACSF to ~$2x10^{11}$ GC/mL and 80-200nL injected at a rate of 10nL/min at depths of 250 um and 450 um below the surface. Lactated Ringer's (0.2mL/20g/hr, s.c.) were given to prevent dehydration. Mice were allowed to recover on a warm heating pad following surgery (<15 minutes).

3.2.4 Visual Area Mapping

Retinotopic maps of azimuth and elevation were used to generate a visual field sign map (Sereno et al., 1994; Garrett et al., 2014) to designate borders between visual areas. See Section 2.2.4 for retinotopic mapping.

3.2.5 Two-Photon Calcium Imaging

Fluorescence was gathered with a resonant two-photon microscope (Neurolabware, Los Angeles, CA) with 900-920 nm excitation light (Mai Tai HP, Spectra-Physics, Santa Clara, CA). Emissions were filtered using a 510/84nm BrightLine bandpass filter (Semrock, Rochester, NY). A 16x (Nikon NA=0.8) water immersion lens was used. Image sequences typically covered a field of approximately 700 μm by 500 um for cell recordings in V1 and LM or approximately 500um μm by 400 um for cell recordings in PM and were acquired at

7.7 or 12 Hz (1024 or 660 lines) using Scanbox acquisition software (Scanbox, Los Angeles, CA) at a depth of 200-250 μm below the pia.

Recordings from binocular V1 were confined to regions adjacent to the intersection of the horizontal and vertical meridians at the border of V1 and LM. Recordings from area LM were restricted to the anterior portion of LM, as close the central visual field coverage as possible, while recordings from PM were performed in both the anterior portion (more central visual field) and posterior portion of PM (more peripheral visual field). Although we did notice an enhancement for spatial frequency tuning in higher elevations of PM, we decided to pool all responses to increase the power.

3.2.5.1 Two-Photon Visual Stimuli

Visual stimuli were generated by custom-written python code using the PsychoPy 1.8 library. For the spatial frequency tuning protocol, full field drifting sinusoidal gratings were presented eight orientations (0-315, 45^{o} steps) and six spatial frequencies (0.03-0.96 c/d, logarithmically spaced) at a fixed temporal frequency (2Hz for LM and V1, 1Hz for PM) using a gamma corrected Acer V193 monitor (53 x 33 cm, 60 Hz refresh rate, 20-30 cd/m^2) or 54" LED LG TV (model 55LB5900, 60 Hz refresh rate, 20-30 cd/m^2). For the speed tuning experiment, full field drifting sinusoidal gratings were presented at four orientations (0,90,180,270), five spatial frequencies (0.03-0.48 c/d, logarithmically spaced) and four temporal frequencies (1-8 Hz, logarithmically spaced). The visual stimulus was spherically corrected. In addition to the 48 grating stimuli, we also showed a blank condition and a condition in which the whole monitor flickered at 2 Hz (FF). The 50 total stimulus conditions were presented in a random order for each of the 8 repetitions. For each trial, the stimulus was presented for 2 seconds, followed by 2

seconds of grey screen. The visual stimulus was presented either first to the ipsilateral or the contralateral eye.

3.2.6 Data Analysis

3.2.6.1 Cellular Responses

Custom-written Python routines were used to remove motion artifact, identify cell ROIs, extract calcium fluorescence traces, and perform analyses. See Section 2.2.6.1

To determine a cell's response to each stimulus trial, the cell's trace during the stimulation period was normalized to the baseline value averaged over the 0.75 seconds preceding stimulus presentation. The cell's response to a given orientation θ_i was defined as the average response across the 8 repeats of each condition: $F(\theta_i)$. An estimate of the cell's spontaneous calcium fluctuation was determined using the cell's trace during the blank condition. For the spatial frequency tuning protocol, at each spatial frequency, a cell's responsiveness was determined using a one-way ANOVA ($p<0.01$) across orientations against the blank condition. For the speed tuning protocol, a cell's responsiveness was first determined using a one-way ANOVA with a Bonferonni correction ($p<0.05/(5 \text{ SFs} * 4 \text{ TFs})= p<0.0025$).

3.2.6.2 Preferred Orientation

See Section 2.2.6.2

3.2.6.3 Preferred Spatial Frequency (Spatial Frequency Tuning Protocol

See Section 2.2.6.3

3.2.6.4 Orientation and Direction Selectivity

See Section 2.2.6.4

3.2.6.5 Ocular Dominance Index

See Section 2.2.6.5

3.2.6.6 Preferred Speed (Speed Tuning Protocol)

To determine a cell's preferred speed, responses across all spatial and temporal frequencies were fit with a two-dimensional elliptical Gaussian (Priebe et al., 2006; Andermann et al., 2011):

$$R(sf, tf) = A\ exp\left(\frac{-(\log_2 sf - \log_2 sf_o)^2}{2(\sigma_{sf})^2}\right)\ exp\left(\frac{-(\log_2 tf - \log_2 tf_p(sf))^2}{2(\sigma_{tf})^2}\right)$$

where A is the neuron's maximum responses, sf_o and tf_o are the preferred spatial and temporal frequency and σ_{sf} and σ_{tf} are the tuning widths for spatial and temporal frequency. From this fit we are able to obtain the dependence of temporal frequency preference on spatial frequency by calculating the speed tuning index, ξ, such that $\log_2 tf_p(sf) = \xi\ (\log_2 sf - \log_2 sf_o) + \log_2 tf_o$. A neuron with a speed tuning index of $\xi = 1$ is a speed-tuned cell, while $\xi = 0$ is not speed-tuned and $\xi = -1$ is anti-tuned. To measure goodness of fit, we used two approaches. First, the fitted data must be well correlated with the raw data (fit correlation greater than 0.5). The confidence intervals for preferred spatial and temporal frequency must not exceed 2 octaves. For speed tuning analysis, the confidence intervals for the speed-tuning index must not exceed 1.

3.2.6.7 Experimental Design and Statistical Analyses

Data was tested for normality before choosing the appropriate statistical tests for differences in cellular distributions. One-way ANOVAs were used to detect differences between areas in percent responsive and Tukey's post hoc multiple comparisons test was

used to detect differences between area pairs. Kruskall-Wallis tests were used to determine differences in cellular distributions between areas for ODI, preferred spatial frequency, orientations selectivity, direction selectivity, binocular matching for orientation and spatial frequency, speed preferences and eye-specific spatial frequency tuning in V1 to LM and V1 to PM afferents. To test differences in eye-specific speed tuning, and in V1 to LM or V1 to PM ODI and spatial frequency afferent tuning, both Mann-Whitney and Kolmogorov-Smirnov tests were used. Statistical analyses were performed using Prism v7.01 (GraphPad).

3.3 Results

To probe eye-specific spatial frequency tuning of V1, LM and PM, we used a transgenic mouse line that expresses GCaMP6s under the control of the CaMK2 promoter (CaMK2-tTA;tetO-GCaMP6s; Wekselblatt et al., 2016). Visual areas were identified using calcium widefield imaging to retinotopically map elevation and azimuth (visual field sign map; Garrett et al., 2014; Figure 1a, bottom left; Figure 1b). The overlaid maps were used as a guide to position two-photon microscopy recordings in the correct areas. Recordings were directed as close to the central visual field as possible in each area, although biases exist in the retinotopic organization of areas LM and PM (Zhuang et al., 2017). Cellular imaging was performed in awake, head-fixed mice that were acclimated to the setup over several days. Mice were shown a visual stimulus through either the contralateral or ipsilateral eye (Figure1a, top right) to probe spatial frequency and speed tuning. For the spatial frequency tuning protocol, the stimulus consisted of two-second presentations of drifting sinusoidal gratings at one of eight directions and one of six spatial frequencies

(0.03-0.96 c/d spaced logarithmically; see Figure 1c). We interleaved the presentation of a full field flickering stimulus with the gratings to detect neurons tuned to very low spatial frequencies. Each stimulus condition was repeated 8 times per eye. We used a similar approach to probe speed tuning with these few exceptions: the visual stimulus consisted of two second presentations of drifting visual gratings at one of four directions (cardinal), one of five spatial frequencies (0.03-0.48 c/d spaced logarithmically) and one of four temporal frequencies (1:8 Hz spaced logarithmically).

We characterized cellular responses to stimulation of either the contralateral eye or ipsilateral eye separately in V1, LM and PM (example traces for spatial frequency tuning protocol in Figure 3.1c). Eye-specific responses (Figure 1d, solid lines) were fit by a difference of Gaussians model to determine preferred spatial frequency (Figure 3.1d, dashed lines). In each area we found cells that were visually responsive to both eyes (Figure 3.1d, see V1 and LM) and cells that were only visually driven when the stimulus was presented to one eye (Figure 3.1d, see PM). Altogether we imaged 5,503 cells from ten animals (V1: 1855 cells, LM: 1714 cells, PM: 1934 cells). We restricted our analysis to cells whose responses at the peak spatial frequency reached significance when compared against the blank condition for spatial frequency tuning protocol ($p<0.01$, ANOVA) or for cells whose responses reached significance when compared against the blank condition, with a Bonferonni correction for multiple comparisons for the speed tuning protocol ($p<0.0025$, ANOVA). Overall, we found that areas V1, LM and PM were well driven by drifting sinusoidal gratings (Figure 3.1d; Left: spatial frequency tuning protocol: V1 mean and SEM: 52.1 +/- 2.14%, LM: 53.2 +/- 3.94%, PM: 31.63 +/- 3.32%; Right: speed tuning protocol: V1 mean and SEM: 59.0% +/- 6.36, LM: 64.9 +/-9.75, PM: 39.5+/- 4.79). Area PM

was less responsive to drifting sinusoidal gratings than V1 and LM, as expected by previously reported and for a higher visual area (Marshel et al., 2011).

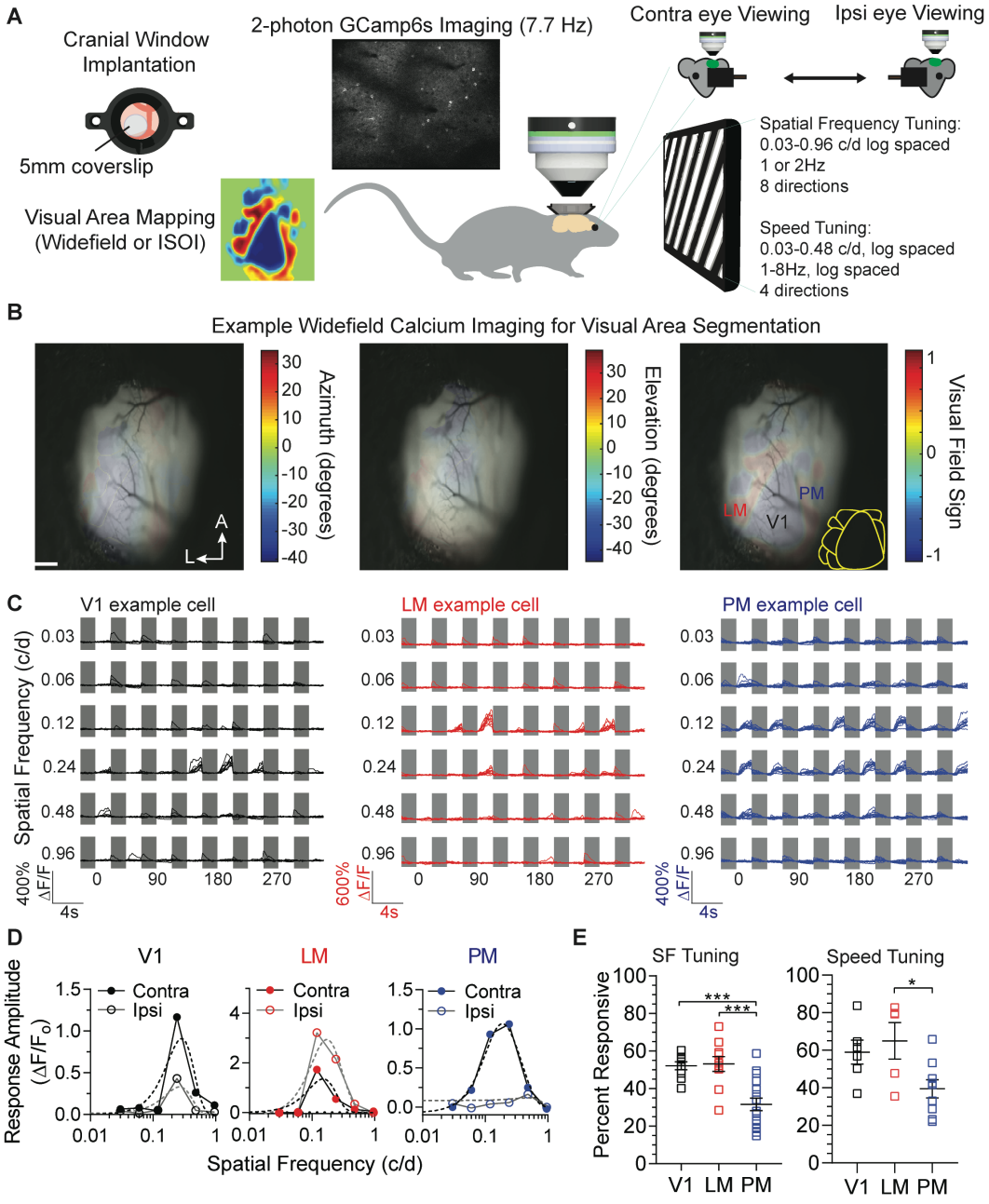

Figure 3.1: Assessment of Spatial Frequency Tuning across V1, LM and PM using GCaMP6s Mice. A. Experimental setup. **B.** Widefield calcium imaging yields retinotopic maps of azimuth (Left) and elevation (Middle), which are used to produce a visual field sign map (Right). The visual field sign map identifies boundaries between visual cortical areas, notably V1, LM and PM. Scale bar is 1mm. Corresponding diagram for mouse visual cortex is shown in bottom right corner. **C.** Visually evoked responses across V1 (left, black), LM (middle, red) and PM (right, blue) were measured in head-fixed, awake mice as they viewed drifting sinusoidal gratings. For the spatial frequency protocol, sinusoidal gratings of six spatial frequencies (0.03,

0.06, 0.12, 0.24, 0.48, 0.96) in eight directions were presented for two seconds (white box) with an intermittent two-second off period (grey box). Each imaging session consisted of eight repeats shown to either the contralateral or ipsilateral eye. **D.** Spatial frequency tuning curves for the example cells shown in B. Filled dots correspond to responses driven by the contralateral eye and open dots correspond to responses driven by the ipsilateral eye. Fits to the tuning curves are shown as dashed lines (contra viewing: black, ipsi viewing: grey). Cells vary in degree of binocularity, with some cells being visually responsive to both eyes and some cells to only one eye (See PM example cell, which was only visually responsive through contra eye) **E.** Total percent of visually responsive neurons recorded by field for the spatial frequency tuning protocol (left) or the speed tuning protocol (right) for each area (V1: black open squares; LM: red open squares and PM: blue open squares). In both comparisons, we found that area PM was less responsive to drifting gratings than areas V1 or LM (Spatial frequency tuning protocol by field Mean and SEM: V1: 52.16% +/- 2.14, n=9 fields, N=10 mice; LM: 53.16% +/- 3.94, n=10 fields, N=10 mice, PM: 31.63% +/- 3.32, n=16 fields, N=10 mice, one-way ANOVA $p<0.0001$, Tukey's multiple comparisons test: V1 vs. PM $p=0.0005$; LM vs. PM $p=0.0002$; Speed tuning protocol by field Mean and SEM: V1: 59.00% +/- 6.36 %, N=6 mice, n=6 fields, LM: 64.99 +/- 9.75, N=5 mice, n=5 fields, PM: 39.46 +/- 4.79, N=6 mice, n= 9 fields, one-way ANOVA $p=0.0263$; Tukey's multiple comparisons test: LM vs. PM $p=0.0420$; V1 vs. PM $p=0.0802$).

3.3.1 Distinct spatial frequency and eye-specific tuning in V1, LM and PM

We characterized the ocular dominance distribution (ODI) of cells in V1, LM and PM as previously described (Salinas et al., 2017). All three areas have a contralateral bias to their ODI distribution (Figure 3.2a, V1 median: 0.62; LM: 0.39, PM: 0.71). However, area LM has fewer contralateral-dominated neurons than area PM, as noted by the leftward shift in the cumulative distribution of ODI (Figure 3.2b). The high contralateral bias in PM could be attributed to PM containing fewer ipsilateral only responsive neurons than V1 (Figure 3.2c). Area LM, known to prefer relatively lower spatial frequencies (Marshel et al., 2011), has a more binocular ODI distribution than area PM, known to prefer relatively higher spatial frequencies (Marshel et al., 2011; Andermann et al., 2011).

We verified the distinct spatial frequency tuning of LM and PM previously reported, with LM preferring lower spatial frequencies than PM (Marshel et al., 2011; Figure 3.2d,e). The contralateral bias to high spatial frequencies is present in all three areas investigated (Figure 3.2e), suggesting that these cells may play a role in high spatial frequency information. The eye-specific response properties of V1, LM and PM suggest that binocular cells specialize in processing low spatial frequency information while contralateral-

dominated cells process higher spatial frequency information. Indeed, within all three areas, ODI is positively correlated with spatial frequency tuning. The coupling of ocularity with spatial frequency tuning has been described previously in primates (Nauhaus et al., 2016). Thus, although mice lack columnar organization for ocular dominance columns, it does appear that eye-specificity could link cell-type specific functional circuitry at multiple levels of cortex.

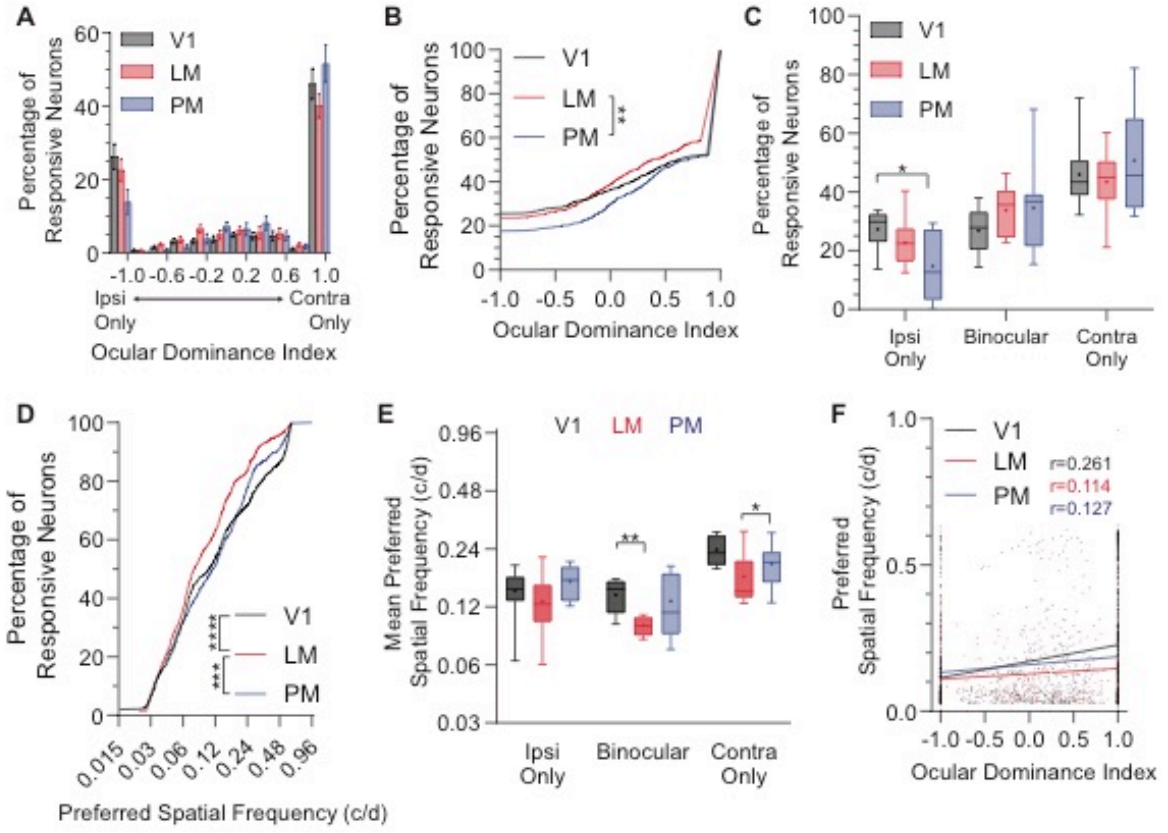

Figure 3.2: Distinct spatial frequency and eye-specific tuning in V1, LM and PM. A. Ocular dominance index was calculated as contra- ipsi / contra + ipsi, placing contralateral dominated cells with an ODI near 1 and ipsilateral dominated cells near -1. Cells responsive during only contra or ipsi eye viewing were given an ODI of 1 or -1, respectively. Ocular dominance distributions were binned by field and the mean plotted for V1 (black), LM (red) and PM (blue). Error bars represent SEM. **B.** Cumulative distribution for ocular dominance indices are shown for V1, LM and PM of the same animals. Area LM has fewer cells dominated by the contralateral eye than area PM (Median ODI for V1= 0.62, n=986 cells; LM median= 0.39, n=867 cells; PM median=0.71, n=527 cells, KW(s)=8.709, LM vs. PM p=0.0099, N=9 animals). **C.** Percentage of responsive neurons grouped into the three categories (ipsi only responsive, binocular, contra only responsive) are plotted for areas V1, LM and PM. Area PM has fewer cells responsive to only the ipsilateral eye than V1 (V1 mean ipsi only responsive: 24.45%, LM mean ipsi only responsive: 21.06%; PM mean ipsi only responsive: 13.86%, Two-way RM ANOVA, Dunnett's multiple comparisons test V1 vs. PM p=0.0245). **D.** Cumulative

distribution of preferred spatial frequency for all neurons in each area for the same animals is shown from V1, LM and PM. Neurons in area LM are tuned to lower spatial frequencies than those in V1 or PM (V1 median preferred spatial frequency: 0.105 c/d, n=986 neurons LM: 0.077 c/d, n=916 neurons, PM: 0.115 c/d, n=527 neurons, KW(s)=24.6, $p<0.0001$, Dunnett's multiple comparisons test V1 vs. LM $p<0.0001$, LM vs. PM $p=0.0009$). **E.** Box and whisker of mean preferred spatial frequency of ipsi only (left), binocular (middle) and contra only (right) responsive cells are plotted for V1 (black), LM (red) and PM (blue). Binocularly responsive cells in LM were tuned to lower spatial frequencies than V1 (V1 binocular mean preferred spatial frequency: 0.139 c/d, LM: 0.096 c/d, PM: 0.129 c/d, Mixed-effects model (REML), eye-specificity factor $p<0.0001$, area factor $p=0.0142$; V1 vs. LM $p=0.0027$, Tukey's multiple comparisons). Contra only responsive cells in LM were tuned to lower spatial frequencies than PM (V1 contra only mean preferred spatial frequency: 0.238 c/d, LM: 0.172 c/d, PM: 0.210 c/d, V1 vs. LM $p=0.0354$, Tukey's multiple comparisons) **F.** Scatter of preferred spatial frequency and ocular dominance index is shown for areas V1 (black), LM (red) and PM (blue) with linear regression plotted (lines). Preferred spatial frequency is significantly correlated with ocular dominance index in each area (V1: $r=0.261$, n=986 neurons, $p<0.0001$; LM: Pearson $r=0.114$, n=867 neurons $p=0.0007$; PM: Pearson $r=0.127$, n=561 neurons, $p=0.0036$, N=9 mice).

3.3.2 Binocular and monocular cells are tuned to orientation and direction

Orientation and direction are important precursors for ventral and dorsal stream processing. Orientation is closely associated with form processing at early levels while high direction selectivity is important for the processing of motion (Blasdel and Fitzpatrick, 1984; Movshon and Newsome 1996; Maunsell and Newsome, 1987). We probed orientation and direction tuning in V1, LM and PM to see if eye-specific or ocular biases exist in their preference for these features, as they do with spatial frequency. In LM and PM, we find that the binocular cells have higher orientation selectivity indices (OSI) than either the contralateral or ipsilateral only cells (Figure 3.3a). The lack of such a distinction in PM may account for the overall less orientation tuning of PM than LM and V1 (Figure 3.3b, $p<0.0001$). It may be that the binocular cells of PM are a result of convergence from lower orientation-tuned contralateral and ipsilateral only cells of V1 and/or LM. We quantified the percentage of orientation-tuned (OSI>0.5) cells by animal and find that more binocular cells are orientation-tuned than monocular cells in V1 and LM (Figure 3.3c). Pooled responses for all three areas based on ocularity suggest that binocular cells are overall more orientation-tuned than monocular cells (Figure 3.3d). We find that the

monocular cells have higher direction selectivity indices (DSI) than the binocular cells in V1, LM and PM (Figure 3.3e). However, we did not find any areal differences in the distribution of pooled DSI preferences (Figure 3.3f). A higher percentage of monocular cells are direction-tuned than binocular cells (Figure 3.3g-h).

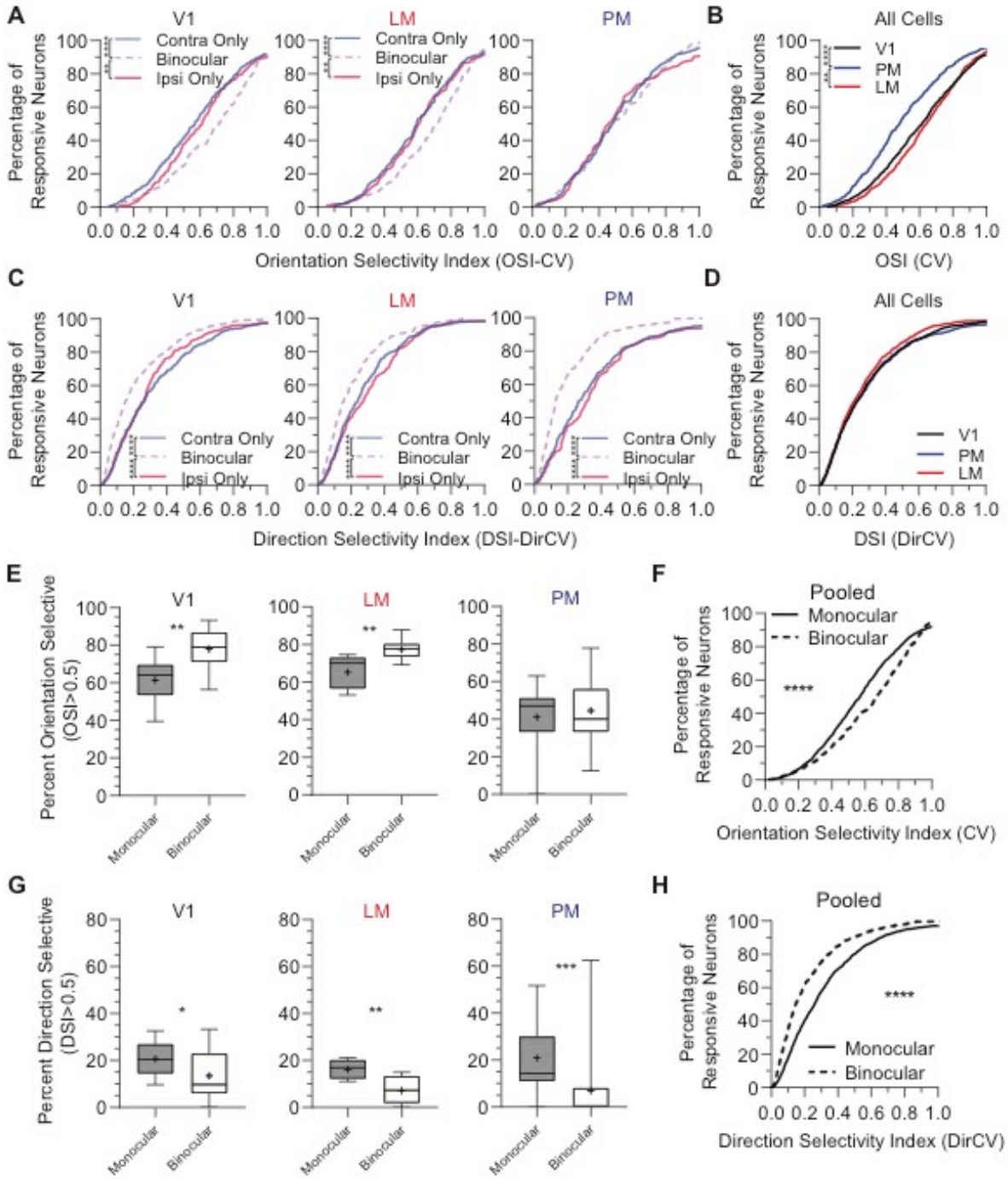

Figure 3.3 Distinct ocular orientation and direction tuning in visual cortex. A. Cumulative distributions of orientation selectivity based on the circular variance method for V1 (left), LM (middle) and PM (right) are plotted based on eye specificity (binocular= purple dashed, contra only= pale blue and ipsi only= pink). In V1 and LM, the binocular cells are more orientation selective than the contralateral or ipsilateral-dominated neurons (V1: binocular median: 0.713, n=264 cells, contra only: 0.57, n=470 cells, ipsi only: 0.61, n=251 cells, Kruskal-Wallis test, p<0.0001, KW(s)=28.66; Post-hoc Dunn's multiple comparisons test: contra only vs. binocular p<0.0001, ipsi only vs. binocular p=0.0061, N=9 mice; LM: binocular median and SEM: 0.72, n=306 cells, contra only: 0.59, n=356 cells, ipsi only: 0.61, n=205 cells, Kruskal-Wallis test, p<0.0001, Post-hoc Dunn's multiple comparisons test: contra only vs. binocular p<0.0001, ipsi only vs. binocular p=0.0024, N=9 mice, KW(s)=23.2). **B.** Cumulative distributions of orientation selectivity are plotted for all cells in V1 (black), LM (red) and PM (blue). Overall, PM is less orientation tuned than V1 and LM (V1: median: 0.62, n=985 cells, LM: 0.64, n=867 cells; PM: 0.48, n=526 cells, Kruskal-Wallis test, p<0.0001, KW(s)= 94.5, N=9 mice). **C.** Box and whisker plots of the percentage of orientation-tuned (OSI>0.5) cells for each animal based on ocularity (monocular=grey, binocular=white) are plotted for V1 (left), LM (middle) and PM (right). In V1 and LM, there are significantly more orientation-tuned binocular cells than monocular cells. (V1 binocular mean and SEM: 77.7 +/- 3.93%, monocular: 60.7 +/- 4.23%, paired t-test, p=0.0033, t=4.13; LM binocular mean and SEM: 77.4 +/- 1.78%, monocular: 65.27 +/- 2.82%, paired t-test, p=0.0018, t=4.58, N=9 animals). **D.** Cumulative distribution of orientation selectivity for all binocular (dashed) and monocular cells (solid) from all three areas. Binocular cells were more orientation tuned than monocular cells (median binocular OSI: 0.669, n=750 cells, monocular: 0.57, n=1629 cells, Mann-Whitney test, p<0.0001, Mann-Whitney (U)= 515940). **E.** Cumulative distributions of direction selectivity based on the circular variance method for V1 (left), LM (middle) and PM (right) are plotted based on eye specificity (binocular= purple, dashed, contra only= pale blue and ipsi only= pink). In all three areas, the monocular neurons (contra only and ipsi only) are more direction selective than the binocular neurons (V1: binocular median: 0.15, n=264 cells, contra only: 0.26, n=470 cells, ipsi only: 0.26, n=251 cells, Kruskal-Wallis test, p<0.0001, Post-hoc Dunn's multiple comparisons test: contra only vs. binocular p<0.0001, ipsi only vs. binocular p<0.0001, N=9 mice, KW(s)=39.78; LM: binocular median: 0.24, n=306 cells, contra only: 0.16, n=356 cells, ipsi only: 0.27, n=205 cells, Kruskal-Wallis test, p<0.0001, Post-hoc Dunn's multiple comparisons test: contra only vs. binocular p<0.0001, ipsi only vs. binocular p<0.0001, N=9 mice, KW(s)=36.08). **F.** Cumulative distributions of direction selectivity are plotted for all cells in V1 (black), LM (red) and PM (blue). **G.** Box and whisker plots of the percentage of direction-tuned (DSI>0.5) cells for each animal based on ocularity (monocular=grey, binocular=white) are plotted for V1 (left), LM (middle) and PM (right). In all three areas, there are significantly more direction-tuned monocular cells than binocular cells. (V1 binocular mean and SEM: 13.46 +/- 3.28%, monocular: 20.63 +/- 2.33%, paired t-test, p=0.0254, t=2.68; LM binocular mean and SEM: 7.15 +/- 1.91%, monocular: 16.09 +/- 1.3%, paired t-test, p=0.0006, t=5.49; PM binocular mean and SEM: 7.02 +/-4.13%, monocular: 20.64 +/- 3.90%, Wilcoxon matched-pairs signed rank test, p=0.0009, Wilcoxon (W)=97.00, N=9 animals). **H.** Cumulative distribution of direction selectivity for all binocular (dashed) and monocular cells (solid) from all three areas. Binocular cells were more orientation tuned than monocular cells (median binocular DSI: 0.15+/- 0.007, n=750 cells, monocular: 0.26+/-0.014, n=1629 cells, Mann-Whitney test, p<0.0001, Mann-Whitney (U)= 2104911, N=9 animals). Significance stars are represented by ****=p<0.0001; ***=p<0.001; **=p<0.01; *=p<0.05.

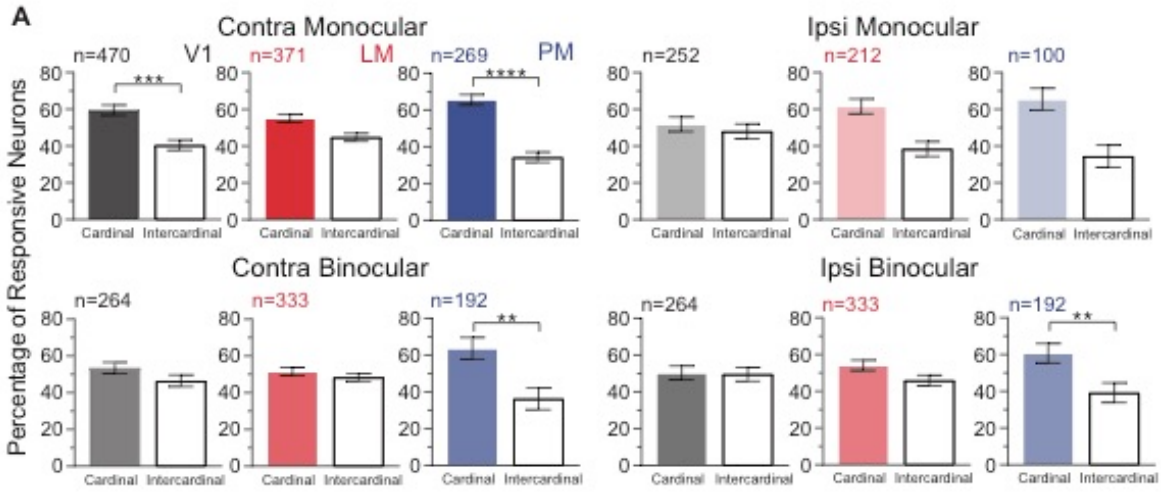

Figure 3.4 Comparison of cardinal preferences of eye-specific responses in V1, LM and PM. A. Preferred directions were binned and averaged across fields for contra monocular (top left), contra binocular (bottom left), ipsilateral monocular (top right) and ipsilateral binocular (bottom right) for responses from V1 (black: cardinal, grey: intercardinal), LM (red: cardinal, grey: intercardinal) and PM (blue: cardinal, grey: intercardinal). Contra monocular responses in V1 were biased to the cardinal directions (Chi-square test p=0.0002) while contra binocular and ipsilateral responses were not biased. LM responses were also not biased to the cardinal directions. In area PM, almost all eye-specific responses are biased to cardinal directions (PM contra monocular Chi-square test= p<0.0001, PM contra binocular Chi-square test p=0.0016, PM ipsilateral binocular Chi-square test p=0.0012; Number of neurons for each group are indicated on graph, N=9 mice).

3.3.3 Eye-specific biases to cardinal directions in V1, LM and PM.

We previously found that the highest spatial frequency tuned cells of V1 were biased to the cardinal directions (Salinas et al., 2017). We asked if this high spatial frequency bias for cardinal directions could be described by eye-specific response properties. In V1, the contralateral dominated neurons have a bias for the cardinal directions, while other eye specific responses did not (Figure 3.4, top right). LM, which is tuned to relatively slower spatial frequencies than PM and V1, did not exhibit any eye-specific bias for cardinal directions (Figure 3.4). All eye-specific responses of area PM were biased to the cardinal directions, although the finding was not found to be statistically significant in the case of the ipsilateral only responses. Perhaps this finding indicates that V1 is sending functionally specific, cardinally biased information to PM, and facilitating its

bias towards cardinal directions. Alternatively, both V1 and PM may obtain their cardinal biases from similar subcortical sources (LP, for example), which also exhibit eye-specific functional organization. The two alternatives are not mutually exclusive. Nonetheless, it may be that the contralateral-dominated neurons are important for detection of landmarks during spatial navigation (Girschick et al., 2011; Hansen et al., 2003).

3.3.4 Binocular Cells are Better Matched in Orientation and Spatial Frequency in Higher Visual Areas.

The preferred spatial frequency of the contralateral eye and ipsilateral eye are correlated at the level of V1 in mouse, but not as well correlated as in higher mammals (Salinas et al., 2017; Skottun and Freeman, 1984: cat, r=0.92; Saint-Amour, 2004: r=0.82). At the level of V1, binocular matching is known to develop over time post eye opening (Wang et al., 2010). The extents to which the two eyes align in terms of spatial frequency or orientation in higher visual areas of mice have yet to be investigated. We find that eye-specific tuning of binocular cells improve up the cortical hierarchy with V1 the least correlated and PM the most correlated (V1 preferred spatial frequency r=0.13, LM r=0.46, PM r=0.78; Figure 3.5a-b). We also find that higher visual areas are better matched in eye-specific orientation in higher visual areas than in V1 (Figure 3.5c), suggesting that the information between the two eyes are better aligned in higher visual areas than in V1.

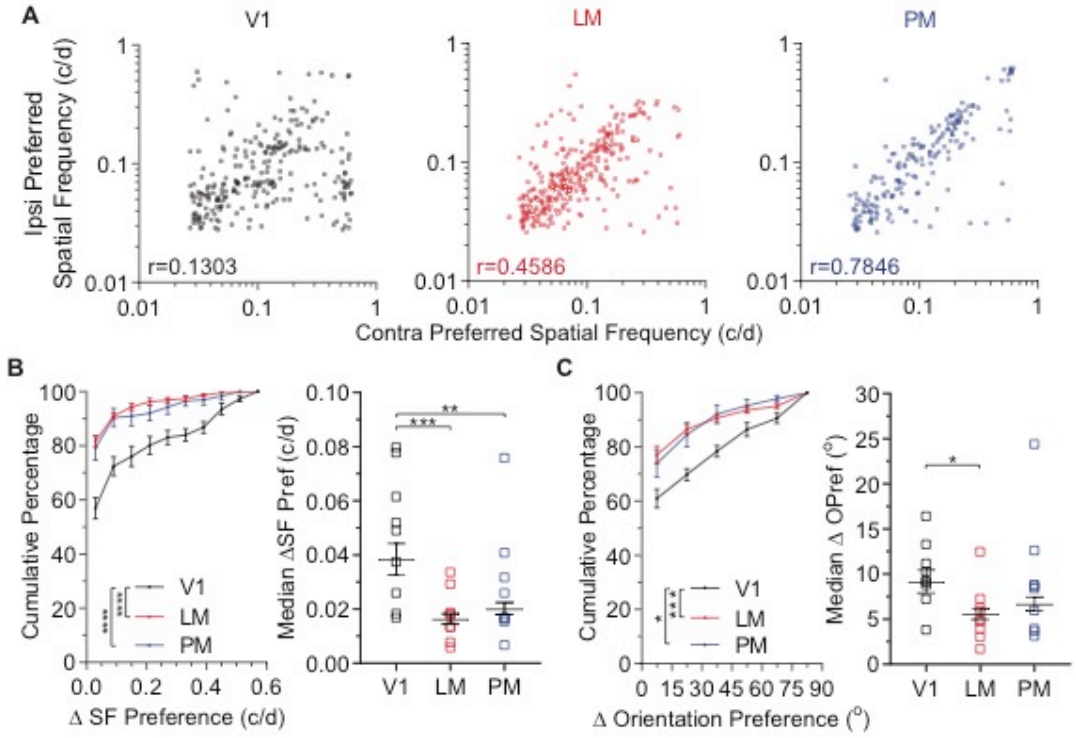

Figure 3.5 Binocular cells are better matched in spatial frequency and orientation in higher visual areas. A. Scatter of ipsilateral and contralateral preferred spatial frequency for V1 (left, black), LM (middle, red) and PM (right, blue). Preferences between the two eyes were significantly correlated for each area but increase in correlation hierarchically (V1 r=0.1303, p=0.0343; LM r=0.4586, p<0.0001; PM r=0.7846, p<0.0001). **B.** Left: Differences in preferred spatial frequency were binned and cumulative distributions plotted for V1 (black), LM (red) and PM (blue). Area LM and PM have significantly lower differences in preferred spatial frequency than V1 (V1 median= 0.0384 c/d, n=264 cells, LM median= 0.0163 c/d, n=333 cells; PM median= 0.0201 c/d, 192 cells; V1 vs. LM p<0.0001; V1 vs. PM p<0.0001, KW(s) =33.43). Right: By animal median difference in preferred spatial frequency confirms that higher visual areas LM and PM are better matched in spatial frequency than V1 (Dunn's multiple comparison's test, V1 vs. LM p=0.0008; V1 vs. PM p=0.0094, Friedman(s)=14, N=9 mice). Line and error bars reflect median and standard error of the median. **C.** Left: Differences in preferred orientation were binned and cumulative distributions plotted for V1 (black), LM (red) and PM (blue). Area LM and PM have significantly lower differences in preferred orientation (V1 median= 9.16 degrees, n=264 cells; LM median= 5.57 degrees, n=333 cells; PM median= 6.67 degrees, n=192 cells; V1 vs. LM p=0.0005, V1 vs. PM p=0.0484, KW(s)=14.46). Right: By animal median difference in preferred orientation (Dunn's multiple comparisons test, V1 vs. LM p=0.0368, Friedman(s)=6.22, N=9 mice). Line and error bars reflect median and standard error of the median. Significance stars are represented by ****=p<0.0001; ***=p<0.001; **=p<0.01; *=p<0.05.

3.3.5 Divergent eye-specific tuning for speed in V1 and PM

Higher visual areas are known to prefer unique speeds (Andermann et al., 2011; Glickfeld et al., 2013). Speed tuning is believed to better distinguish higher visual areas from one another than spatial or temporal frequency alone. To assess if eye-specificity is

coupled to speed tuning in the mouse, we measured visually evoked responses to eight different speed presentations to either the contralateral or ipsilateral eye (Figure 3.6a). Responses were well fit to determine preferred spatial frequency, temporal frequency, speed and the degree of speed tuning, epsilon (Priebe et al., 2006, Figure 3.6b).

Eye-specific responses in V1 were uniquely tuned to different speeds. The contralateral eye dominated responses were tuned to the slowest speeds, the ipsilateral eye dominated responses were tuned to the highest speeds, and the binocular cells were tuned to intermediate speeds (Figure 3.7a, left). In LM, a similar pattern was found, but the distinction between binocular preferred speeds and ipsilateral only preferred speeds is not present (Figure 3.7a, middle). In PM, the contralateral only preferred speeds were significantly lower than the binocular preferred speeds. Thus, there is a recurring motif that the contralateral only responses are tuned to the slowest speeds throughout V1, LM and PM. More ambiguous in the higher visual areas is the distinction between binocular preferred speeds and ipsilateral only preferred speeds, perhaps due to a higher degree of convergence between eye-specific responses onto LM and PM cells. Overall, the three areas are tuned to unique speeds, with V1 and PM preferring overall slower speeds and LM faster speeds (Figure 3.7b).

We analyzed the degree to which the preferred spatial frequency depended on the preferred temporal frequency by the calculation of epsilon from the fitted responses. A high speed tuning index, epsilon, indicates a high degree of speed tuning (Figure 3.7c, bin at epsilon=1). In LM and PM, we found that responses driven by contralateral eye stimulation were more speed tuned than responses driven by stimulating the ipsilateral eye (Figure 3.7c). In our analysis, we also find that area LM has a relatively higher proportion of speed-

tuned cells than area PM (Figure 3.7d). Altogether, these results suggest that eye-specific preferences for speed may drive or facilitate the specialization of higher visual areas.

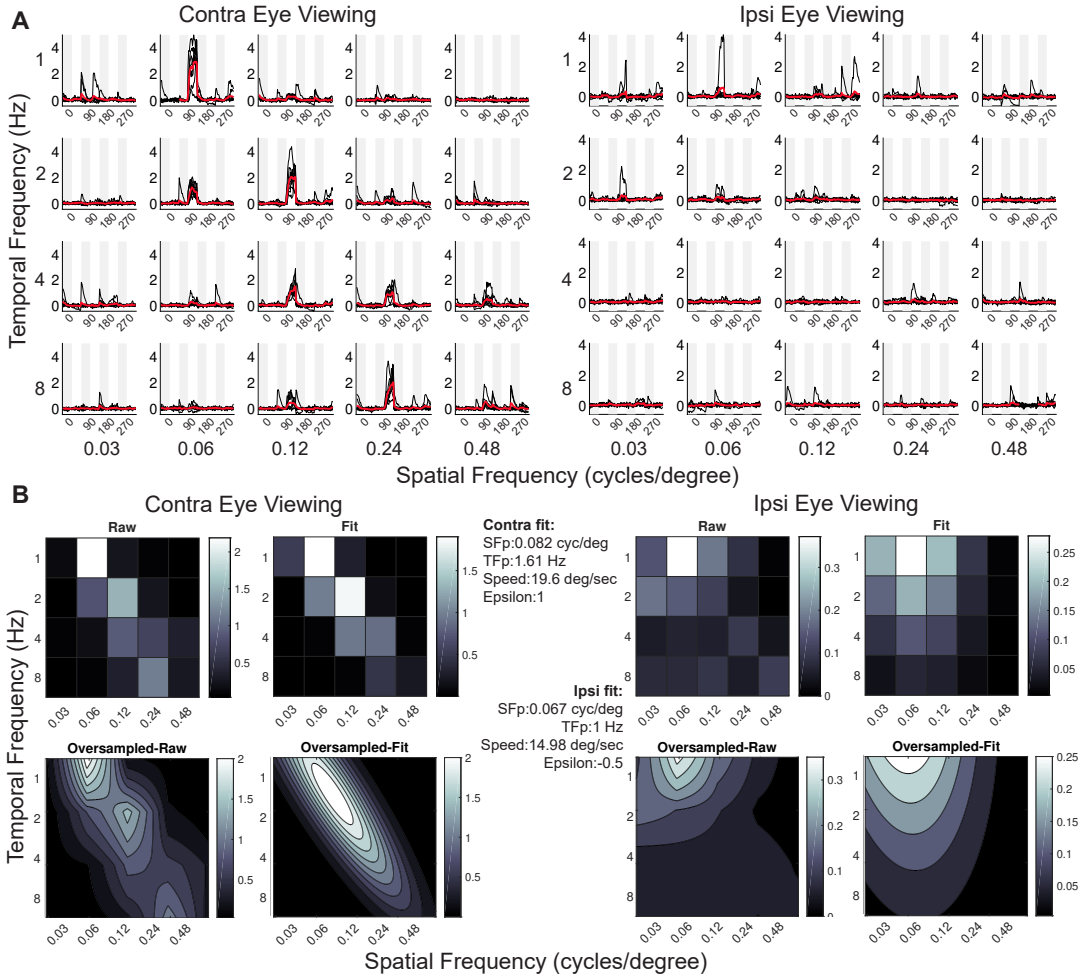

Figure 3.6 Assessment of eye-specific speed tuning. A. Example of a single cell's visually evoked responses measured as mice viewed drifting sinusoidal gratings of various speeds (temporal frequency/ spatial frequency). Drifting sinusoidal gratings of five spatial frequencies (0.03, 0.06, 0.12, 0.24, 0.48 cycles/degree), one of four temporal frequencies (1, 2, 4, 8 Hz) in four directions (0,90,180,270°) were presented for two seconds (white box) with an intermittent two-second off period (grey box). Each imaging session consisted of eight repeats shown to either the contralateral eye (left) or the ipsilateral eye (right). Individual traces are shown in grey and average traces are shown in red. **B.** The average response matrices for each spatial and temporal frequency were fit by a two-dimensional elliptical Gaussian. Calculated preferences for spatial frequency (SFp), temporal frequency (TFp), speed and speed-tuning index (epsilon) is shown in the middle margin for contralateral eye viewing (top) and ipsilateral eye viewing (bottom). The confidence itnervals for the fitted data and a fit correlation were used to assess wellness of fit. To be considered for the preferred speed analysis, the lower and upper bound confidence intervals for the fits of preferred spatial and temporal frequency must each lie within two octaves and the fit correlation must exceed 0.5. To be considered for the degree of speed tuning, we added a threshold for the calculated speed-tuning index: the range for the confidence intervals for epsilon must be less than 1.

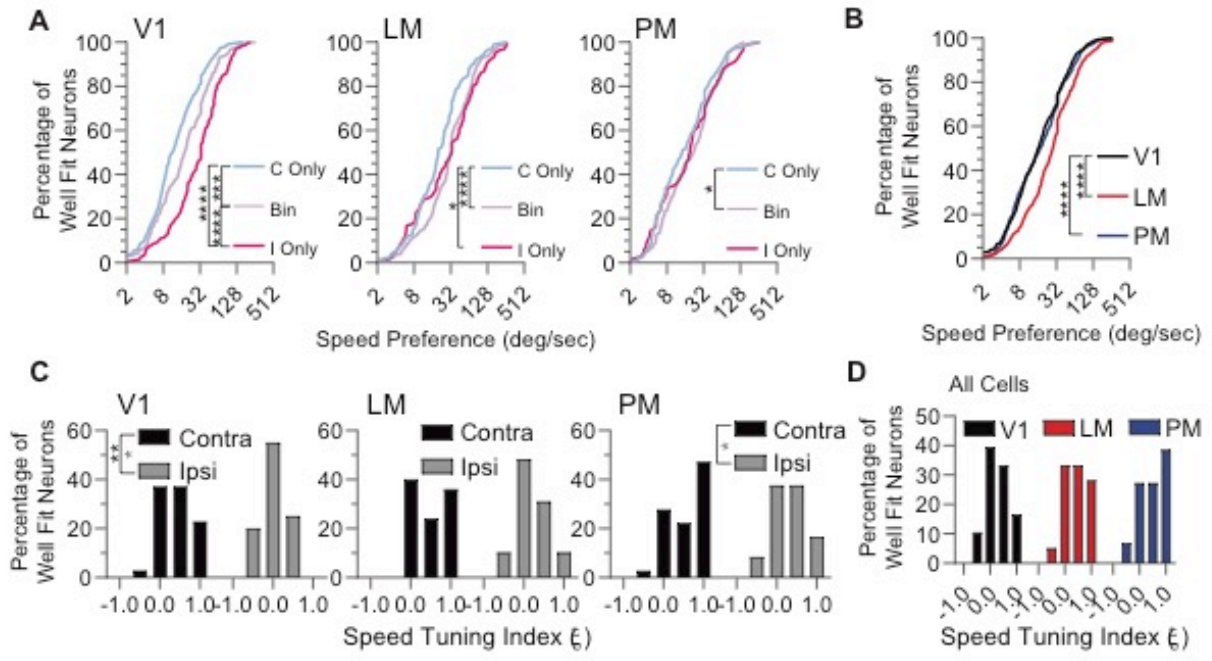

Figure 3.7 Eye-specific speed preferences and speed tuning in V1, LM and PM. A. Cumulative distributions of preferred speed for cells that passed the well-fit criteria. In V1, all three eye-specific responses were significantly different from one another (contra only median preferred speed: 11.26, n=419 cells; binocular: 18.06, n=226 cells; ipsi only: 33.33, n=174 cells, Kruskal-Wallis test, p<0.0001; Dunn's multiple comparisons post hoc test: contra only vs. binocular p=0.0426; contra only vs. ipsi only p<0.0001; binocular vs. ipsi only p=0.0001; KW(s)=85.24; N=8 mice). In LM, contralateral dominated cells were tuned to slower speeds than binocular cells and ipsilateral only cells (contra only median preferred speed: 19.96, n=248 cells; binocular: 32.93, n=296 cells: ipsi only: 33.24, n=101 cells; Kruskal-Wallis test, p<0.0001; Dunn's multiple comparisons post hoc test: contra only vs. binocular p<0.0001; contra only vs. ipsi only p=0.0125; KW(s)=22.29; N=7 mice). In PM, the contralateral only cells are tuned to slower speeds than the binocular cells (contra only median: 14.24, n=245 cells; binocular: 22.04 n=175 cells; ipsi only: 19.20, n=68 cells; Kruskal-Wallis test p=0.0427; Dunn's multiple comparisons post hoc test: contra only vs. binocular p=0.0396 KW(s)=6.308, N=8 mice). **B.** Cumulative distributions for all well fit cells of each area (V1 black, LM red, PM blue). Each area preferred unique speeds from the other, except for V1 and PM (V1 median preferred speed: 16.09, n=819 cells, N=8 mice; LM: 28.05, n=645 cells, N=7 mice; PM: 17.34, n=488 cells, N=8 mice; Kruskal-Wallis test p<0.0001; Dunn's multiple comparisons post hoc test: V1 vs. LM p<0.0001; LM vs. PM p<0.0001, KW(s)=73.28). **C.** Histograms for the speed-tuning index (epsilon), of well-fit cells in V1 (left), LM (middle) and PM (right) for contralateral eye viewing (black) and ipsilateral eye viewing (grey). The highest degree of speed tuning is the bar centered at 1, and indicates that this group of cells changes temporal frequency preference as a function of spatial frequency. In V1 and PM, contralateral eye viewing responses are more speed-tuned than ipsilateral eye viewing responses (V1: contra median 0.359 n=35 cells; ipsi: 0.08, n=20 cells; Mann Whitney test, p=0.0048, MW(U)= 191, N=8 mice; Kolmogorov-Smirnov test p=0.0294, KS(D)=0.4071; PM: contra median: 0.679, n=36 cells; ipsi: 0.106, n= 24 cells; Mann Whitney test p=0.0006, MW(U)=986; Kolmogorov-Smirnov test p=0.0187, KS(D)=0.4028; N=8 mice). No statistical differences were detected for LM (contra median: 0.309, n=25 cells; ipsi: 0.169, n=29 cell;, Mann Whitney test p=0.0600, N=7 mice). **D.** Histogram of speed tuning indices for all well fit cells (contra only, binocular and ipsi only) from areas V1, (black), LM (red) and PM (blue). No statistical differences were found in degree of speed tuning between areas. Significance stars are represented by ****=p<0.0001; ***=p<0.001; **=p<0.01; *=p<0.05.

3.3.6 Functional specificity of V1 projections to LM and PM

It has been demonstrated that the output of V1 to higher visual areas are functionally specific in their preferred speed (Glickfeld et al., 2013) as well as in their orientation and direction tuning (Matsui and Ohki, 2013). Thus, the primary visual cortex may play a role in the processing of distinct functional specialization of HVAs. We asked the question if this functional specialization could potentially arise from the eye-specific functional specialization we have observed in V1. By injecting GCaMP6s virus in the binocular zone of V1 and imaging V1 afferents in LM and PM, (Figure 3.8a) we were able to record visually evoked responses of the output of V1 and characterize eye-specificity and spatial frequency tuning preferences of single boutons (Figure 3.8b).

We find that the eye-specific output of V1 is more contralaterally biased in PM than it is in LM (Figure 3.8c). This matches well with previous findings that the cells in PM are more contralaterally biased than the cells in LM (Figure 3.2b). V1 afferents to PM were also tuned to higher spatial frequencies than the afferents to LM, corroborating previous studies suggesting that the V1 to LM and PM afferents would be distinct and functionally match their targets (Figure 3.8d). We also analyzed the eye-specific spatial frequency tuning properties of the V1 boutons sent to LM and PM, and find that there is eye-specific functional segregation at the level of LM, but not at PM (Figure 3.8e). The contralateral only responsive V1 boutons in LM are tuned to higher spatial frequencies than the binocular boutons, just as we have found in the cellular distributions of V1, LM and PM (Figure 3.8f).

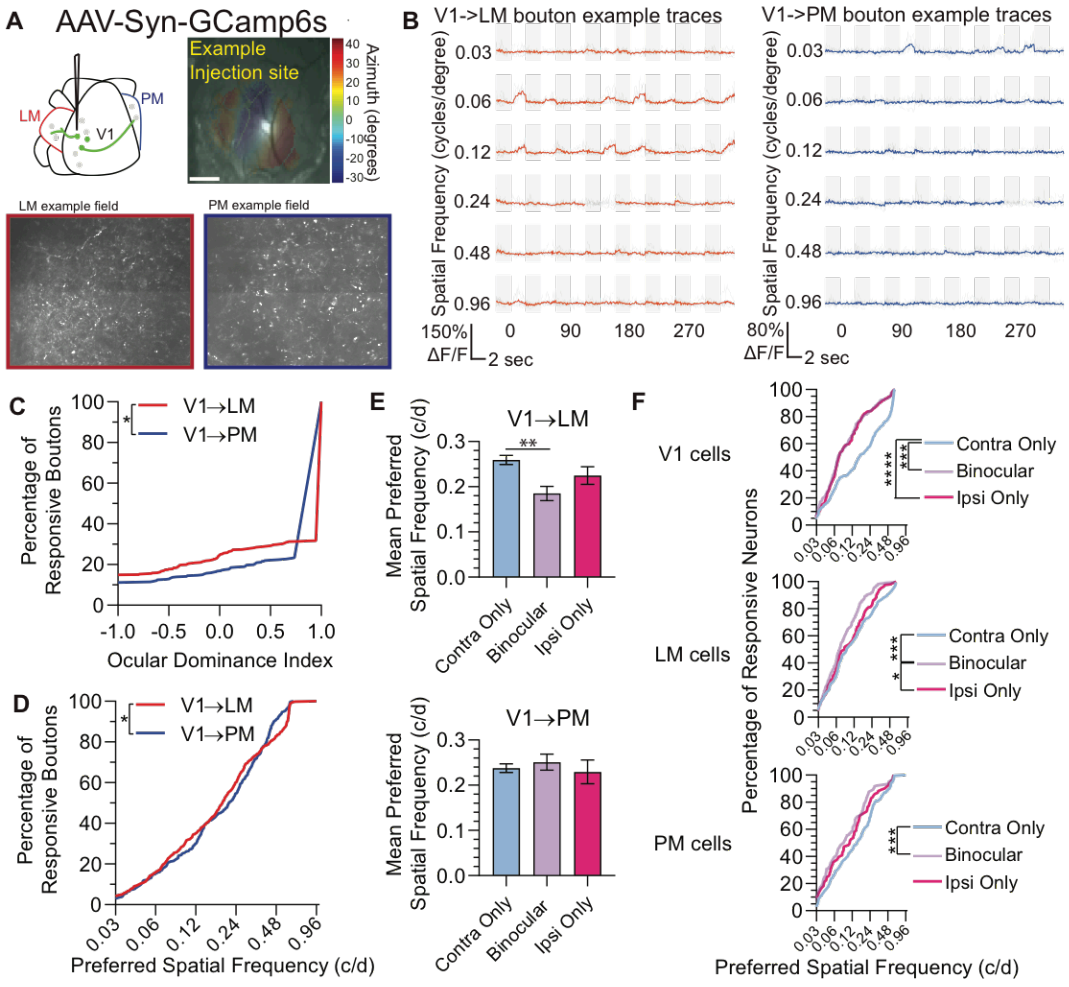

Figure 3.8 Functional specificity of V1 projections to LM and PM. A. Experimental setup. Mice were injected with AAV-SynGCaMP6s into the binocular zone of V1 (top left) and mapped with intrinsic signal imaging for determination of injection site and areal borders (top right). Summed projections of imaging fields in LM (left, red box) and PM (right, blue box) show bright synaptic boutons. **B.** Example traces from an LM field (left, average trace shown in red) and a PM field (right, average trace shown in blue), probed at six spatial frequencies and eight directions. **C.** Cumulative distributions of ocular dominance indices for all significantly responsive boutons of V1 to LM (red) and V1 to PM afferents (blue). The projections to PM are more contralaterally biased than the projections to LM. (V1 to LM median ODI: 1; mean ODI: 0.527, n=576 boutons, N=5 mice; V1 to PM median: 1.0; mean: 0.656, n=401 boutons, N=5 mice; Kolmogorov-Smirnov test p=0.046; KS(D)=0.0893). **D.** Cumulative distributions of preferred spatial frequency for all significantly responsive boutons of V1 to LM (red) and V1 to PM afferents (blue). The projections to PM are higher spatial frequency tuned than the projections to LM. (V1 to LM median: 0.189 cyc/deg, n=576 boutons, N=5 mice; V1 to PM median: 0.212 cyc/deg, n=401 boutons, N=5 mice; Kolmogorov-Smirnov test p=0.0275; KS(D)=0.0952). **E.** Breakdown of the preferred spatial frequency tuning of the afferents from V1 to LM (top) and V1 to PM (bottom) by eye-specificity. In LM, the contralaterally dominated boutons are higher spatial frequency tuned than the binocular boutons (Contra only median: 0.207 cyc/deg, n=382 boutons, binocular median: 0.146 cyc/deg, n=98 boutons N=5 mice; ipsi only median: 0.205 cyc/deg, n=86 boutons; Kruskal-Wallis test p=0.0063, Dunn's multiple comparisons post hoc test, contra only vs. binocular p=0.0069; KW(s)=10.15; N=5 mice). The eye-specific distinction to in V1 afferents does not appear to be present in PM. **F.** Cumulative distributions of eye-specific spatial temporal tuning preferences for cells recorded in V1 (top), LM (middle) and PM (bottom). In all three areas, the contralateral dominated cells are tuned to higher spatial frequencies

than the binocular cells (PM: median contra only: 0.146 cyc/deg, n=254 cells; median binocular: 0.087 cyc/deg, n=180 cells; ipsi only median: 0.111 cyc/deg, n=93 cells, Kruskal-Wallis test p<0.0001; Dunn's multiple comparisons test, contra only vs. binocular p<0.0001, N=9 mice; KW(s)=18.41). In V1, there is also a difference in the contralateral only and ipsilateral only responses. (V1: median contra only: 0.159 cyc/deg, n=470 cells; median binocular: 0.072 cyc/deg, n=264 cells; ipsi only median: 0.0716 cyc/deg, n=252 cells, Kruskal-Wallis test p<0.0001; Dunn's multiple comparisons test, contra only vs. binocular p<0.0001; contra only vs. ipsi only p<0.0001, N=9 mice; KW(s)=60.68). In LM, there is also a difference in preferred spatial frequency for binocular and ipsi only responses (LM: median contra only: 0.091 cyc/deg, n=356 cells; median binocular: 0.0687 cyc/deg, n=304 cells; ipsi only median: 0.0826 cyc/deg, n=205 cells, Kruskal-Wallis test p<0.0001; Dunn's multiple comparisons test, contra only vs. binocular p<0.0001; binocular vs. ipsi only p<0.0345, N=9 mice; KW(s)=20.40). Significance stars are represented by ***=p<0.001; **=p<0.01; *=p<0.05.

3.4 Discussion

The goal of our study was to determine if the functional specialization of eye-specific responses found at the level of V1 is also present in higher visual areas LM and PM. As far as we know, we are the first to probe eye-specific tuning in higher areas of mouse visual cortex. Our study confirms that the asymmetries found in the binocular zone of V1 in the spatial frequency tuning of each eye is also present in higher visual areas of cortex, and extends to other visual stimulus features. The contralateral bias to high spatial frequencies appears to be a pronounced feature of mouse visual cortex, and perhaps serves as an explanation for the bias of PM towards higher spatial frequencies than LM; similarly, the relatively low spatial frequency tuning of area LM may also be owed to the high degree of binocular cells in this area.

The contralateral bias towards high spatial frequencies extends to a high degree of direction selectivity. This also applies to the biases found to the cardinal directions (Salinas et al., 2017). Although we did not find an eye-specific functional specialization for orientation and direction selectivity, we did find an ocular specialization. Monocular cells tended to be more direction selective, and this feature seemed to be conserved in both LM and PM, while binocular cells were more orientation selective. Moreover, all eye-specific responses of area PM are biased to cardinal preferences, indicating a potential role for PM

and V1 contralateral dominated cells in spatial navigation. The orientation matching for spatial frequency and orientation between the two eyes also increases up the proposed cortical hierarchy (V1>LM>PM), suggesting that the eye-specific functional segregation at the level of V1 may scale down in higher visual areas, whose selectivity are more refined to specific types of stimuli (Marshel et al., 2011; Andermann et al., 2011; Roth et al., 2012).

Because spatiotemporal tuning has been determined to better segregate visual areas from one another (Glickfeld et al., 2013), we probed eye-specific preferred speeds. We found that the eye-specific asymmetries found in V1 for spatial frequency tuning also extend to preferred speeds. In all three areas, the contralateral only responses were tuned to the slowest speeds (which could be due to high spatial and low temporal frequency processing). In V1, binocular cells preferred intermediate speeds while ipsilateral only cells preferred the fastest speeds. Thus, it may be that functional specialization of higher visual areas, with their unique speed preferences, could be in part, due to eye-specific functional input from V1. In LM and PM, there appears to be a scaling down in the eye-specific speed distinction up the cortical hierarchy—perhaps owing to convergence of particular eye-specific inputs from V1. Given out current results, we propose that the eye-specific functional output of V1 to higher visual areas could be important for their unique spatial and temporal frequency preferences.

We determined if the V1 afferents to areas LM and PM were distinct in their eye-specificity and in their eye-specific spatial frequency tuning properties. We found that the output of V1 matched the target areas in terms of ODI and spatial frequency tuning. We also found that the output of V1 to LM contained eye-specific spatial frequency tuning, with the contralateral dominated responses preferring the highest spatial frequencies. While we

were unable to restrict our analysis to only the excitatory cells of V1, we were still able to discern differences in spatial frequency and ocular dominance, as would be expected if V1 is a participant in shaping areal selectivity through eye-specific inter-areal connections. This may align with current hierarchical models, where HVA selectivity is dependent on V1. However, it may also be that eye-specific functional specialization at subcortical levels (i.e. LP) drive HVA selectivity.

Many studies have established the relationship between the columnar organization of ocular dominance and orientation pinwheels, and pinwheels with cytochrome oxidase blobs/interblobs (Hubel and Wiesel, 1974a; Bartfeld and Grinvald, 1992; Livingstone and Hubel, 1984). These eye-specific columns are preferentially linked to same eye-specific columns in primate V1, although the segregation is not strict (Malach et al, 1993). More recently, a link between spatial frequency and eye-specificity has been revealed in primates using two-photon calcium imaging. The monocular regions of primate striate cortex prefer lower spatial frequencies than binocular regions (Nauhaus et al., 2016). The discrepancy between our findings and those in primates may be due to anatomical and ethological differences between the two species. Perhaps thinking about how the visual system serves these two species differently may guide an understanding of this apparent discrepancy. Primates, whose binocular visual system is very similar to that of humans, have forward facing eyes, a large binocular visual field and have acuity thresholds much closer to humans. Mice, on the other hand, are afoveate species, with eyes placed largely on the sides of their heads and a relatively small binocular visual field (Dräger 1975). Perhaps a difference in predator vs. prey species could manifest in visual systems primed for

detecting approaching predators in the periphery or finding objects in the central visual field.

While orientation and direction have been shown to be important early features for the processing of form and motion, respectively, why this monocular-binocular distinction exists in mice remains a puzzle. It is intuitive to think that binocular cells should be sharply tuned for orientation, if they are to perform form and object identification processing downstream. Moreover, sensitivity to motion in the periphery might serve as a useful function for looming or approaching objects, and could help serve as an attention shifting mechanism. These operations may need to happen in parallel, and differences in ocularity may be an important mechanism for the simultaneous processing of that information. It is still possible that perhaps eye-specificity and ocularity hold clues about the organizing principles that establish the initial setup of visual cortex during development. Perhaps the mouse, as a rudimentary visual system, could provide a glimpse into how the visual cortex was able to design a visual system capable of parallel processing.

CHAPTER 4: Effects of Monocular Deprivation on eye-specific functional properties of V1, LM and PM

4.1 Introduction

The mammalian visual system has been classically described as a hierarchically organized system that transforms different aspects of the same retinal image along parallel streams for simultaneous processing (Van Essen et al., 1991, Nassi and Callaway 2009). Early in these streams, distinct retinal ganglion cells process functionally distinct spatiotemporal information. Downstream, V1 parses and transmits the spatiotemporal information to specialized higher visual areas (HVAs). The specialization of HVAs is crucial for the encoding of higher-level feature detection, such as global form and motion processing, and their activity is more closely linked to visual perceptual tasks than V1 (reviewed in Kiorpes, 2016). The functional architecture of primate V1 plays a key role in parallel pathway processing (Hubel and Livingstone, 1987; Nassi and Callaway 2009). In mice, V1 seems to play a similar role, containing cells that vary widely in their spatiotemporal tuning, supporting the encoding of multiple visual streams (Gao et al., 2010; Ji et al., 2015). V1 also carries distinct information to HVAs in a target-dependent manner (Glickfeld et al., 2013; Matsui and Ohki, 2013). Mouse HVAs have been grouped into putative dorsal and ventral streams, based largely on their anatomical connectivity (Wang et al., 2011; Wang et al., 2012). HVAs can also be segregated based on their functional diversity and specific preferences for spatiotemporal and orientation/direction selectivity (Marshel et al., 2011; Andermann et al., 2011; Roth et al., 2012; Murakami et al., 2015, Smith et al., 2015).

Functional maps for spatial frequency, eye-specificity and orientation are aligned in primate V1 (Bartfeld and Grinvald, 1992; Obermayer and Blasdel, 1993; Crair et al., 1997a; Nauhaus et al., 2012; Nauhaus et al., 2016) and the modular organization of these feature maps is recapitulated in HVAs (Ts'o et al., 2009; Ghose and Ts'o, 1997; Ghose and Ts'o, 2017). While the basic columnar organization has been demonstrated to be largely independent of visual experience (Hubel and Wiesel, 1963; Sherk and Stryker, 1976, Crair et al., 1998; Rakic, 1976; Horton and Hocking, 1996; Des Rosier et al., 1978; Blasdel, Obermayer and Kiorpes 1995), the maintenance and relationship between some feature maps can be altered with abnormal visual experience (Farley et al., 2007).

The close association between feature maps for eye-specificity and spatial frequency tuning has been demonstrated by studies of ocular dominance plasticity (ODP). Closing an eye during the ocular dominance critical period can cause long-lasting changes in the ocular dominance map and is accompanied by a loss of high spatial frequency tuning of the deprived eye in V1 (Wiesel and Hubel, 1963; Dews and Wiesel, 1970; Hess and Howell, 1977; Levi and Harwerth, 1977; Fagiolini et al., 1994; Prusky et al., 2000; Gordon and Stryker, 1996). Given the hierarchical model suggesting that the receptive fields of HVAs are built upon V1 input, it would seem likely that monocular deprivation may have compounding effects on HVA specialization. In line with this, amblyopic primates have severe deficits in the processing of higher-level feature detection, including contour integration, motion and form processing (Kozma and Kiorpes, 2003; Kiorpes et al., 2006; Kiorpes, 2006). However, it has not been explored whether the differentiation of HVAs into distinctly specialized functional modules depends on visual experience.

A recent study using intrinsic signal optical imaging indicates that the areas become more distinct after eye opening, during a similar time window as the classically defined ocular dominance critical period (Murakami et al., 2017). Also using intrinsic signal imaging, a second study reinforced that dorsal and ventral stream areas have somewhat independent developmental timelines (Smith et al., 2017). However, it is not clear whether visual experience is driving the differentiation of the areas into specialized functional modules. Moreover, to better understand the functional specialization of HVAs, it is critical to characterize the tuning properties of individual cells.

We recently discovered eye-specific functional segregation at the level of V1 in mice (Salinas et al., 2017), indicating that neurons with common eye dominance properties also share similar spatial frequency selectivity. This coupling of eye-specificity with spatial frequency tuning is intriguingly reminiscent of recent findings in primate V1, where maps of spatial frequency run parallel to ocular dominance maps (Nauhaus et al., 2016). Given the distinct spatial frequency information provided by the two eyes, we wondered whether monocular deprivation (MD) would lead to a disruption in the functional specialization of HVAs. Using two-photon calcium imaging, we recorded from thousands of excitatory neurons in L2/3 of areas V1, LM and PM to determine the spatiotemporal and eye-specific receptive field properties. We find that two weeks of MD during the ocular dominance critical period disrupts the functional segregation of HVAs in adulthood. Moreover, the functional segregation of eye-specific responses in V1, LM and PM are disrupted in distinct manners, suggesting that the development of eye-specific response properties may be important for establishing higher visual area specificity.

4.2 Materials and Methods

4.2.1 Animals

All protocols and procedures followed the guidelines of the Animal Care and Use Committee at the University of California, Irvine. To image evoked activity in layer 2/3 excitatory neurons in multiple visual areas, a Camk2a-tTA driver line (RRID: IMSR_JAX:007004) was crossed to a line expressing the calcium indicator GCaMP6s under the control of the tetracycline-responsive regulatory element (tetO) (RRID: IMSR_JAX:024742; Wekselblatt et al., 2016). The founder line was heterozygous for both transgenes and maintained by breeding with wildtype C57BL/6 mice (RRID: IMSR_CRL:642). Mice of either sex were weaned at P18-21 and co-housed with one or more littermate until the day of window implantation (P73-200).

4.2.2 Monocular deprivation

For monocular deprivation experiments, one eye was sutured (either right or left) at P19 and the sutures were monitored for two weeks (Davis et al., 2015). Under isoflurane anesthesia (2% for induction, 1% for maintenance), the non-deprived eye was covered with ophthalmic ointment while the other eye was sutured closed with two-three mattress sutures (7-0 silk, Ethicon). If the eye opened at any time before the two-week window, the mouse was removed from the experiment. Eyes were opened after two weeks and inspected for any damage under a microscope. In total, we gathered data from 8 No MD, 6 CMD and 4 IMD mice. By cell analysis included data from all 18 animals.

4.2.3 Cranial Window Implantation

See Section 2.2.2 Cranial Window Implantation

4.2.4 Visual Area Mapping

Retinotopic maps of azimuth and elevation were used to generate a visual field sign map (Sereno et al., 1994; Garrett et al., 2014) to designate borders between visual areas. See Section 2.2.4 for retinotopic mapping.

4.2.5 Two-Photon Calcium Imaging

See Section 3.2.5 Two-photon Calcium Imaging

4.2.5.1 Two-Photon Visual Stimuli

See Section 3.2.5.1 Two-Photon Visual Stimuli

4.2.6 Data Analysis

4.2.6.1 Cellular Responses

Custom-written Python routines were used to remove motion artifact, identify cell ROIs, extract calcium fluorescence traces, and perform analyses. See Section 2.2.6.1

To determine a cell's response to each stimulus trial, the cell's trace during the stimulation period was normalized to the baseline value averaged over the 0.75 seconds preceding stimulus presentation. The cell's response to a given orientation θ_i was defined as the average response across the 8 repeats of each condition: $F(\theta_i)$. An estimate of the cell's spontaneous calcium fluctuation was determined using the cell's trace during the blank condition. For the spatial frequency tuning protocol, at each spatial frequency, a cell's responsiveness was determined using a one-way ANOVA ($p<0.01$) across orientations against the blank condition. For the speed tuning protocol, a cell's responsiveness was first determined using a one-way ANOVA with a Bonferonni correction ($p<0.05/(5 \text{ SFs} * 4 \text{ TFs})= p<0.0025$).

4.2.6.2 Ocular Dominance Index/ Eye Specificity

Ocular dominance index was also calculated as (C-I)/(C+I), where C is R_{pref} for the contralateral eye and I is R_{pref} for the ipsilateral eye. The R_{pref} was taken at the cell's optimal spatial frequency or optimal spatial and temporal frequency for the speed tuning protocol, for each eye viewing condition. We classified a cell as contralateral only if the cell was only significantly responsive during contralateral eye viewing conditions. These cells were assigned an ODI of 1. A cell that was only responsive during the ipsilateral eye viewing condition was considered ipsilateral only responsive and assigned an ODI of -1.

4.2.6.3 Preferred Speed (Speed Tuning Protocol)

To determine a cell's preferred speed, responses across all spatial and temporal frequencies were fit with a two-dimensional elliptical Gaussian (Priebe et al., 2006; Andermann et al., 2011):

$$R(sf, tf) = A\ exp\left(\frac{-(\log_2 sf - \log_2 sf_o)^2}{2(\sigma_{sf})^2}\right) exp\left(\frac{-(\log_2 tf - \log_2 tf_p(sf))^2}{2(\sigma_{tf})^2}\right)$$

where A is the neuron's maximum responses, sf_o and tf_o are the preferred spatial and temporal frequency and σ_{sf} and σ_{tf} are the tuning widths for spatial and temporal frequency. From this fit we are able to obtain the dependence of temporal frequency preference on spatial frequency by calculating the speed tuning index, ξ, such that $\log_2 tf_p(sf)) = \xi\ (\log_2 sf - \log_2 sf_o) + \log_2 tf_o$. A neuron with a speed tuning index of $\xi = 1$ is a speed-tuned cell, while $\xi = 0$ is not speed-tuned and $\xi = -1$ is anti-tuned. To measure goodness of fit, we used two approaches. First, the fitted data must be well correlated with the raw data (fit correlation greater than 0.5). The confidence intervals for

preferred spatial and temporal frequency must not exceed 2 octaves. For speed tuning analysis, the confidence intervals for the speed-tuning index must not exceed 1.

4.2.7 Experimental Design and Statistical Analyses

Distributions were tested for normality before running statistical tests. When data was not normally distributed, nonparametric tests were used to compare groups. To compare ocular dominance index, spatial frequency, temporal frequency and speed preference between V1, LM and PM in NoMD and CMD mice, the Kruskal-Wallis test was used. Similarly, we used a Kruskal-Wallis test to compare eye-specific speed preferences in No MD and CMD mice. To compare distributions for speed preferences in NoMD and CMD mice in V1, LM and PM, we used a Mann-Whitney and Kolmogorov-Smirnov test.

To quantify functional segregation of HVAs and eye-specific responses, we first used a box-cox transformation (XLSTAT), optimized for all control data, to achieve distributions of spatial and temporal frequency that were more likely to be normally distributed. We then ran the Mahalanobis distance test with a Bonferonni correction for the number of comparisons (XLSTAT) on all cellular spatial and temporal frequency preferences for by-cell analysis, or on preferences obtained from the same animal for by-animal analysis. Fisher distance p-values are reported for inter-areal and eye-specific distance comparisons. Results of the Wilk's lambda test are also reported to show if the mean vectors are significantly different from one another. For comparisons of HVA functional segregation, the inter-areal Mahalanobis distances for each animal in NoMD and CMD mice were then tested with a Two-way ANOVA, mixed-effects (REML) model, with each inter-areal comparison as the repeating factor. The inter-areal distances for NoMD and CMD mice were summed and then compared with Welch's unpaired t test to determine if functional

segregation was impaired with CMD. For Eye-specific segregation, we both pooled the data from V1, LM and PM to determine Mahalanobis distances between eye-specific responses and restricted analysis to each area. By animal-analysis was not used to quantify eye-specific functional segregation for two reasons: 1) There are differential effects of MD on the eye-specific functional segregation in V1, LM and PM, as demonstrated by the distributions for speed preferences and 2) due to the difficulty of achieving a good sample size for each eye-specific response category within each area in a single animal, especially in the case of PM. Statistical analyses were performed using Prism v7.01 (GraphPad).

4.3 Results

4.3.1 Spatiotemporal and Eye-specific Response Properties of V1, LM and PM

To probe eye-specific spatiotemporal tuning, we used a transgenic mouse line that expresses GCaMP6s under the control of the CaMK2 promoter (CaMK2-tTA; tetO-GCaMP6s; Wekselblatt et al., 2016). We used a visual field sign map to delineate areas and imaged visually evoked activity of excitatory neurons in L2/3 of adult mice (Figure 4.1a). By presenting mice with drifting sinusoidal gratings of various temporal and spatial frequencies to each eye individually, we were able to assess eye-specific tuning for spatial frequency, temporal frequency and speed (Figure 4.1b, d). Speed is defined as temporal frequency/ spatial frequency and tuning for speed has been demonstrated to functionally segregate HVAs more robustly than spatial frequency (Glickfeld et al., 2013). Response matrices to the visual stimuli for each eye viewing condition were fit with a 2-dimensional Gaussian (Priebe et al., 2006; Andermann et al., 2011; Glickfeld et al., 2013) to generate spatial and temporal frequency tuning curves and estimate speed tuning (Figure 3.6).

In normally reared adult mice, V1, LM and PM are uniquely responsive to stimuli from each eye and to spatiotemporal stimuli. V1 contains cells that span a broad range of spatiotemporal frequencies, while LM and PM are more selective in their tuning (Figure 4.1b). While all three areas contain neurons that respond to each or both eyes, the higher visual areas differ in their distribution of contralateral only, binocular and ipsilateral only neurons (Figure 4.1c, $p=0.008$). Area LM, which is highly binocular, also prefers relatively lower spatial frequencies and faster speeds. Area PM on the other hand, contains a higher proportion of contralateral only responsive cells and is tuned to relatively higher spatial frequencies and slower speeds (Figure 4.1d). Thus, the functional specialization of HVAs and their eye-specific proportions parallel our findings in V1, where the contralateral eye dominated neurons were tuned to higher spatial frequencies than the binocular or ipsilateral only responses (Salinas et al., 2017). Given the divergence in eye-specific tuning properties of LM and PM, we hypothesized that depriving mice of visual experience through one eye during the ocular dominance critical period may alter the spatiotemporal preferences of LM and PM.

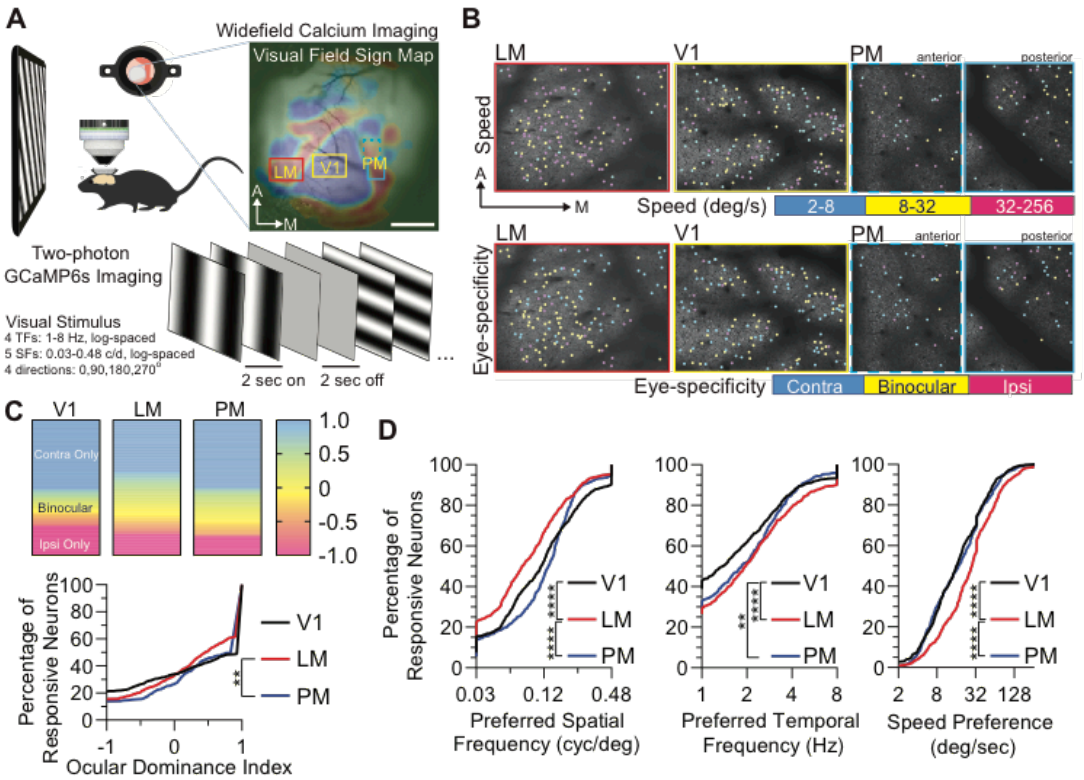

Figure 4.1: Spatiotemporal and Eye-specific Response Properties of V1, LM and PM. A. Experimental setup. Top Right: Widefield visual field sign map were used to delineate higher visual areas (from lateral to medial: LM (boxed in red), V1 (boxed in yellow) and PM (boxed in dark and light blue). Scale bar is 1mm. Top left: The visual field sign map was used to position two-photon calcium imaging experiments carried out while mice viewed drifting sinusoidal gratings of various spatial and temporal frequencies (speeds). The stimulus was shown to either the contralateral or ipsilateral eye to generate eye-specific speed tuning curves (Demonstrated in Figure 2). **B. Top:** Maps of speed preferences for LM, V1 and PM for the same animal. Notably, LM is tuned to faster speeds while V1 is broadly tuned to speed. **Bottom:** Maps of eye-specific responses for the same fields. LM contains many binocular cells while PM is strongly biased by contralateral-dominated responses. **C. Top:** Maps for eye-specificity in V1, LM and PM. Contra Only responses are shown in blue, ipsi only responses in magenta and binocular ODI in between the two extremes. **Bottom:** Cumulative distributions for ocular dominance index, with contra only responses at 1 and ipsi only responses at -1. LM and PM have distinct distributions for ocular dominance index (V1 median: 1.0, mean: 0.3078, n=819 neurons; LM median: 0.454, mean: 0.281, n=645 neurons, PM median: 1, mean: 0.395, n=488 neurons; Kruskal-Wallis test, p=0.0081, Dunn's multiple comparisons post hoc test, LM vs. PM; p<0.0081; KW(s)=9.362, N=8 mice). **D. Left:** Cumulative distributions for preferred spatial frequency of V1 (black), LM (red), and PM (blue). All distributions differ in preferred spatial frequency except for V1 and PM (V1 median: 0.114 cyc/deg; LM median: 0.0768 cyc/deg; PM median: 0.132 cyc/deg; Kruskal-Wallis test, p<0.0001; Dunn's multiple comparisons test, V1 vs. LM p<0.0001; LM vs. PM p<0.0001; KW(s)=55.45). **Middle:** Cumulative distributions for preferred temporal frequency. All distributions differ in their preferred temporal frequency except for LM and PM. (V1 median: 1.38 Hz; LM median: 1.97 Hz; PM median: 1.85 Hz; Kruskal-Wallis test, p<0.0001; Dunn's multiple comparisons test, V1 vs. LM p<0.0001; V1 vs. PM p<0.0044; KW(s)=30.30). **Right:** Cumulative distributions for preferred speed of V1 (black), LM (red), and PM (blue). All distributions differ in their spatial temporal preferences except for V1 and PM (V1 median: 16.1 deg/sec; LM median: 28.1; PM median: 17.34; Kruskal-Wallis test, p<0.0001; Dunn's multiple comparisons test, V1 vs. LM p<0.0001; LM vs. PM p<0.0001; KW(s)=73.28).

4.3.2 Monocular Deprivation disrupts the functional segregation of V1, LM and PM

To determine if the functional specialization of higher visual areas depend upon proper binocular visual experience during the ocular dominance critical period, we monocularly deprived mice of vision through the contralateral eye for two weeks starting at P19 and assessed eye-specific spatiotemporal tuning in adulthood. We again used the visual field sign map to determine areal borders and found no overt differences in the maps between normal and deprived mice. In the spatiotemporal dimension, CMD shifts speed preferences in V1 towards faster speeds (Figure 4.2a, left). However, in area LM, which is normally tuned to lower spatial frequencies, CMD shifts speed responses towards slower speeds (Figure 4.2a, middle). To quantify inter-areal differences in spatiotemporal tuning, we used the Mahalanobis distance. In No MD, the spatiotemporal preferences of each area fall within distinct clusters (Figure 4.3c-d, top). Monocular deprivation impairs the normal functional segregation of areas from on another, decreasing their Mahalanobis distances in the case of LM-PM and V1-LM, and increasing the distance between V1 and PM (Figure 4.3c-d, bottom). By animal analysis further demonstrates these shifts in inter-areal spatiotemporal clustering, diminishing the functional segregation between areas (Figure 4.3e,f).

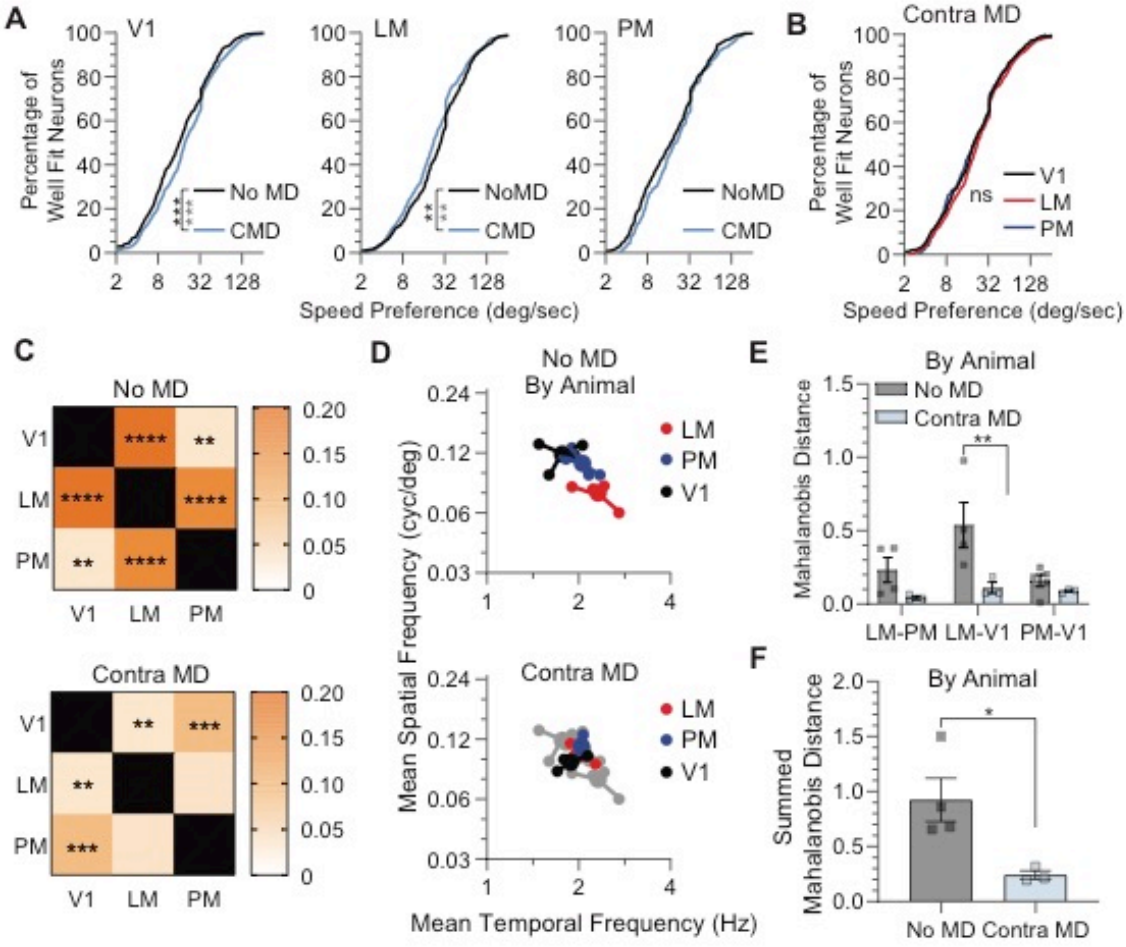

Figure 4.2 Monocular Deprivation disrupts the Functional Segregation of Higher Visual Areas. A. Cumulative distributions for preferred speed in No MD (black) and CMD (light blue) mice for neurons in V1 (left), LM (middle) and PM (right). In V1, CMD shifts speed preferences towards faster speeds (No MD median: 16.09 deg/sec, n=819 neurons; CMD median: 19.43 deg/sec, n=726 neurons; Mann-Whitney Test, MW(U)=266455, p=0.0004; Kolmogorov-Smirnov test, p=0.0010, KS(D)=0.099, NoMD N=8 mice, CMD N=6 mice). In LM, CMD shifts speed preferences towards slower speeds (No MD median: 28.05 deg/sec, n=645 neurons; CMD median: 22.2 deg/sec, n=567 neurons; Mann-Whitney Test, MW(U)=165937, p=0.0054; Kolmogorov-Smirnov test, p=0.0068, KS(D)=0.097, NoMD N=8 mice, CMD N=6 mice). No significant difference in speed preference was found with CMD for PM (No MD median: 17.3 deg/sec, n=488 neurons; CMD median: 21.1 deg/sec, n=216 neurons; Mann-Whitney Test, MW(U)=48079, p=0.0634, NoMD N=8 mice, CMD N=6 mice). **B.** Cumulative distributions for preferred speed of V1 (black), LM (red) and PM (blue) in CMD mice (V1 median: 19.4 deg/sec, n=726 neurons; LM median: 22.2 deg/sec, n=567 neurons; PM median: 21.1 deg/sec, n=216 neurons). Data for control mice are shown in lighter colors. Notice that the areas have lost their distinct speed distributions. **C.** Heatmap of inter-areal Mahalanobis distances in NoMD (top) and CMD (bottom) mice. In NoMD mice, each area is functionally segregated from the other (Summed inter-areal Mahalanobis distances: 0.401, V1 vs. LM: 0.202, p<0.0001; V1 vs. PM: 0.033, p=0.0064, LM vs. PM: 0.167, p<0.0001, N=8 mice). CMD results in diminished functional segregation between LM and PM as well as LM and V1 (Summed inter-areal Mahalanobis distances: 0.1623; V1 vs. LM: 0.033, p=0.0058; V1 vs. PM: 0.093, p=0.0004; LM vs. PM: 0.036, p=0.058, ns) **D.** Scatter for mean preferred spatial frequency and mean preferred temporal frequency for V1 (black), LM (red) and PM (blue) in NoMD (top) and CMD (bottom) mice. Each individual point is an animal while larger points represent the mean of the means. Control data is shown in grey on the CMD chart. **E.** By animal mean inter-areal Mahalanobis distances for each area comparison in

NoMD (grey) and CMD (blue) mice. Each individual point represents an animal. Error bar represents SEM. Deprivation significantly alters inter-areal Mahalanobis distances (Two-way ANOVA, Mixed-effects model (REML), deprivation factor p=0.0218; Sidak's multiple comparisons post-hoc test, LM-V1 p=0.0091, No MD N=5 mice, CMD N=3 mice). **F.** By animal mean summed Mahalanobis distance for inter-areal comparisons in NoMD (grey) and CMD (blue) mice. Each individual point represents an animal. Error bar represents SEM (Welch's unpaired t test, p=0.0385, mean difference: -0.6812 +/- 0.2012).

4.3.3 Monocular Deprivation disrupts the functional segregation of eye-specific responses

We have previously reported eye-specific asymmetries in tuning for spatial frequencies in binocular V1 (Salinas et al., 2017). Here, we grouped neural responses into three eye-specific categories (contralateral only, binocular, ipsilateral only) and tested whether these groups were functionally segregated in terms of spatiotemporal tuning (Figure 4.3). In all three areas, neurons dominated by contralateral eye input are tuned to the slowest speeds (Figure 4.3a). In V1, neurons linked by eye-specificity are tuned to distinct speeds, with binocular neurons preferring intermediate and ipsilateral-dominated neurons preferring the fastest speeds (Figure 4.3a, left). Ipsilateral-dominated neurons of LM are also tuned to significantly faster speeds than their contralateral-dominated counterparts (Figure 4.3a, middle). In contrast, in PM, neurons linked by eye-specificity are less distinct in their speed preferences (Figure 4.3a, right).

CMD results in a shift of the speed preferences of eye-specific responses in V1, so much so, that the binocular speed preferences are no longer distinct from the ipsilateral-dominated speed preferences (Figure 4.3b, left). The effect of CMD on shifting eye-specific speed preferences in LM was less robust (Figure 4.3b, middle). In CMD mice, the eye-specific speed preferences are no longer distinct (Figure 4.3b,right). CMD has differential effects on intra-areal eye-specific clustering (Figure 4.3d). While V1 and LM seem to lose

their eye-specific functional segregation, area PM, whose neurons linked by eye-specificity were quite matched in controls, is more functionally segregated with CMD (Figure 4.3d).

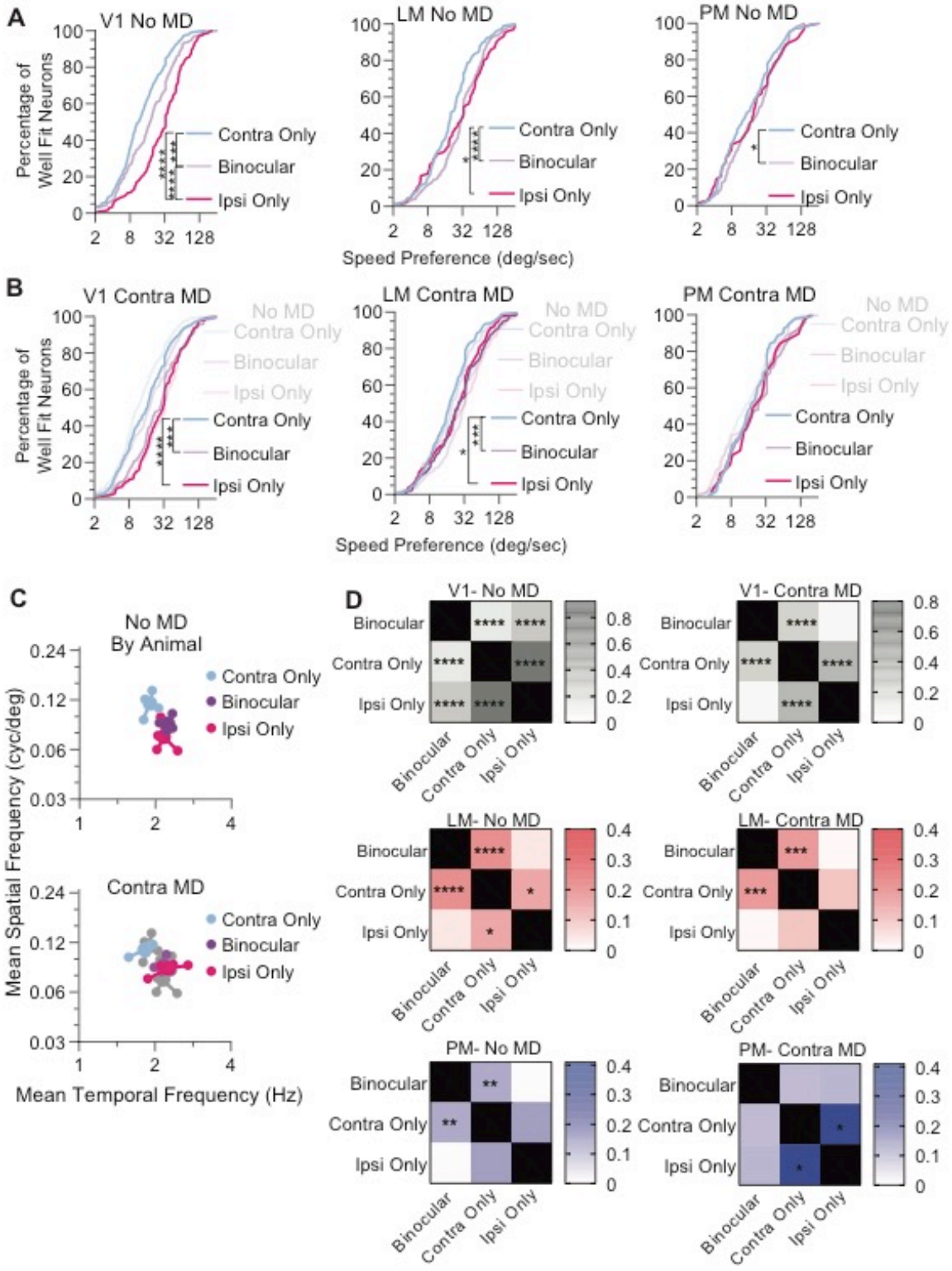

Figure 4.3 Monocular Deprivation disrupts the Functional Segregation of Eye-specific Responses. A. Cumulative distributions for preferred speed of contralateral eye-dominated (light blue), binocular (purple) and ipsilateral eye-dominated (magenta) responsive neurons in V1 (left), LM (middle) and PM (right) in No MD mice. **Left**: In V1, all eye-specific responsive neurons are tuned to unique speeds (contralateral only median: 11.26 deg/sec n=419 neurons; binocular median: 18.06 deg/sec, n=226 neurons; ipsilateral only median: 33.33 deg/sec, n=174 neurons; Kruskal-Wallis test, KW(s)=85.2, p<0.0001; Dunn's multiple comparisons test, Contra only vs. binocular: p=0.0002; contra only vs. ipsi only: p<0.0001; binocular vs. ipsi only: p<0.0001, N=8 mice). **Middle**: In LM, contralateral dominated neurons are tuned to slower speeds than binocular and ipsilateral neurons (contralateral only median: 19.96 deg/sec, n=248 neurons; binocular median: 32.93 deg/sec, n=296 neurons; ipsilateral only median: 33.24 deg/sec, n=101 neurons; Kruskal-Wallis test, KW(s)=22.3, p<0.0001; Dunn's multiple comparisons test, Contra only vs. binocular: p<0.0001; contra only vs. ipsi only: p=0.0125; N=8 mice). **Right**: In PM, contralateral dominated responses are tuned to slower speeds than binocular neurons (contralateral only median: 14.24 deg/sec, n=245 neurons; binocular median: 22.04 deg/sec, n=175 neurons; ipsilateral only median: 19.2 deg/sec, n=60 neurons; Kruskal-Wallis test, KW(s)=6.308, p<0.0427; Dunn's multiple comparisons test, Contra only vs. binocular: p=0.0396, N=8 mice). **B.** Cumulative distributions for preferred speed of contralateral eye-dominated (light blue), binocular (purple) and ipsilateral eye-dominated (magenta) responsive neurons in V1 (left), LM (middle) and PM (right) in CMD mice. Control data is shown in lighter colors for reference. **Left**: In V1, all eye-specific responsive neurons are tuned to unique speeds except binocular and ipsilateral only neurons with CMD (contralateral only median: 16.51 deg/sec, n=391 neurons; binocular median: 27.92 deg/sec, n=174 neurons; ipsilateral only median: 31.21 deg/sec, n=161 neurons; Kruskal-Wallis test, KW(s)=, p<0.0001; Dunn's multiple comparisons test, Contra only vs. binocular: p<0.0001; contra only vs. ipsi only: p<0.0001; N=6 mice). **Middle:** In LM, contralateral dominated neurons are tuned to slower speeds than binocular and ipsilateral neurons with CMD (contralateral only median: 18.03 deg/sec, n=246 neurons; binocular median: 26.44 deg/sec, n=193 neurons; ipsilateral only median: 25.78 deg/sec, n=128 neurons; Kruskal-Wallis test, KW(s)=15.36, p=0.0005; Dunn's multiple comparisons test, Contra only vs. binocular: p=0.0007; contra only vs. ipsi only: p=0.0229; N=8 mice). **Right:** No significant difference in preferred speed was found with CMD in PM (contralateral only median: 17.48 deg/sec, n=96 neurons; binocular median: 23.64 deg/sec, n=81 neurons; ipsilateral only median: 21.48 deg/sec, n=39 neurons; Kruskal-Wallis test, KW(s)=2.14, p=0.344, N=6 mice). **C.** Scatter for mean preferred spatial frequency and mean preferred temporal frequency for contralateral only (light blue), binocular (purple) and ipsilateral only (magenta) in No MD (top) and CMD (bottom) mice. Each individual point is an animal while larger points represent the mean across animals. Control data is shown in grey on the CMD chart. **D.** Heatmaps for intra-areal eye-specific Mahalanobis distances in V1 (top, black), LM (middle, red) and PM (bottom, blue) for No MD. **Top:** In V1, No MD eye-specific responses are functionally segregated (No MD: Summed Mahalanobis Distance=1.42; V1: contra only vs. binocular: 0.142, p<0.0001; contra only vs. ipsi only: 0.926, p<0.0001; binocular vs. ipsi only: 0.348, p<0.0001; Wilk's lambda test p<0.0001, N=8 mice). V1 cells of CMD mice have shorter Mahalanobis distances and less segregation than controls (CMD Summed Mahalanobis distance= 0.6813; contra only vs. binocular: 0.243, p<0.0001; contra only vs. ipsi only: 0.396, p<0.0001; binocular vs. ipsi only: 0.0423, ns; Wilk's lambda test p<0.0001, N=6 mice). **Middle:** In LM, No MD contralateral only responses are functionally segregated from other eye-specific responses (No MD: Summed Mahalanobis Distance=0.310; V1: contra only vs. binocular: 0.156, p<0.0001; contra only vs. ipsi only: 0.1217, p=0.0132; binocular vs. ipsi only: 0.0315, p=0.310, ns; Wilk's lambda test p<0.0001, N=8 mice). LM cells of CMD mice have shorter Mahalanobis distances and less segregation than controls (CMD Summed Mahalanobis distance= 0.228; contra only vs. binocular: 0.140, p=0.00057; contra only vs. ipsi only: 0.079, p=0.037, ns; binocular vs. ipsi only: 0.008, p=0.713, ns; Wilk's lambda test p=0.0027, N=6 mice). **Bottom:** In PM, No MD contralateral only responses are functionally segregated from binocular neurons (No MD: Summed Mahalanobis Distance=0.262; V1: contra only vs. binocular: 0.118, p=0.0027; contra only vs. ipsi only: 0.137, p=0.0269, ns; binocular vs. ipsi only: 0.007, p=0.847, ns; Wilk's lambda test p=0.0048, N=8 mice). The functional specializations of eye-specific responses are rearranged in PM of CMD mice (CMD Summed Mahalanobis distance= 0.262; contra only vs. binocular: 0.094, p=0.132, ns; contra only vs. ipsi only: 0.357, p=0.0081; binocular vs. ipsi only: 0.1002, p=0.271, ns; Wilk's lambda test p=0.0297, N=6 mice).

4.3.4 Monocular Deprivation alters eye-specific speed tuning properties

Visual areas of mice are not only specialized for distinct speeds, but also have varying degrees for speed tuning, or the dependence of temporal frequency preference on spatial frequency (Andermann et al., 2011). Area PM has been demonstrated to have a relatively higher degree of speed tuning than area V1. We assessed if CMD had an affect on the overall speed tuning of areas V1, LM and PM by comparing speed tuning indices obtained from the fitted data (Figure 4.4a). Speed tuning indices of 1 are speed-tuned cells, while speed tuning indices of 0 have no speed tuning. The distribution for speed tuning in V1, although slighted shifted to the left with CMD, was not found to be significantly different between the groups. However, it appears that there may be less speed-tuned neurons in V1 with CMD and that our sample size could have affected the lack of difference in the distributions. CMD appeared not to have disrupted the degree of speed tuning in LM and PM.

Since speed tuning has been demonstrated to negatively correlate with speed preferences (Andermann et al., 2011), and because contralateral eye-dominated responses are preferentially tuned to higher spatial frequencies, we asked if there was an eye-specific distinction in speed tuning NoMD and CMD mice (Figure 4.4b). In No MD mice, in areas V1 and PM, speed-tuning indices of the contralateral eye responses were significantly more speed tuned than ipsilateral eye responses. Interestingly, this eye-specific speed tuning is absent in CMD mice. In CMD mice, both areas LM and PM contain eye-specific speed tuning. Since CMD resulted in a shift of speed preferences in V1 and LM, we asked if speed preferences for speed-tuned neurons were different in CMD and No MD mice. We find that the speed-tuned neurons of PM are shifted towards slower speeds in CMD mice (Figure

4.4c). Our results suggest that CMD during the critical period disrupts eye-specific speed tuning in V1 and may lead to shifted speed preferences for neurons tuned for speed in area PM.

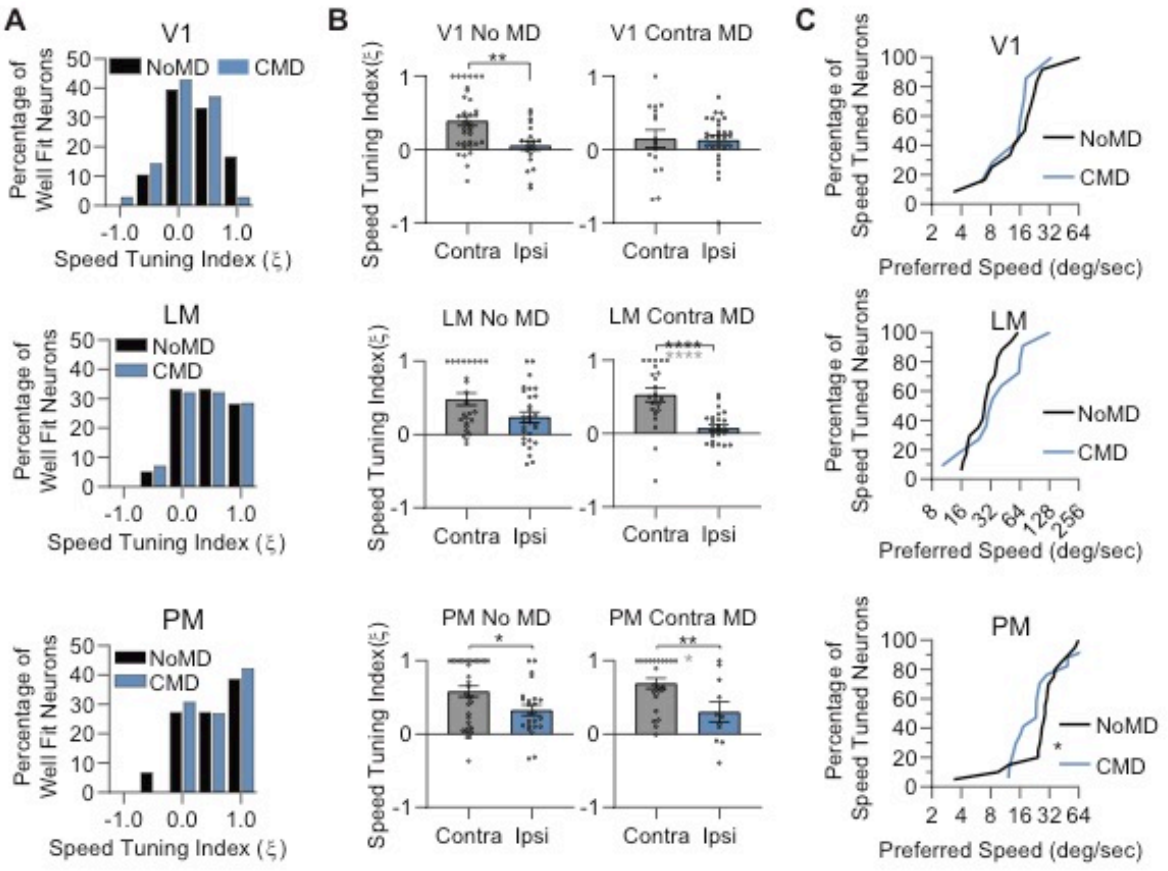

Figure 4.4 Monocular deprivation effects on speed tuning. A. Histograms for speed tuning indices in No MD (black) and CMD (light blue) for all cells in V1 (top, median: 0.25, mean: 0.28), LM (middle, median: 0.34, mean: 0.41) and PM (bottom, median: 0.46, mean: 0.49). **B.** Speed tuning indices segregated by eye-specific responses in No MD (left column) and CMD (right column) mice for V1 (top), LM (middle) and PM (bottom). Individual points on the graph are speed-tuning indices from individual cells. Mean and SEM are plotted. In No MD mice, the contralateral eye is more speed tuned than the ipsilateral eye in both V1 and PM (V1: contralateral mean: 0.39, median: 0.36, n=35 neurons; ipsilateral mean: 0.053, median: 0.085, n=20 neurons, Welch's unpaired t-test p=0.0016, r^2=0.172; PM: contralateral mean: 0.58, median: 0.68, n=36 neurons; ipsilateral mean: 0.33, median: 0.29, n=24 neurons, Kolmogorov-Smirnov test p=0.0187, KS(D)=0.403; LM: contralateral mean: 0.48, median: 0.31, n=25 neurons; ipsilateral mean: 0.24, median: 0.17, n=29 neurons, Kolmogorov-Smirnov test p=0.118, KS(D)=0.296). In CMD mice, eye-specific tuning for speed is not different in V1 (contralateral mean: 0.15, median: 0.12, n=16 neurons; ipsilateral mean: 0.13, median: 0.18, n=29 neurons). In contrast, in CMD mice, both LM and PM responses driven by the contralateral eye are more speed tuned than those driven by the ipsilateral eye (LM: contralateral mean: 0.53, median: 0.52, n=22 neurons; ipsilateral mean: 0.076, median: 0.071, n=25 neurons, Kolmogorov-Smirnov test p<0.0001, KS(D)=0.658; Mann-Whitney test p<0.0001; mW(U)=84; PM: contralateral mean: 0.69, median: 0.67, n=23 neurons; ipsilateral mean: 0.30, median: 0.24, n=11 neurons, Kolmogorov-Smirnov test p=0.118, KS(D)=0. 510; Mann-Whitney test p=0.0064, MW(U)=54). **C.** Cumulative distributions for speed preferences of cells that are tuned for speed in No MD (black) and CMD (light blue) mice are shown for V1 (top), LM (middle) and

PM (bottom). In PM, the preferred speeds of speed-tuned neurons are significantly shifted towards slower speeds with CMD (No MD median: 28.9 deg/sec, n=20 neurons; CMD median: 23.4 deg/sec, n=17 neurons, p=0.0213, KS(D)=0.497).

4.4 Discussion

Higher visual areas have distinct spatiotemporal tuning properties that depend upon binocular visual experience in early life

In this study we found pronounced effects of monocular deprivation during the critical period on the functional specialization of visual areas. CMD shifted speed preferences differentially in V1 and LM, bringing the two closer together in the spatiotemporal domain. The distribution of speed preferences, which is the best way to segregate higher visual areas from one another, became nearly identical for V1, LM and PM with CMD. We quantified the difference between inter-areal clusters in the spatiotemporal domain with the Mahalanobis distance and found that CMD reduces the differences between the three areas. Overall, there is a reduction in the differentiation of V1 and HVAs in mice that are deprived of visual input through the contralateral eye.

It has been shown that the functional specialization of HVAs refines over the course of development (Murakami et al., 2017; Smith et al., 2017). The summed Mahalanobis distances for HVAs are relatively small at P20 and adult-like by P25 (Murakami et al., 2017), a time window that overlaps with the ocular dominance critical period. Our study demonstrates that CMD during this time window can dramatically shift spatiotemporal preferences of visual areas into adulthood, resulting in a reduction of adult-like areal segregation. It has been proposed that areas of the putative dorsal stream take longer to develop than areas of the putative ventral stream (Smith et al., 2017). Here, we show that spatiotemporal tuning of area LM, grouped in the putative ventral stream, was altered with

CMD, while the selectivity of PM, grouped in the putative dorsal stream, seemed to be unaffected. Here, areas from both streams appear to be vulnerable to MD, although in an eye-specific dependent manner. The difference may lie in the type of manipulation and the measurement: Smith and colleagues dark reared mice from E14 to P40 and used intrinsic signal optical imaging to compare response magnitude to visual stimulation.

Neurons linked by eye-specificity may serve as an efficient routing mechanism from the retina to functionally specialized HVAs

We have found an asymmetry in the eye-specific tuning for spatial frequency in V1 of mice, whereby cells dominated by the contralateral eye prefer higher spatial frequencies than binocular and ipsilateral only responses (Salinas et al., 2017). In normal mice, areas LM and PM have unique proportions of eye-specific responses in conjunction with disparate spatial frequency tuning: LM is more binocular and tuned to lower spatial frequencies while PM is more contralaterally-biased and is tuned to higher spatial frequencies. Thus, the areal distributions parallel the eye-specific functional organization shown in V1. Here, we asked if neurons linked by eye-specificity in HVAs are functionally segregated, as in V1, and if this segregation is experience-dependent.

In the spatiotemporal domain, contralateral only responses are tuned to slower speeds (low temporal frequency/ high spatial frequency), binocular cells are tuned to intermediate speeds and ipsilateral only cells are tuned to the fastest speeds (high temporal frequency/ low spatial frequency). LM and PM share some of the eye-specific functional segregation found in V1, with the contralateral only cells tuned to the slowest speeds. However, the distances between clusters of eye-specific preferences are smaller in LM and PM, suggesting that convergence of functionally specific cells may lead to better

interocular matching of features in downstream areas of cortex. CMD disrupts the functional segregation of eye-specific responses most pronouncedly in V1, but also in LM and PM, bringing the spatiotemporal frequency preferences of eye-specific responses closer together.

Retinal ganglion cells carry distinct channel information and terminate in eye-specific zones of the thalamus and superior colliculus. Subregions of the dorsal lateral geniculate nucleus house functionally distinct cell types, which project to distinct layers of cortex (Krahe et al., 2011). For example, a subset of highly direction-selective and high spatial frequency tuned cells of the shell region projecting to superficial layers of V1 (Cruz-Martin et al., 2014). Thus, the functional distinction of eye-specific responses in V1 and HVAs may be a result of cell type-specific projections from subcortical structures that receive input from the retina (reviewed in Seabrook et al., 2017). This early eye-specific functional segregation may serve as an efficient routing mechanism for organizing the functional architecture of V1 and HVAs.

The mouse visual system as a model for understanding developmental mechanisms of higher visual area processing

CMD led to a reduction in the functional specialization of V1 and HVAs, but it did not eliminate speed tuning in LM and PM. However, there is a functional specialization of eye-specific responses for speed tuning, with neural responses to the contralateral eye carrying more speed-tuned information than the responses to the ipsilateral eye. This eye-specific distinction in speed tuning suggests that a subset of contralateral-dominated neurons may be important for downstream motion processing. This agrees with our previous findings of a contralateral bias for high direction selectivity (Salinas et al., 2017). CMD eliminated the

eye-specific speed tuning distinction in V1 and exacerbated it in LM. While the eye-specific distinction for speed tuning was not disrupted with CMD in PM, the preferred speeds of speed-tuned neurons in PM, was shifted towards slower speeds. These findings suggest that CMD causes a cascade of shifting preferences, impacting the tuning of cells relevant for motion processing.

In primates, visual cortical phase maps of ocular dominance, spatial frequency and orientation are aligned (Nauhaus et al., 2017). Multiple studies demonstrate that the functional architecture of V1 is repeated in HVAs (Ts'o et al., 2009; Ghose and Ts'o, 1997; Ghose and Ts'o, 2017). Here we provide evidence that eye-specific functional specialization occurs in V1 and HVAs of mice, and that the maintenance of this organization may be required for proper HVA development. This finding suggests that the organization of mouse visual cortex is fundamentally similar to the organization of primate visual cortex, even without columnar organization. The collapse of HVA selectivity onto one another in the spatiotemporal domain with CMD could be indicative that, as in amblyopic primates, monocular deprivation causes disturbances in visual processing related to both motion processing and form detection (Kozma and Kiorpes, 2003; Kiorpes et al., 2006; Kiorpes, 2006). Our study provides validation in studying the mouse visual system to understand how MD impacts visual processing related to higher order feature detection and to reveal mechanisms underlying the development of the visual system.

CHAPTER 5: Discussion

5.1: Summary

One way the visual cortex has tackled visual perception is by creating functionally organized modules with neurons that prefer similar stimuli, linking them and stacking them into simultaneous processing stages. This repetition allows filtering and processing of multiple feature dimensions within the circuitry to complete on-demand tasks simultaneously and flexibly. Spatiotemporal filtering is one of the earliest stages of the process, beginning first with the functionally distinct retinal ganglion cells and passed on to the thalamus and visual cortex. The parallel channels process and transform distinct features of the visual scene from these filters, such as information related to motion, depth and form, into two proposed streams of information processing: the dorsal and the ventral pathways (Ungerleider and Mishkin 1982; Maunsell and Newsome, 1987; Goldman-Rakic, 1988).

Inherently coupled to the task of parallel processing is the eye-specific organization arising upon the mixing of inputs from the two eyes in later stages of the visual system. Eye-specific segregation is largely maintained in the thalamus and superior colliculus. Inputs from the two eyes first converge predominantly in primary visual cortex (V1). In V1, at least in mice, neurons vary greatly in their spatiotemporal and orientation tuning in what largely appears to be a random “salt and pepper fashion”, although weak local clustering exists (Ohki and Reid 2007; Ringach et al., 2016). Despite this apparent disorderliness, hierarchically higher order visual areas are comprised of neurons with unique spatiotemporal tuning and are grouped into putative dorsal and ventral streams (Marshel et al., 2011; Andermann et al., 2011; Glickfeld et al., 2013; Wang et al., 2012).

Electrophysiological evidence suggests that despite its broad distribution of spatiotemporal tuning (Niell and Stryker, 2008) and apparent lack of obvious functional domains (but see Ji et al., 2015), V1 contains distinct channels of information, which differ substantially in their tuning for spatial frequency, among other visual properties like contrast sensitivity and temporal frequency (Gao et al., 2010; Ji et al., 2015).

One possible interpretation of how higher visual areas acquire their selectivity is through like-to-like connectivity from V1, such that the cells in V1 which share the spatiotemporal tuning properties of a higher visual area make synaptic contacts preferentially with that area. There is evidence that such target specificity exists in mice (Glickfeld et al., 2013; Matsui and Ohki, 2013). However, the dependence of V1 activity on the functional selectivity of HVAs has been called to question. Inactivating adult V1 does not alter spatiotemporal tuning of HVAs (although inactivating the SC seems to shift velocity tuning of V1 and HVAs, Tohmi et al., 2014). Many studies have demonstrated that monocular deprivation (MD) shifts neural preferences towards the non-deprived eye and results in a reduction of acuity at the level of V1 (Prusky and Douglas 2003), linking a shift in eye-specific responses with a shift in spatial frequency tuning. However, there is an absence of understanding how early visual experience shapes higher visual area processing, whose activity in primates is thought to better reflect visual percepts (Kiorpes, 2016). In the case of MD, when interocular inputs have been disrupted and there is a loss of high spatial frequency tuning in V1, what might be the effects on higher visual area selectivity, if any?

We first sought to understand if eye-specificity is linked to spatial frequency tuning at the level of binocular V1 to determine if eye-specificity may be involved in carrying

distinct channels of information related to preferred spatial frequency. We imaged visually evoked activity from thousands of excitatory neurons in L2/3 of transgenic mice expressing the genetically encoded calcium indicator GCaMP6s. We found an asymmetry in the tuning for spatial frequency between the contralateral and ipsilateral eye, such that neurons dominated by the contralateral eye were tuned to the highest spatial frequencies and were prominently direction selective, while binocular and ipsilateral responses were tuned to lower spatial frequencies (Salinas et al., 2017). Cells preferring high spatial frequencies were tuned to the cardinal directions (0,90,270,180^{o}). Cardinal direction selectivity is a known feature of higher visual area PM (Roth et al., 2012), who has been postulated to play a role in spatial navigation, projecting to retrosplenial cortex. These asymmetries in V1 appear to link eye-specificity with spatial frequency, a now known feature of primate V1 (Nauhaus et al., 2016), and a potential explanation for a shift in spatial frequency tuning after depriving an eye during the ocular dominance critical period. We hypothesized that the asymmetries found at the level of V1 may be repeated in higher visual areas (HVAs) of cortex, as has been demonstrated with the functional organization of feature maps in primates (Ts'o et al., 2009; Ghose and Ts'o, 1997; Ghose and Ts'o, 2017).

We assessed if these eye-specific tuning biases were present in two higher visual areas grouped into the putative ventral and dorsal streams: areas LM and PM. We characterized tuning properties for early stimulus features (spatial frequency, temporal frequency, orientation and direction) and found motifs between the three areas, which substantiated our hypothesis, that eye-specific response properties in V1 are repeated in higher visual areas, potentially linking distinct processing channels. Contralateral eye dominated responses were always tuned to the highest spatial frequencies of a given area.

The eye-specific bias from the population ODI reflected each area's unique spatial frequency tuning properties. We also found the same ocular distinction for direction and orientation tuning in all areas. The binocular cells were more selective for orientation while cells dominated by one eye were more direction selective. Moreover, area PM was biased to the cardinal directions, similar to the contralateral dominated neurons of V1, while LM preferred intercardinal directions just as much as cardinal directions. Next, we show that information regarding eye-specificity and spatial frequency is carried from V1 to higher visual areas LM and PM by recording from V1 afferents in LM and PM. Despite the difference in eye-specific tuning for spatial frequency found in LM and PM, these HVAs were better matched in interocular preferences for spatial frequency and orientation, suggesting that convergence of inputs results in better alignment between the two eyes downstream from V1. Indeed, when we assessed the eye-specific spatial frequency tuning of V1 afferents to LM and PM we detected a difference in eye-specific spatial frequency tuning in V1 afferents to LM, but not PM.

The functional motifs we find in V1, LM and PM, and the eye-specific afferents from V1 to LM and PM could be an indication that neurons linked by eye-specificity are functional channels that endow higher visual areas their specialization. This finding does not depend on the classical hierarchical cortical model (i.e. that V1 output is required for HVA specialization) being true for mice, since eye-specificity from subcortical structures that project to both V1 and HVAs could be responsible. For example, besides the central visual pathway (retina->dLGN->V1->HVAs), there is also the extrageniculate pathway (retina->SC->LP->HVAs) as well as a minor indirect route from the superior colliculus to the dLGN and both V1 and HVAs (Tohmi et al, 2014). Eye-specific inputs remain largely

segregated in the dLGN, but binocularity does exist (Huh et al., 2018; Zeater et al., 2015). In primates, there is binocularity in the SC (Economides et al., 2018). Thus, it is not impossible that eye-specific routing from subcortical structures could participate in HVA selectivity.

Because speed has been shown to better segregate the functional selectivity of HVAs, we assessed eye-specific spatiotemporal tuning in V1, LM and PM. Eye-specific responses are functionally segregated in V1 and appear to become less segregated in a hierarchical fashion. The contralateral eye responses were also much more speed tuned than the ipsilateral eye responses. Thus, neurons linked by eye-specificity prefer distinct features in terms of spatiotemporal frequency, orientation and direction in V1 and higher visual areas of mouse visual cortex. Moreover, the eye-specific responses may be carrying information related to distinct stream processing: the contralateral dominated neurons are more tuned for speed, direction selective and prefer higher spatial frequencies. The binocular neurons are tuned for orientation and intermediate speeds while the ipsilateral only responses are tuned for faster speeds.

We then perturbed binocular visual processing during the ocular dominance critical period via two weeks of monocular deprivation through the contralateral eye and assessed eye-specific spatiotemporal tuning in V1, LM and PM. We find that monocular deprivation through either the contralateral eye results in a de-differentiation of higher visual areas, such that the spatiotemporal tuning of V1, LM and PM become more similar. Monocular deprivation also disrupted the eye-specific functional segregation of visual cortex found in normally reared mice. While the degree of speed tuning was not eliminated with CMD, it was impacted in area PM, an area much more speed tuned than V1. Altogether our data demonstrates that the maturation of higher visual areas is dependent on proper binocular

visual experience and suggests that the functional specialization of eye-specific responses could be an efficient routing mechanism to differentiate higher visual areas.

5.2: Limitations

Using two-photon calcium imaging in awake mice, we were able to record from thousands of neurons in layer 2/3 of visual cortex as mice transiently viewed visual stimuli through each eye. To accomplish these experiments we took advantage of a transgenic mouse model, which expresses the genetically encoded calcium indicator, GCaMP6s, in all excitatory neurons. While GCaMPs have improved substantially since they were first introduced (Chen et al., 2013) and have been demonstrated to detect single action potentials in soma and even dendritic spines, calcium imaging is still a correlate of neural activity. One limitation of our experiments is thus inferring neural activity from these calcium transients. Because the field is heavily based on classical electrophysiological experiments, it is important to point out that there are some discrepancies between our reports on the prevalence of eye-specific responses and the literature using electrophysiological measurements. For instance, we report far more contralateral dominated and ipsilateral dominated neurons in binocular V1 than previously described (Dräger, 1975; Mrsic-Flogel et al., 2007; Gordon and Stryker, 1996). While some of the discrepancies may be due to choice of stimulus conditions (using only lower spatial frequencies will help balance out the percent contralateral and ipsilateral responsive neurons, since both have preferences for low SFs), it is also possible that the difference lies in the technique. Studies using calcium indicators also report higher prevalence of contralateral dominated neurons (Scholl et al., 2017). It could be that the difference in

assessing “baseline” activity using calcium imaging is inherently different than in electrophysiology, allowing us to isolate cell responses that electrophysiological recordings cannot. The fact that the binocular neurons’ response amplitudes are greater than the contralateral or ipsilateral-dominated neurons substantiates this. It is also possible that, since we are able to record from hundreds of cells at a time, that our sampling size is far larger and less susceptible to bias from searching for visually responsive cells. On the other hand, it could be that calcium imaging is unable to detect very weak responses, missing the non-dominant eye input to cells that we identify to be monocular. We were able to determine that contralateral eye responses were tuned to higher spatial frequencies than ipsilateral eye responses using electrophysiological techniques (unpublished data), but we were unable to confirm the ODI distributions using electrophysiological methods. Due to the rise and fall time of the indicator, it was also impossible to determine if the eye-specific responses related to complex or simple cells, which would have been informative for the interpretation of the study.

There have been reports that locomotion can alter visual tuning properties in mouse visual cortex (Niell and Stryker 2010; Mineault et al., 2016). One limitation of our study is we did not measure locomotion or relate it to the tuning of V1 and HVAs. However, we measured pupil dilation as a correlate for behavioral state, in contralateral and ipsilateral eye viewing sessions to be sure that there were not behavioral state changes potentially causing the differences in eye-specific spatial frequency tuning. This was substantiated by similar eye-specific spatial frequency tuning preferences from animals that were anesthetized. Moreover, it has been demonstrated that peak speed preferences are not different when the animal is stationary vs. when the animal is moving for V1, PM and

another higher visual area, RL (Andermann et al., 2011). Still, it would be interesting to know if locomotion has any differential effect on eye-specific responses, especially since the contralateral eye dominated neurons are linked to early features important for motion detection. Moreover, all higher visual areas receive direct input from LP, which itself received input from the superior colliculus of the extrageniculate pathway. This pathway may provide context and modulate visual processing related to motion (Dean and Redgrave, 1984b; Roth et al., 2016).

Our recordings were restricted to layer 2/3 of the cortex. While this is the predominantly feedforward layer in primates, mice exhibit even less of the strict laminar segregation of primates, and layer 4 in mice is also a feedforward layer. It would be informative to know if cells of layer 4 also exhibit the same eye-specific response properties of cells in layer 2/3. This could help with the interpretation, since layer 4 is the predominant layer receiving input from the dLGN, while superficial layers (including layer 2/3) receive input from the LP. If no such eye-specific functional organization could be found in layer 4, it might hint that the inputs are coming from the LP. However, to aid in this limitation, other work in our lab has demonstrated that inputs from the dLGN carry functionally segregated eye-specific responses, at least in terms of spatial frequency tuning to V1 (Huh et al., 2018). Thus, our findings may not just be a consequence of the mouse visual system being heavily influenced by superior colliculus activity, but may be applicable to understanding hierarchical primate vision.

We have found interesting effects on the spatiotemporal tuning of HVAS with CMD. While these experiments are useful for understanding the transformations that take place from V1 to higher visual areas, they do not add to our understanding of what higher visual

areas of mice do. While inferences can be made based on preferences for early feature detectors, we are still limited in what we can say about mouse higher visual area processing due to the fact that we really don't know what many of the areas do or have clearly define homologs for primate visual areas. The lack of an understanding of HVA function and visual processing tasks catered towards mice make it difficult to relate our findings to those of primates. Still, our studies demonstrate that, at the cellular level, the mouse visual system is fundamentally similar to primates and warrants further exploration on the function of mouse HVAs.

5.3: Recommendations for Future Work

There are many implications for our findings that eye-specific responses are tuned to unique speeds and that monocular deprivation during the ocular dominance critical period disrupts the differentiation of higher visual areas. It may be that MD impairs higher order visual processing for complex features, such as global form or motion processing. Future studies linking eye-specific responses to the detection of higher visual processing tasks would make the findings more compelling and suggest that the mouse could serve as a useful model for understanding mechanisms of amblyopia. The experiment on tuning for plaids vs. gratings would be a great experiment to do under each eye viewing condition, to see if the eye-specific responses are distinctly important for stream processing.

We were able to characterize eye-specific V1 afferents to LM and PM, but we did not do so in mice that were visually deprived. It would be interesting to know if the eye-specific routing of information from V1 to HVAs is perturbed in CMD. Does V1 start to send higher spatial frequency tuned information to LM? It would also be beneficial to know if V1 activity, during the time of deprivation, is important for the functional segregation of HVAs.

Are V1 and the HVAs all receiving functionally segregated eye-specific information from subcortical structures or are the HVAs dependent on V1 activity to develop, as would be expected if the cortex develops hierarchically.

References

Adams, Michelle M., et al. "Visual cortical projections and chemoarchitecture of macaque monkey pulvinar." *Journal of Comparative Neurology* 419.3 (2000): 377-393.

Ahmadlou, Mehran, Larry S. Zweifel, and J. Alexander Heimel. "Functional modulation of primary visual cortex by the superior colliculus in the mouse." *Nature communications* 9.1 (2018): 3895.

Andermann, Mark L., et al. "Functional specialization of mouse higher visual cortical areas." *Neuron* 72.6 (2011): 1025-1039.

Anderson PA, Movshon JA (1989) Binocular combination of contrast signals. *Vision Research* **29(9)**:1115–1132

Antonini, Antonella, and Michael P. Stryker. "Rapid remodeling of axonal arbors in the visual cortex." *Science* 260.5115 (1993): 1819-1821.

Antonini, Antonella, Michela Fagiolini, and Michael P. Stryker. "Anatomical correlates of functional plasticity in mouse visual cortex." *Journal of Neuroscience* 19.11 (1999): 4388-4406.

Apkarian PA, Nakayama K, Tyler CW (1981) Binocularity in the human visual evoked potential: Facilitation, summation and suppression. *Electroenceph and Clinical Neurophysiol* **51(1)**:32-48

Applebury, M. L., et al. "The murine cone photoreceptor: a single cone type expresses both S and M opsins with retinal spatial patterning." *Neuron* 27.3 (2000): 513-523.

Ayzenshtat, Inbal, Jesse Jackson, and Rafael Yuste. "Orientation tuning depends on spatial frequency in mouse visual cortex." *eNeuro* 3.5 (2016).

Baden, Tom, et al. "A tale of two retinal domains: near-optimal sampling of achromatic contrasts in natural scenes through asymmetric photoreceptor distribution." *Neuron* 80.5 (2013): 1206-1217.

Bagolini B, Porciatti V, Falsini B (1988) Binocular interaction and steady-state evoked potentials. *Graefe's Arch Clin Exp Ophthalmol* **226(5)**:401-406

Baroncelli, L., C. Braschi, and L. Maffei. "Visual depth perception in normal and deprived rats: effects of environmental enrichment." *Neuroscience* 236 (2013): 313-319.

Bartfeld, Eyal, and Amiram Grinvald. "Relationships between orientation-preference pinwheels, cytochrome oxidase blobs, and ocular-dominance columns in primate striate cortex." *Proceedings of the National Academy of Sciences* 89.24 (1992): 11905-11909.

Basole, Amit, Leonard E. White, and David Fitzpatrick. "Mapping multiple features in the population response of visual cortex." *Nature* 423.6943 (2003): 986.

Benevento, L. A., and K. Yoshida. "The afferent and efferent organization of the lateral geniculo-prestriate pathways in the macaque monkey." *Journal of Comparative Neurology* 203.3 (1981): 455-474.

Berezovskii, Vladimir K., Jonathan J. Nassi, and Richard T. Born. "Segregation of feedforward and feedback projections in mouse visual cortex." *Journal of Comparative Neurology*519.18 (2011): 3672-3683

Bergeron A, Tardif E, Lepore F, Guillemot JP (1998) Spatial and temporal matching of receptive field properties of binocular cells in area 19 of the cat. *Neuroscience* **86(1)**: 121-134

Beurdeley M, Spatazza J, Lee HHC, Sugiyama S, Bernard C, Di Nardo AA, Hensch TK, Prochiantz A (2012) Otx2 binding to perineuronal nets persistently regulates plasticity in the mature visual cortex. *J Neurosci*, **32(27)**: 9429–9437

Bi, Hua, et al. "Neuronal responses in visual area V2 (V2) of macaque monkeys with strabismic amblyopia." *Cerebral Cortex* 21.9 (2011): 2033-2045.

Bickford, Martha E., et al. "Retinal and tectal “driver-like” inputs converge in the shell of the mouse dorsal lateral geniculate nucleus." *Journal of Neuroscience* 35.29 (2015): 10523-10534

Bienkowski, Michael S., et al. "Extrastriate connectivity of the mouse dorsal lateral geniculate thalamic nucleus." *Journal of Comparative Neurology* 527.9 (2019): 1419-1442.

Blake R, Levinson E (1977) Spatial properties of binocular neurones in the human visual system. *Exp Brain Res* **27(2)**:221

Blake F, Sloane M, Fox R (1981) Further Developments in binocular summation. *Perception and Psychophys*, **30**:266-276

Blakemore, C., and Fj Vital-Durand. "Organization and post-natal development of the monkey's lateral geniculate nucleus." *The Journal of Physiology* 380.1 (1986): 453-491.

Blakemore, Colin, J. Garey, and F. Vital-Durand. "The physiological effects of monocular deprivation and their reversal in the monkey's visual cortex." *The Journal of Physiology* 283.1 (1978): 223-262.

Blasdel, Gary G., and Jennifer S. Lund. "Termination of afferent axons in macaque striate cortex." *Journal of Neuroscience* 3.7 (1983): 1389-1413.

Blasdel, GARY G., and D. A. V. I. D. Fitzpatrick. "Physiological organization of layer 4 in macaque striate cortex." *Journal of Neuroscience* 4.3 (1984): 880-895.

Blasdel, Gary, Klaus Obermayer, and Lynne Kiorpes. "Organization of ocular dominance and orientation columns in the striate cortex of neonatal macaque monkeys." *Visual neuroscience* 12.3 (1995): 589-603.

Boothe, Ronald G., Velma Dobson, and Davida Y. Teller. "Postnatal development of vision in human and nonhuman primates." *Annual review of neuroscience* 8.1 (1985): 495-545.

Bullier, J., and H. Kennedy. "Projection of the lateral geniculate nucleus onto cortical area V2 in the macaque monkey." *Experimental Brain Research* 53.1 (1983): 168-172.

Brindley, G. S., P. C. Gautier-Smith, and W. Lewin. "Cortical blindness and the functions of the non-geniculate fibres of the optic tracts." *Journal of neurology, neurosurgery, and psychiatry* 32.4 (1969): 259.

Bruce, CHARLES J., Robert Desimone, and Charles G. Gross. "Both striate cortex and superior colliculus contribute to visual properties of neurons in superior temporal polysensory area of macaque monkey." *Journal of Neurophysiology* 55.5 (1986): 1057-1075.

Bussey, Timothy J., Lisa M. Saksida, and Lawrence A. Rothblat. "Discrimination of computer-graphic stimuli by mice: a method for the behavioral characterization of transgenic and gene-knockout models." *Behavioral neuroscience* 115.4 (2001): 957.

Calderone, Jack B., and Gerald H. Jacobs. "Regional variations in the relative sensitivity to UV light in the mouse retina." *Visual neuroscience* 12.3 (1995): 463-468.

Callaway, Edward M., and Liqun Luo. "Monosynaptic circuit tracing with glycoprotein-deleted rabies viruses." *Journal of Neuroscience* 35.24 (2015): 8979-8985.

Campbell FW, Green DG (1965) Monocular versus binocular visual acuity. *Nature* **208**(5006):191–192

Campbell FW, Maffei L (1970) Electrophysiological evidence for the existence of orientation and size detectors sin the human visual system. *J Physiology* **207(3)**:635-652

Cang, Jianhua, et al. "Roles of ephrin-as and structured activity in the development of functional maps in the superior colliculus." *Journal of Neuroscience* 28.43 (2008): 11015-11023.

Chapman, Barbara, and Michael P. Stryker. "Development of orientation selectivity in ferret visual cortex and effects of deprivation." *Journal of Neuroscience* 13.12 (1993): 5251-5262.

Chen TW, Wardill TJ, Sun Y, Pulver SR, Renninger SL, Baohan A, Schreiter ER, Kerr RA, Orger MB, Jayaraman V, Looger LL, Svoboda K, Kim DS (2013) Ultrasensitive fluorescent proteins for imaging neuronal activity. *Nature* **499(7458)**:295-300

Chino, Yuzo M., et al. "Postnatal development of binocular disparity sensitivity in neurons of the primate visual cortex." *Journal of Neuroscience* 17.1 (1997): 296-307.

Coleman, Jason E., et al. "Rapid structural remodeling of thalamocortical synapses parallels experience-dependent functional plasticity in mouse primary visual cortex." *Journal of Neuroscience* 30.29 (2010): 9670-9682.

Conley, Michael, and David Fitzpatrick. "Morphology of retinogeniculate axons in the macaque." *Visual neuroscience*2.3 (1989): 287-296.

Coogan, Thomas A., and Andreas Burkhalter. "Hierarchical organization of areas in rat visual cortex." *Journal of Neuroscience* 13.9 (1993): 3749-3772.

Crair, Michael C., et al. "Ocular dominance peaks at pinwheel center singularities of the orientation map in cat visual cortex." *Journal of Neurophysiology* 77.6 (1997): 3381-3385.

Crair, Michael C., et al. "Relationship between the ocular dominance and orientation maps in visual cortex of monocularly deprived cats." *Neuron* 19.2 (1997): 307-318.

Crair, Michael C., Deda C. Gillespie, and Michael P. Stryker. "The role of visual experience in the development of columns in cat visual cortex." *Science* 279.5350 (1998): 566-570.

Crook, J. M., et al. "Visual resolution of macaque retinal ganglion cells." *The Journal of physiology* 396.1 (1988): 205-224.

Cruz-Martín, Alberto, et al. "A dedicated circuit links direction-selective retinal ganglion cells to the primary visual cortex." *Nature* 507.7492 (2014): 358.

Czajkowski, Rafał, et al. "Encoding and storage of spatial information in the retrosplenial cortex." *Proceedings of the National Academy of Sciences* 111.23 (2014): 8661-8666.

Daniel, P. M., and D. Whitteridge. "The representation of the visual field on the cerebral cortex in monkeys." *The Journal of physiology* 159.2 (1961): 203-221.

Davis MF, Figueroa Velez DX, Guevarra RP, Yang MC, Habeeb M, Carathedathu MC, Gandhi SP (2015) Inhibitory neuron transplantation into adult visual cortex creates a new critical period that rescues impaired vision. *Neuron* **86(4)**:1055-1066

Dean, Paul, and Peter Redgrave. "The superior colliculus and visual neglect in rat and hamster. I. Behavioural evidence." *Brain Research Reviews* 8.2-3 (1984): 129-141.

Dean, Paul, and Peter Redgrave. "Superior colliculus and visual neglect in rat and hamster. III. Functional implications." *Brain Research Reviews* 8.2-3 (1984): 155-163.

DeAngelis, Gregory C., Izumi Ohzawa, and R. D. Freeman. "Spatiotemporal organization of simple-cell receptive fields in the cat's striate cortex. I. General characteristics and postnatal development." *Journal of neurophysiology* 69.4 (1993): 1091-1117.

DeAngelis, Gregory C., and William T. Newsome. "Organization of disparity-selective neurons in macaque area MT." *Journal of Neuroscience* 19.4 (1999): 1398-1415.

Dec, Krystyna, Remigiusz Tarnecki, and Boguslaw Zernicki. "Single unit responses to moving spots in the superior colliculus of the cat's isolated midbrain." *Acta neurobiol. exp* 38 (1978): 103-112.

Derrington, A. M., and P. Lennie. "Spatial and temporal contrast sensitivities of neurones in lateral geniculate nucleus of macaque." *The Journal of physiology* 357.1 (1984): 219-240.

Des Rosiers, M. H., et al. "Functional plasticity in the immature striate cortex of the monkey shown by the [14C] deoxyglucose method." *Science* 200.4340 (1978): 447-449.

De Valois RL, Albrecht DG, Thorell LG (1982a) Spatial frequency selectivity of cells in macaque visual cortex. *Vision Research* **22(5)**: 545–559

De Valois RL, Yund EW, Hepler N (1982b) The orientation and direction selectivity of cells in macaque visual cortex. *Vision Research* **22(5)**: 531–544

Dews, P. B., and T. N. Wiesel. "Consequences of monocular deprivation on visual behaviour in kittens." *The Journal of Physiology* 206.2 (1970): 437-455.

Dräger, U. C., and David H. Hubel. "Responses to visual stimulation and relationship between visual, auditory, and somatosensory inputs in mouse superior colliculus." *Journal of Neurophysiology* 38.3 (1975): 690-713.

Dräger, Ursula C. "Receptive fields of single cells and topography in mouse visual cortex." *Journal of Comparative Neurology* 160.3 (1975): 269-289.

Dräger, Ursula C., and D. H. Hubel. "Topography of visual and somatosensory projections to mouse superior colliculus." *Journal of Neurophysiology* 39.1 (1976): 91-101

Dräger, Ursula C., and John F. Olsen. "Origins of crossed and uncrossed retinal projections in pigmented and albino mice." *Journal of Comparative Neurology* 191.3 (1980): 383-412.

Dubbs A, Guevara J, Yuste R (2016) Moco:fast motion correction for calcium imaging. *Front Neuroinform* **10**:6

Durand S, Iyer R, Mizuseki K, de Vries S, Mihalas S, Reid RC (2016) A comparison of visual response properties in the lateral geniculate nucleus and primary visual cortex of awake and anesthetized mice. *J Neurosci* **36(48)**: 12144-12156

D'Souza, Rinaldo David, et al. "Recruitment of inhibition and excitation across mouse visual cortex depends on the hierarchy of interconnecting areas." *Elife* 5 (2016): e19332.

Ecker, Jennifer L., et al. "Melanopsin-expressing retinal ganglion-cell photoreceptors: cellular diversity and role in pattern vision." *Neuron* 67.1 (2010): 49-60.

Ellis, Erika M., et al. "Shared and distinct retinal input to the mouse superior colliculus and dorsal lateral geniculate nucleus." *Journal of neurophysiology* 116.2 (2016): 602-610.

El-Shamayleh, Yasmine, et al. "Visual motion processing by neurons in area MT of macaque monkeys with experimental amblyopia." *Journal of Neuroscience* 30.36 (2010): 12198-12209.

Espinosa, J. Sebastian, and Michael P. Stryker. "Development and plasticity of the primary visual cortex." *Neuron* 75.2 (2012): 230-249.

Espinoza, Sergio G., and Hardy C. Thomas. "Retinotopic organization of striate and extrastriate visual cortex in the hooded rat." *Brain research* 272.1 (1983): 137-144.

Fagiolini, Michela, et al. "Functional postnatal development of the rat primary visual cortex and the role of visual experience: dark rearing and monocular deprivation." *Vision research* 34.6 (1994): 709-720.

Fahey, Paul G., et al. "A global map of orientation tuning in mouse visual cortex." *bioRxiv* (2019): 745323.

Farley, Brandon J., et al. "Alteration of visual input results in a coordinated reorganization of multiple visual cortex maps." *Journal of Neuroscience* 27.38 (2007): 10299-10310.

Ferrera, Vincent P., Tara A. Nealey, and John HR Maunsell. "Mixed parvocellular and magnocellular geniculate signals in visual area V4." *Nature* 358.6389 (1992): 756.

Felleman, Daniel J., and DC Essen Van. "Distributed hierarchical processing in the primate cerebral cortex." *Cerebral cortex (New York, NY: 1991)* 1.1 (1991): 1-47.

Fitzpatrick, David, Jennifer S. Lund, and Gary G. Blasdel. "Intrinsic connections of macaque striate cortex: afferent and efferent connections of lamina 4C." *Journal of Neuroscience* 5.12 (1985): 3329-3349.

Fries, W. "The projection from the lateral geniculate nucleus to the prestriate cortex of the macaque monkey." *Proceedings of the Royal Society of London. Series B. Biological Sciences* 213.1190 (1981): 73-80.

Fu Y, Tucciarone JM, Espinosa JS, Sheng N, Darcy DP, Nicoll RA, Huang J, Stryker MP (2014) A cortical circuit for gain control by behavioral state. *Cell* **156(6):** 1139-1152

Gandhi SP, Yanagawa Y, Stryker MP (2008) Delayed plasticity of inhibitory neurons in developing visual cortex. *Proc Natl Acad Sci USA* **105(43)**:16797–16802

Gao, Enquan, Gregory C. DeAngelis, and Andreas Burkhalter. "Parallel input channels to mouse primary visual cortex." *Journal of Neuroscience* 30.17 (2010): 5912-5926.

Garrett, Marina E., et al. "Topography and areal organization of mouse visual cortex." *Journal of Neuroscience* 34.37 (2014): 12587-12600.

Ghose, Geoffrey M., and Daniel Y. Ts' O. "Form processing modules in primate area V4." *Journal of Neurophysiology* 77.4 (1997): 2191-2196.

Ghose, Geoffrey M., and Y. Daniel. "Integration of color, orientation, and size functional domains in the ventral pathway." *Neurophotonics* 4.3 (2017): 031216.

Girard, P., P. A. Salin, and J. Bullier. "Response selectivity of neurons in area MT of the macaque monkey during reversible inactivation of area V1." *Journal of Neurophysiology* 67.6 (1992): 1437-1446.

Girshick AR, Landy MS, Simoncelli EP (2011) Cardinal rules: visual orientation perception reflects knowledge of environmental statistics. *Nat Neurosci* **14(7)**:926-932

Glickfeld, Lindsey L., et al. "Cortico-cortical projections in mouse visual cortex are functionally target specific." *Nature neuroscience* 16.2 (2013): 219.

Glickfeld, Lindsey L., Mark H. Histed, and John HR Maunsell. "Mouse primary visual cortex is used to detect both orientation and contrast changes." *Journal of Neuroscience* 33.50 (2013): 19416-19422.

Glickfeld, Lindsey L., and Shawn R. Olsen. "Higher-order areas of the mouse visual cortex." *Annual review of vision science* 3 (2017): 251-273.

Goldman-Rakic, Patricia S. "Topography of cognition: parallel distributed networks in primate association cortex." *Annual review of neuroscience* 11.1 (1988): 137-156.

Gordon, Joshua A., and Michael P. Stryker. "Experience-dependent plasticity of binocular responses in the primary visual cortex of the mouse." *Journal of Neuroscience* 16.10 (1996): 3274-3286.

Gouras, Peter. "Antidromic responses of orthodromically identified ganglion cells in monkey retina." *The Journal of physiology* 204.2 (1969): 407-419.

Hammond P, Fothergill LK (1994) Cat striate cortex: monocular and interocular comparison of spatial-frequency selectivity. *Anais da Academia Brasileira de Ciencias* **66**(1):95-113

Hammond P, Pomfrett CJD (1991) Interocular mismatch in spatial frequency and directionality characteristics of striate cortical neurons. Exp Brain Res **85(3)**:631-640

Han, Yunyun, et al. "The logic of single-cell projections from visual cortex." *Nature* 556.7699 (2018): 51.

Hansen, Bruce C., et al. "Perceptual anisotropies in visual processing and their relation to natural image statistics." *Network: Computation in Neural Systems* 14.3 (2003): 501-526.

Harris, Laurence R. "The superior colliculus and movements of the head and eyes in cats." *The Journal of physiology* 300.1 (1980): 367-391.

Harting, John K., et al. "Projection of the mammalian superior colliculus upon the dorsal lateral geniculate nucleus: organization of tectogeniculate pathways in nineteen species." *Journal of Comparative Neurology* 304.2 (1991): 275-306.

Harvey, Christopher D., et al. "Intracellular dynamics of hippocampal place cells during virtual navigation." *Nature* 461.7266 (2009): 941.

Harwerth, R. S., et al. "Behavioral studies on the effect of abnormal early visual experience in monkeys: Temporal modulation sensitivity." *Vision Research* 23.12 (1983): 1511-1517.

Harwerth, Ronald S., et al. "Multiple sensitive periods in the development of the primate visual system." *Science* 232.4747 (1986): 235-238.

Haverkamp, Silke, et al. "The primordial, blue-cone color system of the mouse retina." *Journal of Neuroscience* 25.22 (2005): 5438-5445.

Hawken MJ, Parker AJ *(*1987*)* Spatial properties of neurons in the monkey striate cortex*. Proc R Soc Lond B Biol Sci* 231(1263)*:*251–288

Hendry, Stewart HC, and R. Clay Reid. "The koniocellular pathway in primate vision." *Annual review of neuroscience*23.1 (2000): 127-153.

Herkenham, Miles. "Laminar organization of thalamic projections to the rat neocortex." *Science* 207.4430 (1980): 532-535.

Hess, R. F., and E. R. Howell. "The threshold contrast sensitivity function in strabismic amblyopia: evidence for a two type classification." *Vision research* 17.9 (1977): 1049-1055.

Hess, Robert F., et al. "A deficit in strabismic amblyopia for global shape detection." *Vision research* 39.5 (1999): 901-914.

Hicks, T. P., B. B. Lee, and T. R. Vidyasagar. "The responses of cells in macaque lateral geniculate nucleus to sinusoidal gratings." *The Journal of physiology* 337.1 (1983): 183-200.

Horton, Jonathan C., and David H. Hubel. "Regular patchy distribution of cytochrome oxidase staining in primary visual cortex of macaque monkey." *Nature* 292.5825 (1981): 762.

Horton, Jonathan C., and Davina R. Hocking. "An adult-like pattern of ocular dominance columns in striate cortex of newborn monkeys prior to visual experience." *Journal of Neuroscience* 16.5 (1996): 1791-1807.

Horton, Jonathan C., and Davina R. Hocking. "Timing of the critical period for plasticity of ocular dominance columns in macaque striate cortex." *Journal of Neuroscience* 17.10 (1997): 3684-3709

Howarth, Michael, Lauren Walmsley, and Timothy M. Brown. "Binocular integration in the mouse lateral geniculate nuclei." *Current Biology* 24.11 (2014): 1241-1247.

Hoy, Jennifer L., et al. "Vision drives accurate approach behavior during prey capture in laboratory mice." *Current Biology* 26.22 (2016): 3046-3052

Hoy JL, Niell CM (2015) Layer-specific refinement of visual cortex function after eye opening in the awake mouse. *J Neurosci* **35(8)**:3370–3383

Hoyt, Creig S. "Amblyopia: a neuro-ophthalmic view." *Journal of neuro-ophthalmology* 25.3 (2005): 227-231.

Huang ZJ, Kirkwood A, Pizzorusso T, Porciatti V, Morales B, Bear MF, Maffei L, Tonegawa S (1999) BDNF regulates the maturation of inhibition and the critical period of plasticity in mouse visual cortex. *Cell* 98(6):739–755

Huberman, Andrew D., et al. "Architecture and activity-mediated refinement of axonal projections from a mosaic of genetically identified retinal ganglion cells." *Neuron* 59.3 (2008): 425-438.

Huberman, Andrew D., et al. "Genetic identification of an On-Off direction-selective retinal ganglion cell subtype reveals a layer-specific subcortical map of posterior motion." *Neuron* 62.3 (2009): 327-334.

Huberman AD, Niell CM (2011) What can mice tell us about how vision works? *Trends Neurosci* **34(9)**:464–473

Hubel, David H., and Margaret S. Livingstone. "Segregation of form, color, and stereopsis in primate area 18." *Journal of neuroscience* 7.11 (1987): 3378-3415.

Hubel, David H., and Torsten N. Wiesel. "Receptive fields of single neurones in the cat's striate cortex." *The Journal of physiology* 148.3 (1959): 574-591.

Hubel, David H., and Torsten N. Wiesel. "Receptive fields, binocular interaction and functional architecture in the cat's visual cortex." *The Journal of physiology* 160.1 (1962): 106-154.

Hubel, David H., and Torsten N. Wiesel. "Binocular interaction in striate cortex of kittens reared with artificial squint." *Journal of neurophysiology* 28.6 (1965): 1041-1059.

Hubel, David H., and Torsten N. Wiesel. "Receptive fields and functional architecture in two nonstriate visual areas (18 and 19) of the cat." *Journal of neurophysiology* 28.2 (1965): 229-289.

Hubel, D. H., and T. N. Wiesel. "Anatomical demonstration of columns in the monkey striate cortex." *Nature* 221.5182 (1969): 747.

Hubel, David H., and Torsten N. Wiesel. "The period of susceptibility to the physiological effects of unilateral eye closure in kittens." *The Journal of physiology* 206.2 (1970): 419-436.

Hubel, David H., and Torsten N. Wiesel. "Sequence regularity and geometry of orientation columns in the monkey striate cortex." *Journal of Comparative Neurology* 158.3 (1974): 267-293.

Hubel, David H., and Torsten N. Wiesel. "Uniformity of monkey striate cortex: a parallel relationship between field size, scatter, and magnification factor." *Journal of Comparative Neurology* 158.3 (1974): 295-305.

Hubel, David Hunter, et al. "Plasticity of ocular dominance columns in monkey striate cortex." *Philosophical Transactions of the Royal Society of London. B, Biological Sciences* 278.961 (1977): 377-409.

Hubel, David H., Torsten N. Wiesel, and Michael P. Stryker. "Anatomical demonstration of orientation columns in macaque monkey." *Journal of Comparative Neurology* 177.3 (1978): 361-379.

Huberman, Andrew D., et al. "Architecture and activity-mediated refinement of axonal projections from a mosaic of genetically identified retinal ganglion cells." *Neuron* 59.3 (2008): 425-438.

Huberman, Andrew D., et al. "Genetic identification of an On-Off direction-selective retinal ganglion cell subtype reveals a layer-specific subcortical map of posterior motion." *Neuron*62.3 (2009): 327-334.

Huberman AD, Niell CM (2011) What can mice tell us about how vision works? *Trends Neurosci* **34(9)**:464–473

Hughes, Howard C. "Anatomical and neurobehavioral investigations concerning the thalamo-cortical organization of the rat's visual system." *Journal of Comparative Neurology*175.3 (1977): 311-335

Huh, Carey YL, et al. "Early Visual Experience Shapes Binocularity in the Mouse Thalamocortical Pathway." (2018).

Jacoby J, Schwartz GW. (2017) Three small-receptive-field ganglion cells in the mouse retina are distinctly tuned to size, speed and object motion. *J Neurosci* **37(3**): 610-625

Jaepel, Juliane, et al. "Lateral geniculate neurons projecting to primary visual cortex show ocular dominance plasticity in adult mice." *Nature neuroscience* 20.12 (2017): 1708.

Ji, Weiqing, et al. "Modularity in the organization of mouse primary visual cortex." *Neuron* 87.3 (2015): 632-643.

Jones, K. R., Peter D. Spear, and Lilian Tong. "Critical periods for effects of monocular deprivation: differences between striate and extrastriate cortex." *Journal of Neuroscience* 4.10 (1984): 2543-2552.

Juavinett, Ashley L., and Edward M. Callaway. "Pattern and component motion responses in mouse visual cortical areas." Current Biology 25.13 (2015): 1759-1764.

Juavinett, Ashley L., et al. "Automated identification of mouse visual areas with intrinsic signal imaging." *Nature protocols*12.1 (2017): 32.

Kalatsky, Valery A., and Michael P. Stryker. "New paradigm for optical imaging: temporally encoded maps of intrinsic signal." *Neuron* 38.4 (2003): 529-545.

Kang, Erin, et al. "Visual acuity development and plasticity in the absence of sensory experience." *Journal of Neuroscience* 33.45 (2013): 17789-17796.

Kang E, Durand S, LeBlanc JJ, Hensch TK, Chen C, Fagiolini M (2013) Visual acuity development and plasticity in the absence of sensory experience. *J Neurosci* **33(45)**:17789–17796

Kaplan, E., and R. M. Shapley. "X and Y cells in the lateral geniculate nucleus of macaque monkeys." *The Journal of Physiology* 330.1 (1982): 125-143.

Kay, Jeremy N., et al. "Retinal ganglion cells with distinct directional preferences differ in molecular identity, structure, and central projections." *Journal of Neuroscience* 31.21 (2011): 7753-7762.

Kerlin AM, Andermann ML, Berezovskii VK, Reid RC (2010) Broadly tuned response properties of diverse inhibitory neuron subtypes in mouse visual cortex. *Neuron* **67(5)**:858–871

Khaytin, Ilya, et al. "Functional organization of temporal frequency selectivity in primate visual cortex." *Cerebral Cortex* 18.8 (2007): 1828-1842.

Kim, In-Jung, et al. "Molecular identification of a retinal cell type that responds to upward motion." *Nature* 452.7186 (2008): 478.

Kim, Mean-Hwan, et al. "Exclusive functional subnetworks of intracortical projection neurons in primary visual cortex." *BioRxiv* (2017): 153247.

Kim, Dae-Shik, and Tobias Bonhoeffer. "Reverse occlusion leads to a precise restoration of orientation preference maps in visual cortex." *Nature* 370.6488 (1994): 370.

Kiorpes, Lynne, and Suzanne P. McKee. "Neural mechanisms underlying amblyopia." *Current opinion in neurobiology* 9.4 (1999): 480-486.

Kiorpes, Lynne, et al. "Neuronal correlates of amblyopia in the visual cortex of macaque monkeys with experimental strabismus and anisometropia." *Journal of Neuroscience* 18.16 (1998): 6411-6424.

Kiorpes, Lynne. "Visual processing in amblyopia: animal studies." *Strabismus* 14.1 (2006): 3-10.

Kiorpes, Lynne, Chao Tang, and J. Anthony Movshon. "Sensitivity to visual motion in amblyopic macaque monkeys." *Visual neuroscience* 23.2 (2006): 247-256.

Kiorpes, Lynne. "The puzzle of visual development: behavior and neural limits." *Journal of Neuroscience* 36.45 (2016): 11384-11393.

Klüver, Heinrich, and Paul C. Bucy. "" Psychic blindness" and other symptoms following bilateral temporal lobectomy in Rhesus monkeys." *American Journal of Physiology* (1937).

Kondo, Satoru, and Kenichi Ohki. "Laminar differences in the orientation selectivity of geniculate afferents in mouse primary visual cortex." *Nature neuroscience* 19.2 (2016): 316.

Kovács, Ilona, et al. "A new test of contour integration deficits in patients with a history of disrupted binocular experience during visual development." *Vision research* 40.13 (2000): 1775-1783.

Kozma, Petra, and Lynne Kiorpes. "Contour integration in amblyopic monkeys." *Visual neuroscience* 20.5 (2003): 577-588.

Krahe, Thomas E., et al. "Morphologically distinct classes of relay cells exhibit regional preferences in the dorsal lateral geniculate nucleus of the mouse." *Journal of Neuroscience*31.48 (2011): 17437-17448.

Kreile, Anne K., Tobias Bonhoeffer, and Mark Hübener. "Altered visual experience induces instructive changes of orientation preference in mouse visual cortex." *Journal of Neuroscience* 31.39 (2011): 13911-13920.

Le Vay, Simon, Torsten N. Wiesel, and David H. Hubel. "The development of ocular dominance columns in normal and visually deprived monkeys." *Journal of Comparative Neurology* 191.1 (1980): 1-51.

Lee AM, Hoy JL, Bonci A, Wilbrecht L, Stryker MP, Niell CM (2014) Identification of a brainstem circuit regulating visual cortical state in parallel with locomotion. *Neuron* **83(2)**:455-466

Levelt, Christiaan N., and Mark Hübener. "Critical-period plasticity in the visual cortex." *Annual review of neuroscience* 35 (2012): 309-330.

Leventhal, Audie G., R. W. Rodieck, and B. Dreher. "Retinal ganglion cell classes in the Old World monkey: morphology and central projections." *Science* 213.4512 (1981): 1139-1142.

Levi, D. M., and RONALD S. Harwerth. "Spatio-temporal interactions in anisometropic and strabismic amblyopia." *Investigative Ophthalmology & Visual Science* 16.1 (1977): 90-95.

Li, Ye, David Fitzpatrick, and Leonard E. White. "The development of direction selectivity in ferret visual cortex requires early visual experience." *Nature neuroscience* 9.5 (2006): 676.

Lien, Anthony D., and Massimo Scanziani. "Tuned thalamic excitation is amplified by visual cortical circuits." *Nature neuroscience* 16.9 (2013): 1315.

Liu, Yong-Jun, Qian Wang, and Bing Li. "Neuronal responses to looming objects in the superior colliculus of the cat." *Brain, Behavior and Evolution* 77.3 (2011): 193-205.

Livingstone, Margaret S., and David H. Hubel. "Anatomy and physiology of a color system in the primate visual cortex." *Journal of Neuroscience* 4.1 (1984): 309-356.

Livingstone, Margaret S., and David H. Hubel. "Psychophysical evidence for separate channels for the perception of form, color, movement, and depth." *Journal of Neuroscience* 7.11 (1987): 3416-3468.

Lomber, Stephen G., et al. "Restoration of visual orienting into a cortically blind hemifield by reversible deactivation of posterior parietal cortex or the superior colliculus." *Experimental brain research* 142.4 (2002): 463-474.

Lysakowski, A., G. P. Standage, and L. A. Benevento. "An investigation of collateral projections of the dorsal lateral geniculate nucleus and other subcortical structures to cortical areas V1 and V4 in the macaque monkey: a double label retrograde tracer study." *Experimental brain research* 69.3 (1988): 651-661.

Maffei L, Fiorentini A (1973) The visual cortex as a spatial frequency analyzer. *Vision Research* **13(7)**: 1255-267

Malach, R., et al. "Relationship between intrinsic connections and functional architecture revealed by optical imaging and in vivo targeted biocytin injections in primate striate cortex." *Proceedings of the National Academy of Sciences* 90.22 (1993): 10469-10473.

Malonek, D., R. B. H. Tootell, and A. Grinvald. "Optical imaging reveals the functional architecture of neurons processing shape and motion in owl monkey area MT." *Proceedings of the Royal Society of London. Series B: Biological Sciences* 258.1352 (1994): 109-119.

Malpeli, Joseph G., Peter H. Schiller, and Carol L. Colby. "Response properties of single cells in monkey striate cortex during reversible inactivation of individual lateral geniculate laminae." *Journal of neurophysiology* 46.5 (1981): 1102-1119.

Mao, Dun, et al. "Sparse orthogonal population representation of spatial context in the retrosplenial cortex." *Nature communications* 8.1 (2017): 243.

Marques, Tiago, et al. "A role for mouse primary visual cortex in motion perception." *Current Biology* 28.11 (2018): 1703-1713.

Marshel, James H., et al. "Functional specialization of seven mouse visual cortical areas." *Neuron* 72.6 (2011): 1040-1054.

Marshel, James H., et al. "Anterior-posterior direction opponency in the superficial mouse lateral geniculate nucleus." *Neuron* 76.4 (2012): 713-720.

Matsui, Teppei, and Kenichi Ohki. "Target dependence of orientation and direction selectivity of corticocortical projection neurons in the mouse V1." *Frontiers in neural circuits* 7 (2013): 143.

Matteucci, Giulio, et al. "Nonlinear processing of shape information in rat lateral extrastriate cortex." *Journal of Neuroscience* 39.9 (2019): 1649-1670.

Maunsell, John HR, and William T. Newsome. "Visual processing in monkey extrastriate cortex." *Annual review of neuroscience* 10.1 (1987): 363-401.

Maurer, Daphne, et al. "Rapid improvement in the acuity of infants after visual input." *Science* 286.5437 (1999): 108-110.

Merigan, William H., and Thomas A. Eskin. "Spatio-temporal vision of macaques with severe loss of Pβ retinal ganglion cells." *Vision Research* 26.11 (1986): 1751-1761.

Merigan, William H., and Laurence M. Katz. "Spatial resolution across the macaque retina." *Vision research* 30.7 (1990): 985-991.

Merigan, W. H., Laurence M. Katz, and J. H. Maunsell. "The effects of parvocellular lateral geniculate lesions on the acuity and contrast sensitivity of macaque monkeys." *Journal of Neuroscience* 11.4 (1991): 994-1001.

Merigan, William H., and John HR Maunsell. "How parallel are the primate visual pathways?." *Annual review of neuroscience*16.1 (1993): 369-402.

Merlin, Sam, et al. "Deletion of Ten-m3 induces the formation of eye dominance domains in mouse visual cortex." *Cerebral Cortex* 23.4 (2012): 763-774.

Mineault PJ, Tring E, Trachtenberg JT, Ringach DL (2016) Enhanced spatial resolution during locomotion and heightened attention in mouse primary visual cortex. *J Neurosci* **36(24)**:6382–6392

Mishkin, Mortimer, and Leslie G. Ungerleider. "Contribution of striate inputs to the visuospatial functions of parieto-preoccipital cortex in monkeys." *Behavioural brain research*6.1 (1982): 57-77.

Mishkin, Mortimer, Leslie G. Ungerleider, and Kathleen A. Macko. "Object vision and spatial vision: two cortical pathways." *Trends in neurosciences* 6 (1983): 414-417.

Movshon JA, Thompson ID, Tolhurst DJ (1978a) Spatial summation in the receptive fields of simple cells in the cat's striate cortex. *J Physiol* **283**: 53-77

Movshon, J. Anthony, and William T. Newsome. "Visual response properties of striate cortical neurons projecting to area MT in macaque monkeys." *Journal of Neuroscience*16.23 (1996): 7733-7741.

Mrsic-Flogel, Thomas D., et al. "Altered map of visual space in the superior colliculus of mice lacking early retinal waves." *Journal of Neuroscience* 25.29 (2005): 6921-6928.

Mrsic-Flogel TD, Hofer SB, Ohki K, Reid RC, Bonhoeffer T, Hübener M (2007) Homeostatic regulation of eye-specific responses in visual cortex during ocular dominance plasticity. *Neuron* **54(6)**:961–972

Muir, Dylan Richard, et al. "Model-based analysis of pattern motion processing in mouse primary visual cortex." *Frontiers in neural circuits* 9 (2015): 38.

Murakami, Tomonari, Teppei Matsui, and Kenichi Ohki. "Functional segregation and development of mouse higher visual areas." *Journal of Neuroscience* 37.39 (2017): 9424-9437.

Murphy KM, Mitchell DE (1986) Bilateral amblyopia following a short period of reverse occlusion. *Nature* **323(6088)**: 536-538

Nassi, Jonathan J., and Edward M. Callaway. "Parallel processing strategies of the primate visual system." *Nature reviews neuroscience* 10.5 (2009): 360.

Nath A, Schwartz GW (2016) Cardinal orientation selectivity is represented by two distinct ganglion cell types in mouse retina. *J Neurosci* **36(11)**:3208–3221

Nauhaus, Ian, et al. "Orthogonal micro-organization of orientation and spatial frequency in primate primary visual cortex." *Nature neuroscience* 15.12 (2012): 1683.

Nauhaus, Ian, Kristina J. Nielsen, and Edward M. Callaway. "Efficient receptive field tiling in primate V1." *Neuron* 91.4 (2016): 893-904.

Niell CM, Stryker MP (2010) Modulation of visual responses by behavioral state in mouse visual cortex. *Neuron* **65(4)**:472–479

Niell, Cristopher M., and Michael P. Stryker. "Highly selective receptive fields in mouse visual cortex." *Journal of Neuroscience* 28.30 (2008): 7520-7536.

Newsome, William T., and Edmond B. Pare. "A selective impairment of motion perception following lesions of the middle temporal visual area (MT)." *Journal of Neuroscience*8.6 (1988): 2201-2211.

Norcia, Anthony M., et al. "Experience-expectant development of contour integration mechanisms in human visual cortex." *Journal of Vision* 5.2 (2005): 3-3.

Norton, Thomas T., and Vivien A. Casagrande. "Laminar organization of receptive-field properties in lateral geniculate nucleus of bush baby (Galago crassicaudatus)." *Journal of Neurophysiology* 47.4 (1982): 715-741.

Norton, THOMAS T., et al. "Contrast-sensitivity functions of W-, X-, and Y-like relay cells in the lateral geniculate nucleus of bush baby, Galago crassicaudatus." *Journal of Neurophysiology* 59.6 (1988): 1639-1656.

Obermayer, Klaus, and Gary G. Blasdel. "Geometry of orientation and ocular dominance columns in monkey striate cortex." *Journal of Neuroscience* 13.10 (1993): 4114-4129.

Ogino, Tetsuo, and Kenji Ohtsuka. "Effects of superior colliculus inhibition on visual motion processing in the lateral suprasylvian visual area of the cat." *Investigative ophthalmology & visual science* 41.3 (2000): 955-960.

Ohki, Kenichi, et al. "Functional imaging with cellular resolution reveals precise micro-architecture in visual cortex." *Nature* 433.7026 (2005): 597.

Ohki, Kenichi, and R. Clay Reid. "Specificity and randomness in the visual cortex." *Current opinion in neurobiology* 17.4 (2007): 401-407.

Olavarria, Jaime, and Vicente M. Montero. "Organization of visual cortex in the mouse revealed by correlating callosal and striate-extrastriate connections." *Visual neuroscience* 3.1 (1989): 59-69.

Osakada, Fumitaka, et al. "New rabies virus variants for monitoring and manipulating activity and gene expression in defined neural circuits." *Neuron* 71.4 (2011): 617-631.

Palagina, Ganna, Jochen F. Meyer, and Stelios M. Smirnakis. "Complex visual motion representation in mouse area V1." *Journal of Neuroscience* 37.1 (2017): 164-183.

Panzera, Lauren C., and Michael Blake Hoppa. "Genetically Encoded Voltage Indicators Are Illuminating Subcellular Physiology of the Axon." *Frontiers in Cellular Neuroscience* 13 (2019): 52.

Pasik, Tauba, and Pedro Pasik. "The visual world of monkeys deprived of striate cortex: effective stimulus parameters and the importance of the accessory optic system." *Vision Research* 11 (1971): 419-IN55.

Perry, V. H., R. Oehler, and A. Cowey. "Retinal ganglion cells that project to the dorsal lateral geniculate nucleus in the macaque monkey." *Neuroscience* 12.4 (1984): 1101-1123.

Pirenne MH (1943) Binocular and uniocular threshold of vision. *Nature* **152**, 698-699

Piscopo, Denise M., et al. "Diverse visual features encoded in mouse lateral geniculate nucleus." *Journal of Neuroscience*33.11 (2013): 4642-4656.

Polack, Pierre-Olivier, and Diego Contreras. "Long-range parallel processing and local recurrent activity in the visual cortex of the mouse." *Journal of Neuroscience* 32.32 (2012): 11120-11131.

Poort, Jasper, et al. "Learning enhances sensory and multiple non-sensory representations in primary visual cortex." *Neuron*86.6 (2015): 1478-1490.

Porciatti V, Pizzorusso T, Maffei L (1999) The visual physiology of the wild type mouse determined with pattern VEPs. *Vision Research* 39(18):3071–3081

Priebe, Nicholas J., Stephen G. Lisberger, and J. Anthony Movshon. "Tuning for spatiotemporal frequency and speed in directionally selective neurons of macaque striate cortex." *Journal of Neuroscience* 26.11 (2006): 2941-2950.

Prusky, Glen T., Paul WR West, and Robert M. Douglas. "Behavioral assessment of visual acuity in mice and rats." *Vision research* 40.16 (2000): 2201-2209.

Prusky, Glen T., and Robert M. Douglas. "Developmental plasticity of mouse visual acuity." *European Journal of Neuroscience* 17.1 (2003): 167-173.

Purpura, Keith, et al. "Light adaptation in the primate retina: analysis of changes in gain and dynamics of monkey retinal ganglion cells." *Visual neuroscience* 4.1 (1990): 75-93.

Rakic, Pasko. "Prenatal genesis of connections subserving ocular dominance in the rhesus monkey." *Nature* 261.5560 (1976): 467.

Rezak, Michael, and L. A. Benevento. "A comparison of the organization of the projections of the dorsal lateral geniculate nucleus, the inferior pulvinar and adjacent lateral pulvinar to primary visual cortex (area 17) in the macaque monkey." *Brain research* 167.1 (1979): 19-40.

Rhim, Issac, et al. "Maps of cone opsin input to mouse V1 and higher visual areas." *Journal of neurophysiology* 117.4 (2017): 1674-1682.

Ringach, Dario L., et al. "Spatial clustering of tuning in mouse primary visual cortex." *Nature communications* 7 (2016): 12270.

Rivlin-Etzion, Michal, et al. "Transgenic mice reveal unexpected diversity of on-off direction-selective retinal ganglion cell subtypes and brain structures involved in motion processing." *Journal of Neuroscience* 31.24 (2011): 8760-8769.

Rochefort, Nathalie L., et al. "Development of direction selectivity in mouse cortical neurons." *Neuron* 71.3 (2011): 425-432

Rodman, Hillary R., Charles G. Gross, and Thomas D. Albright. "Afferent basis of visual response properties in area MT of the macaque. I. Effects of striate cortex removal." *Journal of Neuroscience* 9.6 (1989): 2033-2050.

Rodman, Hillary R., Charles G. Gross, and Thomas D. Albright. "Afferent basis of visual response properties in area MT of the macaque. II. Effects of superior colliculus removal." *Journal of Neuroscience* 10.4 (1990): 1154-1164.

Rompani SB, Mullner FE, Wanner A, Zhang C, Roth CN, Yonehara K, Roska B (2017) Different modes of visual integration in the lateral geniculate nucleus revealed by single-cell-initiated transsynaptic tracing. *Neuron* **93(4)**:767-776

Roth MM, Helmchen F, Kampa BM (2012) Distinct functional properties of primary and posteromedial visual area of mouse neocortex. *J Neurosci* **32(28)**:9716–9726

Roth, Morgane M., et al. "Thalamic nuclei convey diverse contextual information to layer 1 of visual cortex." *Nature neuroscience* 19.2 (2016): 299.

Saint-Amour D, Lepore F, Guillemot JP (2004) Binocular fusion/suppression to spatial frequency differences at the border of areas 17/18 of the cat. *Neuroscience* **124(1)**:121-136.

Salinas, Kirstie J., et al. "Contralateral bias of high spatial frequency tuning and cardinal direction selectivity in mouse visual cortex." *Journal of Neuroscience* 37.42 (2017): 10125-10138.

Schiller PH, Finlay BL, Volman SF (1976a) Quantitative studies of single-cell properties in monkey striate cortex: II. Orientation specificity and ocular dominance. *J Neurophysiol* **39(6)**: 1320-33

Schiller, Peter H., and Joseph G. Malpeli. "Properties and tectal projections of monkey retinal ganglion cells." *Journal of Neurophysiology* 40.2 (1977): 428-445.

Schiller, Peter H., Nikos K. Logothetis, and Eliot R. Charles. "Role of the color-opponent and broad-band channels in vision." *Visual neuroscience* 5.4 (1990): 321-346.

Schiller, PETER H., and JOSEPH G. Malpeli. "Functional specificity of lateral geniculate nucleus laminae of the rhesus monkey." *Journal of neurophysiology* 41.3 (1978): 788-797.

Scholl B, Burge J, Priebe NJ (2013) Binocular integration and disparity selectivity in mouse primary visual cortex. *J Neurophysiol* **109(12)**:3013-3024

Scholl B, Pattadkal JJ, Priebe NJ (2017) Binocular disparity selectivity weakened after monocular deprivation in mouse V1. *J Neurosci* **37(27)**:6517-6526

Sclar, Gary, John HR Maunsell, and Peter Lennie. "Coding of image contrast in central visual pathways of the macaque monkey." *Vision research* 30.1 (1990): 1-10.

Sereno, Martin I., Colin T. McDonald, and John M. Allman. "Analysis of retinotopic maps in extrastriate cortex." *Cerebral Cortex* 4.6 (1994): 601-620.

Shapley, Robert, Ehud Kaplan, and Robert Soodak. "Spatial summation and contrast sensitivity of X and Y cells in the lateral geniculate nucleus of the macaque." *Nature* 292.5823 (1981): 543.

Shatz, Carla J., and Michael P. Stryker. "Ocular dominance in layer IV of the cat's visual cortex and the effects of monocular deprivation." *The Journal of physiology* 281.1 (1978): 267-283.

Sherk, Helen, and Michael P. Stryker. "Quantitative study of cortical orientation selectivity in visually inexperienced kitten." *Journal of Neurophysiology* 39.1 (1976): 63-70.

Silveira, L. C. L., and V. H. Perry. "The topography of magnocellular projecting ganglion cells (M-ganglion cells) in the primate retina." *Neuroscience* 40.1 (1991): 217-237.

Sincich, Lawrence C., Cristina M. Jocson, and Jonathan C. Horton. "Neuronal projections from V1 to V2 in amblyopia." *Journal of Neuroscience* 32.8 (2012): 2648-2656.

Sklansky J (1982) Finding the convex hull of a simple polygon. *Pattern Recognition Letters* **1(2)**:79-83

Skottun BC, Freeman RD (1984) Stimulus specificity of binocular cells in the cat's visual cortex: Ocular dominance and the matching of left and right eyes. *Exp Brain Res* **56**: 206–216

Smith, Ikuko T., et al. "Stream-dependent development of higher visual cortical areas." *Nature neuroscience* 20.2 (2017): 200.

Sommeijer, Jean-Pierre, et al. "Thalamic inhibition regulates critical-period plasticity in visual cortex and thalamus." *Nature neuroscience* 20.12 (2017): 1715-1721.

Stephany, Céleste-Élise, et al. "Distinct circuits for recovery of eye dominance and acuity in murine amblyopia." *Current Biology* 28.12 (2018): 1914-1923.

Sun W, Tan Z, Mensh BD, Ji N (2016) Thalamus provides layer 4 of primary visual cortex with orientation- and direction-tuned inputs*. Nat Neurosci* **19(2)**:308–315

Suzuki S, Abe K (1985) Topological structural analysis of digitized binary images by border following. *Computer Vision, Graphics, and Image Processing* **30(1)**, 32-46

Swindale, N. V., F. Vital Durand, and C. Blakemore. "Recovery from monocular deprivation in the monkey. III. Reversal of anatomical effects in the visual cortex." *Proceedings of the Royal Society of London. Series B. Biological Sciences* 213.1193 (1981): 435-450.

Szél, Ágoston, and Pál Röhlich. "Two cone types of rat retina detected by anti-visual pigment antibodies." *Experimental eye research* 55.1 (1992): 47-52.

Tafazoli, Sina, et al. "Emergence of transformation-tolerant representations of visual objects in rat lateral extrastriate cortex." *Elife* 6 (2017): e22794.

Talbot, S. A., and W. H. Marshall. "Physiological studies on neural mechanisms of visual localization and discrimination." *American Journal of Ophthalmology* 24.11 (1941): 1255-1264.

Tobimatsu S. Kato M. (1996). The effect of binocular stimulation on each component of transient and steady-state VEPs. *Electroencephalography & Clinical Neurophysiology* **100(3)**: 177–183

Tohmi, Manavu, et al. "The extrageniculate visual pathway generates distinct response properties in the higher visual areas of mice." *Current Biology* 24.6 (2014): 587-597.

Tootell, Roger B., et al. "Functional anatomy of macaque striate cortex. V. Spatial frequency." *Journal of Neuroscience*8.5 (1988): 1610-1624.

Ts'o, Daniel Y., Mark Zarella, and Guy Burkitt. "Whither the hypercolumn?." *The Journal of Physiology* 587.12 (2009): 2791-2805.

Tychsen, Lawrence, et al. "Early versus delayed repair of infantile strabismus in macaque monkeys: II. Effects on motion visually evoked responses." *Investigative ophthalmology & visual science* 45.3 (2004): 821-827.

Ungerleider, Leslie G., et al. "Subcortical projections of area MT in the macaque." *Journal of Comparative Neurology* 223.3 (1984): 368-386.

Van Essen, David C., Charles H. Anderson, and Daniel J. Felleman. "Information processing in the primate visual system: an integrated systems perspective." *Science* 255.5043 (1992): 419-423.

Vermaercke, Ben, and Hans P. Op de Beeck. "A multivariate approach reveals the behavioral templates underlying visual discrimination in rats." *Current Biology* 22.1 (2012): 50-55.

Vinck M, Batista-Brito R, Knoblich U, Cardin JA. (2015) Arousal and locomotion make distinct contributions to cortical activity patterns and visual encoding. *Neuron* **86(3)**:740-754

Vreysen S, Zhang B, Chino YM, Arckens L, Van den Bergh G (2012) Dynamics of spatial frequency tuning in mouse visual cortex. *J Neurophysiol* **107(11)**:2937–2949

Wagor E, Mangini NJ, Pearlman AL (1980) Retinotopic organization of striate and extrastriate visual cortex in the mouse. *J Comp Neurol* **193(1)**:187–202

Wang, Bor-Shuen, Rashmi Sarnaik, and Jianhua Cang. "Critical period plasticity matches binocular orientation preference in the visual cortex." *Neuron* 65.2 (2010): 246-256.

Wang BS, Feng L, Liu M, Liu X, Cang J (2013) Environmental enrichment rescues binocular matching of orientation preference in mice that have a precocious critical period. *Neuron* **80(1)**:198–209

Wang, Quanxin, and Andreas Burkhalter. "Area map of mouse visual cortex." *Journal of Comparative Neurology* 502.3 (2007): 339-357.

Wang, Quanxin, Enquan Gao, and Andreas Burkhalter. "In vivo transcranial imaging of connections in mouse visual cortex." *Journal of neuroscience methods* 159.2 (2007): 268-276.

Wang, Quanxin, Enquan Gao, and Andreas Burkhalter. "Gateways of ventral and dorsal streams in mouse visual cortex." *Journal of Neuroscience* 31.5 (2011): 1905-1918.

Wang, Quanxin, Olaf Sporns, and Andreas Burkhalter. "Network analysis of corticocortical connections reveals ventral and dorsal processing streams in mouse visual cortex." *Journal of Neuroscience* 32.13 (2012): 4386-4399.

Wässle, Heinz. "Parallel processing in the mammalian retina." *Nature Reviews Neuroscience* 5.10 (2004): 747.

Wekselblatt, Joseph B., et al. "Large-scale imaging of cortical dynamics during sensory perception and behavior." *Journal of neurophysiology* 115.6 (2016): 2852-2866.

White, Leonard E., David M. Coppola, and David Fitzpatrick. "The contribution of sensory experience to the maturation of orientation selectivity in ferret visual cortex." *Nature* 411.6841 (2001): 1049.

White, Leonard E., and David Fitzpatrick. "Vision and cortical map development." *Neuron* 56.2 (2007): 327-338.

Wiesel, Torsten N., and David H. Hubel. "Single-cell responses in striate cortex of kittens deprived of vision in one eye." *Journal of neurophysiology* 26.6 (1963): 1003-1017.

Wiesel, Torsten N., and David H. Hubel. "Ordered arrangement of orientation columns in monkeys lacking visual experience." *Journal of comparative neurology* 158.3 (1974): 307-318.

Wurtz, Robert H., and Michael E. Goldberg. "Activity of superior colliculus in behaving monkey. 3. Cells discharging before eye movements." *Journal of Neurophysiology* 35.4 (1972): 575-586.

Xu, Xiangmin, et al. "A comparison of koniocellular, magnocellular and parvocellular receptive field properties in the lateral geniculate nucleus of the owl monkey (Aotus trivirgatus)." *The Journal of physiology* 531.1 (2001): 203-218.

Yonehara K, Farrow K, Ghanem A, Hillier D, Balint K, Teixeira M, Jüttner J, Noda M, Neve RL, Conzelmann KK, Roska B (2013) The first stage of cardinal direction selectivity is localized to the dendrites of retinal ganglion cells. *Neuron* **79(6)**:1078–1085

Yoshida, K., and L. A. Benevento. "The projection from the dorsal lateral geniculate nucleus of the thalamus to extrastriate visual association cortex in the macaque monkey." *Neuroscience Letters* 22.2 (1981): 103-108.

Yoshioka, T., and S. H. C. Hendry. "The koniocellular visual pathway in rhesus monkeys: organization of neurochemically distinct neurons in the lateral geniculate nucleus." *J. Neurosci*(1999).

Zeater, Natalie, et al. "Binocular visual responses in the primate lateral geniculate nucleus." *Current Biology* 25.24 (2015): 3190-3195.

Zeki, Semir M. "Functional specialisation in the visual cortex of the rhesus monkey." *Nature* 274.5670 (1978): 423.

Zhang, Yifeng, et al. "The most numerous ganglion cell type of the mouse retina is a selective feature detector." *Proceedings of the National Academy of Sciences* 109.36 (2012): E2391-E2398.

Zhao X, Chen H, Liu X, Cang J (2013) Orientation-selective responses in the mouse lateral geniculate nucleus. *J Neurosci* **33(31)** 12751-12763

Zheng, Jianghe, et al. "Development of temporal response properties and contrast sensitivity of V1 and V2 neurons in macaque monkeys." *Journal of Neurophysiology* 97.6 (2007): 3905-3916.

Zhuang, Jun, et al. "An extended retinotopic map of mouse cortex." *Elife* 6 (2017): e18372.